SAND79-8199
Unlimited Release

Solar Energy Storage by Reversible Chemical Processes Final Report

Rockwell International

Prepared by Sandia Laboratories, Albuquerque, New Mexico 87115 and Livermore, California 94550 for the United States Department of Energy under Contract DE-AC04-76DP00789.

Printed January 1980

Sandia Laboratories energy report

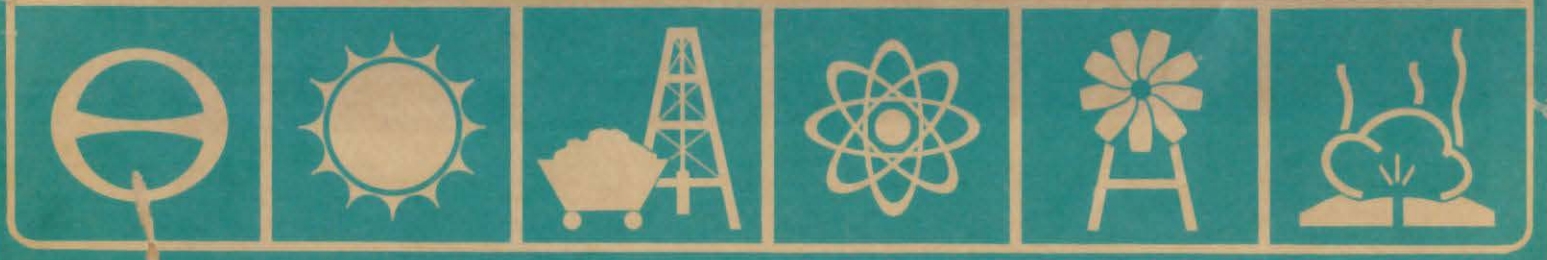

Issued by Sandia Laboratories, operated for the United States Department of Energy by Sandia Corporation.

NOTICE

Printed in the United States of America
Available from
National Technical Information Service
U. S. Department of Commerce
5285 Port Royal Road
Springfield, VA 22161
Price: Printed Copy $9.00; Microfiche $3.00

SOLAR ENERGY STORAGE
BY
REVERSIBLE CHEMICAL PROCESSES
FINAL REPORT

Rockwell International

Atomics International Division
8900 DeSoto Avenue
Canoga Park, California 91304

CONTRACT: FAO-92-7671

CONTENTS

CONTENTS

TABLES

TABLES

FIGURES

FIGURES

FIGURES

I. INTRODUCTION AND SUMMARY

A. HISTORICAL REVIEW AND EVALUATION

Investigation at Rockwell International of solar energy storage by reversible chemical reactions was initiated early in 1973 in the course of a company-sponsored conceptual design study of a 100-MWe solar central station plant.[I-1] To quote from Reference I-1: "The reactions studied in detail were the dehydration of $Ca(OH)_2$ and $Mg(OH)_2$. The heat of hydration of CaO of about 500 calories per gram is several times as high as the heat of fusion of a salt." It was recognized that the high temperatures necessary for dehydration at practical rates (~350°C with the $Mg(OH)_2$ system, the lower of the two) required the use of concentrating solar collectors – a potential disadvantage. There were a number of potential advantages, however: high energy storage density; simple, long-time storage at ambient temperature; portability, like a solid fuel; low cost and ready availability of the storage materials; relative simplicity of the chemical reactions; and the availability of high temperatures from the hydration step, a feature that is attractive for application to the generation of electric power. Under Rockwell Independent Research and Development funding, experimental work began later that year on the MgO - $Mg(OH)_2$ system. The goal was to evaluate the thermal and chemical performance under cyclic behavior, using electric resistance heating to simulate a solar source. The lower decomposition temperature for $Mg(OH)_2$, as compared with $Ca(OH)_2$, led in the early Rockwell-sponsored work to concentrating the study effort on the former type of material. This sponsorship continued into 1977. To date, two patents have issued from this phase of the development effort.[I-2]

Development in other areas was supported by a grant from the National Science Foundation and by contract from the Energy Research and Development Administration. Under the grant, cycling experiments were made with both the magnesium and calcium oxide-hydroxide systems that showed reproducible behavior.[I-3] The reactors employed in these experiments contained small (~200 g) fixed beds in layers 1/2 to 3/4 in. thick. These could be dehydrated to ~90% in 2 to 4 h – a condition that is compatible with the daily availability of

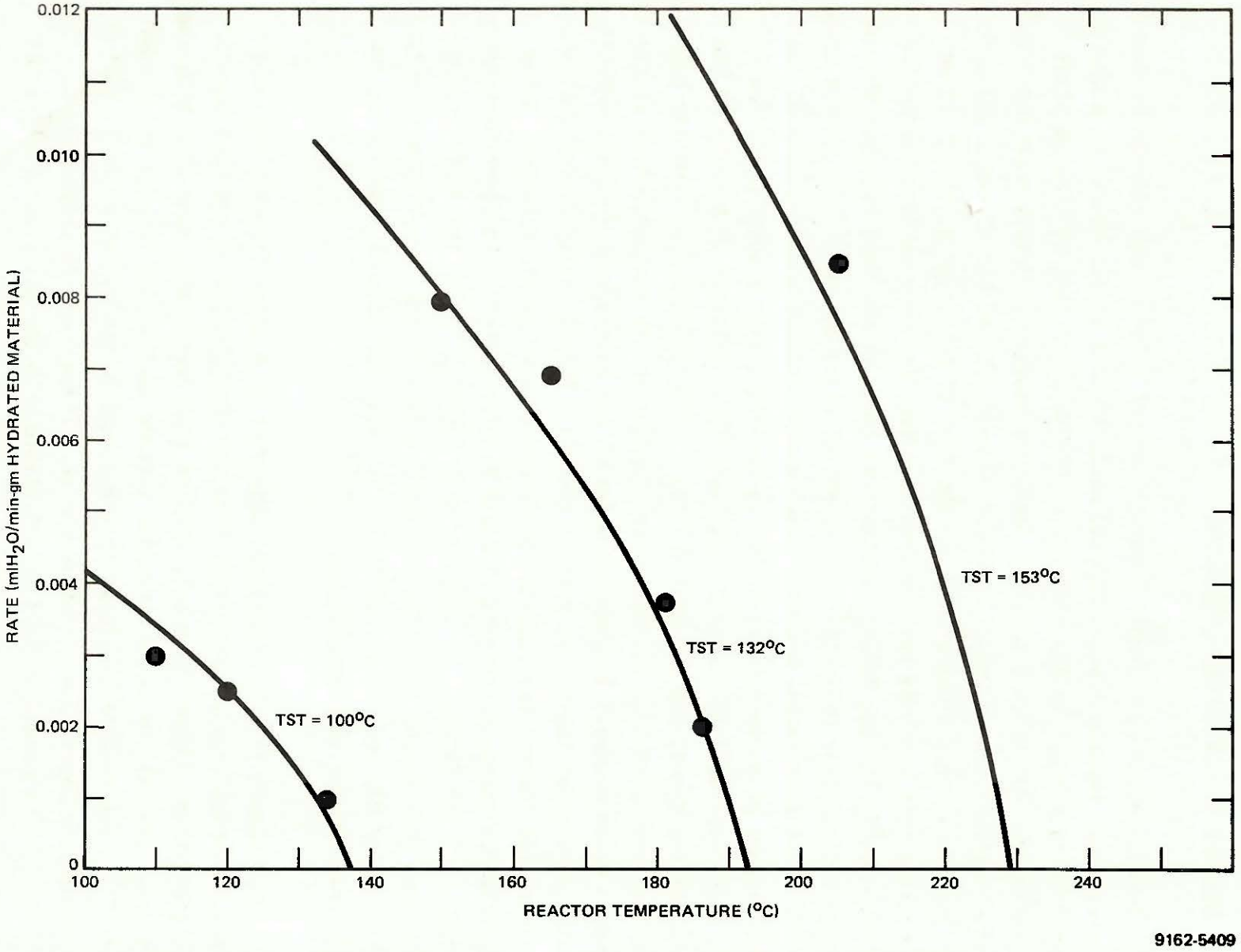

Figure I-1. Rate of Hydration of MgO as a Function of MgO Bed Temperature

sunlight – and hydrated in ~1 h. Thinner layers reacted more rapidly, as discussed in more detail below. These results suggested that the reactions may be heat transfer limited because of the low thermal conductivity of the oxide and hydroxide, especially in powder form or in highly porous layers.

A conceptual design based on the use of MgO - $Mg(OH)_2$ to store thermal energy was prepared for air conditioning a building (both cooling and heating) with solar power. It was decided to use a gas, circulating between a fixed bed of storage material and the load, for heat and mass transfer. A laboratory apparatus to evaluate performance of this fixed-bed concept was designed and sized to contain 20 lb of $Mg(OH)_2$ – a quantity of material that has storage capacity of ~6000 Btu.

Under the ERDA contract, the initial multitask effort included gas heat transfer tests and thermal cycling tests. Results of experiments in the 20-lb, fixed-bed MgO - $Mg(OH)_2$ apparatus showed that circulating gas was a feasible concept, using superheated steam as the heat and mass transfer fluid in direct contact with active material.[I-4] Inert gases such as air were found to affect the kinetics (especially hydration).[I-5] Also, there was a need to contain the material in thin layers in order to have a reasonably fast reaction.

It was found that the reaction rate of MgO depended strongly on the extent of superheat. The rates decreased with increasing bed temperature for a given steam saturation temperature (TST) as shown in Figure I-1. At TST = 132°C, for example, the rate becomes essentially zero at about 60° of superheat. This observation is consistent with other published studies of MgO hydration, but could not have been predicted from these studies alone.[I-6] This phenomenon is not observed for CaO, which was found to hydrate rapidly at temperatures very close to the $Ca(OH)_2$ - CaO equilibrium temperature for the particular steam pressure existing. The practical effect of this upper temperature limitation on MgO hydration is to reduce the efficiency of heat engine operation that could be performed with the $Mg(OH)_2$ - MgO cycle. On this basis alone, the $Ca(OH)_2$ - CaO cycle would be more attractive. Other reasons for preferring the calcium system are that it has a higher storage density than the magnesium system, and the chemical is much cheaper.

TABLE I-1

PERFORMANCE OF $Mg(OH)_2$ - MgO AND $Ca(OH)_2$ - CaO

	$Mg(OH)_2$ - MgO	$Ca(OH)_2$ - CaO
Cycling (% utilization)	60 to 70	95
Dehydration Temperature (^oC)	350	500
Hydration Temperature (^oC at 15 psig)	up to 200	up to 500
Net Heat of Reaction (Btu/lb)	300	430
Latent Heat (fraction of total)	1/2	1/3
Cost ($/ton)	150	30

TABLE I-2

POTASH 2 SYSTEM REQUIREMENTS

Electrical	9.45 MWe, 24 h per day, 7 days per week
Process Steam	89.7E6 Btu/h at 240^oF, 24 h per day, 7 days per week
Direct Fired Process Heat	69.6E6 Btu/h at 570^oF, 24 h per day, 7 days per week
Building Heating/Cooling	Included in electrical
Storage	41 h at full load

Repeated cycling tests were performed using a fixed-bed apparatus, where the bed thickness was about 1/8 in. This short path for reaction, and a total active material mass of less than 10 g, allowed very rapid heating and cooling and a high cycling frequency. The total cycle time was ~30 min, ~20 min for dehydration and ~10 min for hydration. The apparatus was arranged with a section where the solid material was confined and could be heated electrically, and a glass tube (part of the glass envelope around the system) was located where water from the dehydration could be collected and stored as a liquid. Heating the tube provided steam for hydrating. After charging with hydroxide, the glass system was evacuated and sealed. The extent of the reaction in either direction was measured by the volume of water in the tube. In this program,[I-7] 500 cycles were achieved with $Mg(OH)_2$, and 211 cycles with $Ca(OH)_2$.

As the cycling progressed, changes were observed in the capacity to hydrate and dehydrate, and in the rates. The data are summarized in Table I-1. In general, the results promoted confidence that these systems could store and deliver thermal energy over hundreds of cycles. No gross incompatibility with the Type 304 stainless steel parts was apparent. Also, the design of the experimental apparatus was proved fundamentally sound. It provided the basis for the refined apparatus used in the later, more extensive cycling, which is discussed elsewhere in this report.

Several application studies of oxide-hydroxide energy storage were made under the ERDA contract. In addition to more extensive investigation of the heating and cooling of buildings,[I-8] these included seasonal storage for crop drying (corn), process steam generation, and water pumping;[I-9] total solar concepts (a shopping center and an industrial plant "Potash 2"); and solar central electric power plants.[I-10] In general, these studies showed technical feasibility. For the Potash 2 plant and a 100-MWe central station power plant, where detailed comparisons were made, economic advantages were projected over alternate thermal storage systems. The Potash 2 system requirements are summarized in Table I-2 to indicate the scope of that design study.

Detailed engineering design and cost analyses were conducted as part of the Potash 2 and 100-MWe central station plant studies. The CaO - $Ca(OH)_2$ storage system chosen for this application was projected to be less costly than the mixture of rock and Exxon's HT-43 organic fluid used in Reference I-11. Both fixed-bed and fluidized-bed reactor designs were more economical than the rotating drum. In comparing the fixed-bed and fluidized-bed concepts, the principal advantages of the fixed bed are the relatively simpler system design and the better-understood technology resulting from more experimental investigation. On the other hand, the large reactor size[I-11] (6 ft in diameter for the plant vessels) and expected low heat transfer coefficients (~1 Btu/h-ft^2-^oF) represent a combination that has not been tested for achieving uniform, controlled reaction characteristics. The moving solids concept appeared overall to offer more advantages. These include: high heat transfer coefficients (to 100 Btu/h-ft^2-^oF); high mass transfer, leading to high reaction rates for both reactions; smaller and fewer reactor vessels; storage bins of low-alloy (and low-cost) steel; and the potential for better startup, shutdown, control, and operational flexibility, because of smaller reactor size and smaller quantities of solids involved.

The engineering design studies of moving solids reactors for these applications were not as extensive as the fixed bed. More work on moving solids systems was therefore proposed and included among other studies in the program entitled "Solar Energy Storage by Reversible Chemical Processes," under Federal Agency Order 92-7671. The results obtained under this Federal Agency Order Program is the principal subject of this report.

B. SUMMARY OF RESULTS OF THIS PROGRAM

Rockwell International* began work in August 1977 on a six-task program:

*The Atomics International Division of Rockwell International carried out the technical scope of work. This division has subsequently been reorganized to form the Energy Systems Group (ESG) of Rockwell International. ESG is responsible for the program at this time.

1) Characterization of Storage Materials
2) Cycling Experiments
3) Calorimetry and Kinetics Experiments
4) Fluidized-Bed System Analysis
5) Rotating Drum System Analysis
6) Alternate System Evaluation, Assessment, and Ranking

Essentially all goals were met. Results are briefly described in the following sections, along with some recommendations for future work.

1. Experimental Tasks

The broad objectives of the first three experimental-type tasks were to verify that a fixed-bed configuration of CaO - $Ca(OH)_2$ could be chemically cycled many times without degradation of material utilization (or reaction kinetics), and to measure the inherent heats of reaction and intrinsic chemical reaction rates of this system.

a. Characterization of Storage Materials

The starting material for all the experimental investigations was analytical-grade $Ca(OH)_2$. Characterization included chemical analyses, determination of surface area and particle size, electron spectroscopy for chemical analysis (ESCA), scanning electron microscopy (SEM), and chromatography of the gases involved. All samples of $Ca(OH)_2$ used in the investigation came from the same lot of as-manufactured material.

The starting material was of high purity, with average particle size of about 1.8 μm and surface area of about 17 m^2/g. Larger particles appear to be formed from several smaller, adherent platelets.

The material could be stored in air for short periods without appreciable change in composition, specifically H_2O and CO_2 pickup. No attempt was made to form the powder into granules prior to loading into an apparatus. It was used

"right out of the bottle." It was satisfactory as a reference material for the present program. Further investigation, however, should be made of the range of particle size and shapes with and without the use of binders to establish the optimum characteristics for thermal storage use in fixed-bed and moving solids reactors.

b. Cycling Experiments

Three identical experimental rigs were built and operated to observe behavior on cycling. Both the equipment and the instrumentation included improvements over previous work, but basically used the same design: a Type 304 stainless steel reactor, with automatically controllable temperature, contained in a sealed Pyrex glass envelope. In all three rigs, $CaO - Ca(OH)_2$ was successfully cycled in one system to a maximum over 1100 times (equivalent to more than 3 years of daily solar cycles). Dehydration was at $550^{o}C$ for 44 minutes; hydration was performed by allowing the reactor to cool to a temperature below the equilibrium temperature for the available steam generated in a heated tube attached to the Pyrex envelope. Typically, a hydration began at $375^{o}C$, with the temperature rising to $400^{o}C$. The total hydration period was 14 min, with the steam generator reaching about $110^{o}C$.

Over 90% utilization, based on available lime, was consistently attainable, provided that noncondensible gases were periodically removed from the system. These gases probably existed as the result of (1) small leaks and (2) generation of hydrogen caused by corrosion of metallic parts of the reactor. In the fixed-bed, "dead-end" reactor employed, the noncondensibles retarded reaction during the preset periods of time allowable in the automatically controlled cycle by (1) blanketing the water condenser walls during dehydration, and (2) accumulating in the solid reactant during hydration. In a moving solids reactor (or even a fixed-bed reactor in which the vapor phase is continuously passed through the reactor during hydration and noncondensibles are continuously vented during dehydration), the inert gas blanketing problem is expected to be of less importance. No metallographic examination was made post-operation. From visual observation of the stainless steel reactors at the

conclusion of 484, 837, and 1171 cycles, deterioration was progressive with cycling. Although no mechanism could be positively established, several hypotheses can be made. It is well known that Type 304 stainless steel, heated to the 425 to 815°C range, undergoes microstructural changes because of the precipitation of carbides ($M_{23}C_6$) at the grain boundaries. This process, called sensitization, results in susceptibility to intergranular corrosion and subsequent embrittlement. Water and especially steam are effective corrosion agents on sensitized steel. Also, there are substantial changes in crystalline specific volumes in the transition from one chemical form to the other. For example, the specific volume of crystalline $Ca(OH)_2$ is 45.2% greater than CaO. It is conceivable that the forces resulting from such volume changes could mechanically damage the stainless steel reactor parts, especially if the latter have already been weakened by corrosion.

Within a single half-cycle, however, it was found that the surface area of the oxide form is considerably higher than that of the hydroxide, suggesting that the departure of water results in the formation of pores, with possibly little variation in macrogeometric structure. A moderate decrease in specific surface area of the charge (hydroxide basis) was observed. Particle size underwent a cyclic variation suggesting periodic agglomeration and refracturing. This changing structure could also result in stresses in the corrosion-weakened walls of the reactor, causing rupture of the retaining screen.

Chemical changes in the active material include increased contents of Fe, with some Ni and Cr – the constituents of stainless steel. The most significant change is the increase in $CaCO_3$, which may reflect reaction with the CO_2 in leaked air.

In any future structural materials work, a first priority should be to examine the microstructure of the stainless steel in these three reactors. Guided by these findings, a systematic evaluation of alternative alloys can be made to find a material more suitable than stainless steel. Even with stainless steel, it is possible to select heats that are resistant to intergranular corrosion, if that mechanism is involved. Future reactors, made of the superior

material, would surely reduce the generation of hydrogen. This is one of the gases identified by chromatographic analysis (along with hydrocarbons and CO_2) in the noncondensible fraction removed from the reactors by "cold evacuation" (pumping at 50°C). Some provision will inevitably be necessary, however, for removing noncondensible gases in any practical reactor. Two improvements in future experimental reactors would be better valving to vacuum, and a means of replenishing the water supply over long cycling campaigns.

c. Calorimetry and Kinetics Experiments

A pressure differential scanning calorimeter (PDSC) was successfully used to:

1) Develop equilibrium constants (pressure-temperature relationships) for the reaction $Ca(OH)_2 = CaO + H_2O$, in excellent agreement with JANAF data over the 450 to 550°C range
2) Measure, in single tests, values of the heat of reaction for $Ca(OH)_2 = CaO + H_2O$ within 90 to better than 95% of published values
3) Determine a value of 36 kcal/mole for the activation energy of the reaction $Ca(OH)_2 = CaO + H_2O$ into an inert atmosphere (N_2) at ambient pressure, in agreement with several other investigators (For experiments conducted at low pressures, however, values reported in the literature tend to be considerably lower. This is as yet unexplained.)
4) Establish that the dehydration reaction kinetics are determined by phase-boundary control (the "shrinking core" model) (Also, for the very small (1.8 μm average) particle size and the minute (0.5 to 100 mg) quantities of material studied, formation of oxide on the surface of the initially hydroxide particles does not appear to impede water transport.).

It is felt that the current PDSC studies, employing the very thin layer charges in intimate contact with the heat transfer surfaces and the surrounding

atmosphere, represent, perhaps, the closest approach to intrinsic surface kinetic measurements attempted for the CaO - $Ca(OH)_2$ system.

Future work will require the determination of steam-atmosphere kinetics of both hydration and dehydration. While operation of the PDSC in steam was not demonstrated, tests by ESG have shown that the equipment does function at $125^{o}C$.

2. Analytical Tasks

a. Fluidized-Bed and Rotating Drum (Moving Solids) System Analyses

Engineering studies were made to assess performance of these two thermal energy storage concepts when incorporated into a commercial 100-MWe solar-electric power plant, to provide capability to generate 100 MWe during 6 night-time (or sunless) hours. The principal features of day and nighttime operation are illustrated schmatically in Figures I-2 and I-3.

During a sunny day, liquid sodium is used as a heat transfer fluid between the solar receiver to the steam boiler-superheater and to the $Ca(OH)_2$ dehydration system. At night, the sodium transfers heat, generated by the hydration of CaO, to the steam generator. Both modes of operation employ arrangements of reactant storage bins, fluidized-bed reactors, and fluidized-bed heat recovery components (heat exchangers).

During sunny days, a portion of the solar-heated sodium is directed through tube bundles in a fluidized-bed reactor system (fluidized with nitrogen and steam), where at $800^{o}F$ it dehydrates $Ca(OH)_2$ coming from storage at $550^{o}F$. At night, the same reactor system fluidizes and hydrates CaO at $760^{o}F$ with turbine exhaust steam. A second fluidized-bed system fluidizes and hydrates CaO at $1000^{o}F$ with steam from one of the turbine's lower stages. Pneumatic conveying is used for solids transport. In both modes, there is heat exchange (solids heat recovery) with boiler feedwater, and nitrogen is used as the fluidizing gas in the heat recovery units.

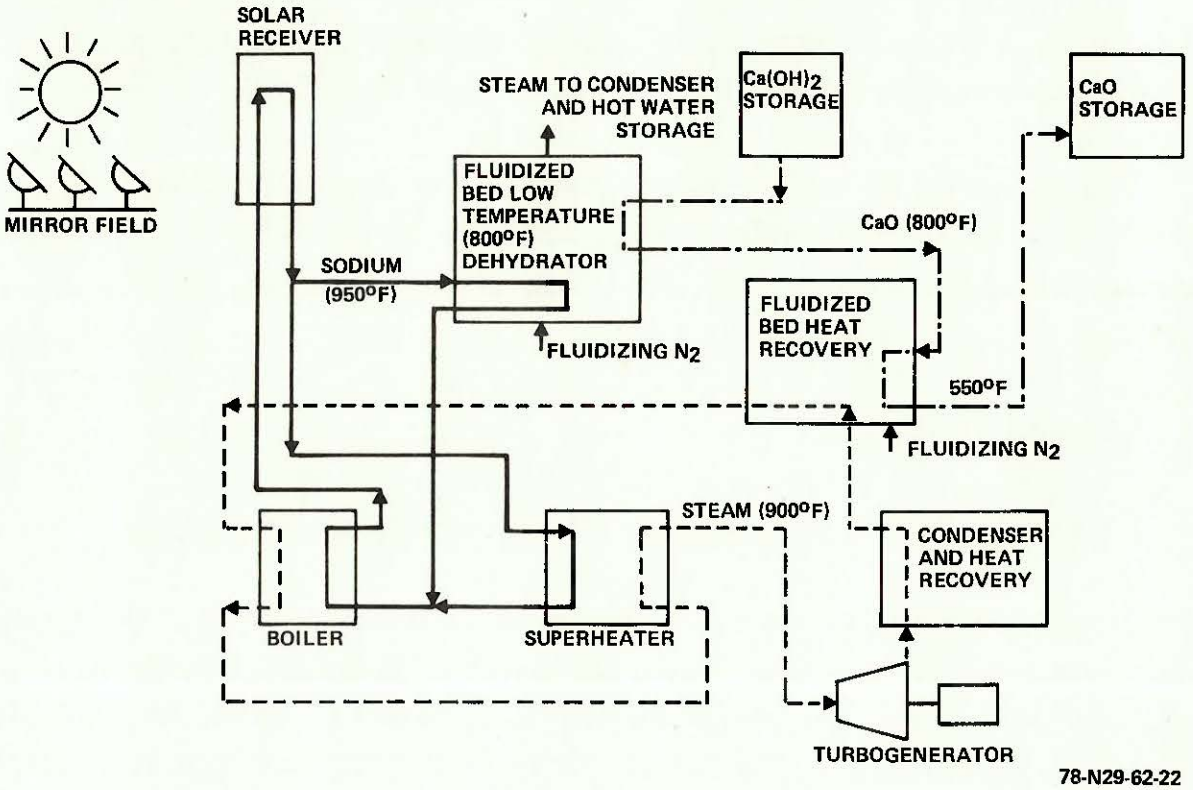

Figure I-2. Central Solar Power Station With CaO - $Ca(OH)_2$ Heat Storage, Day Operation

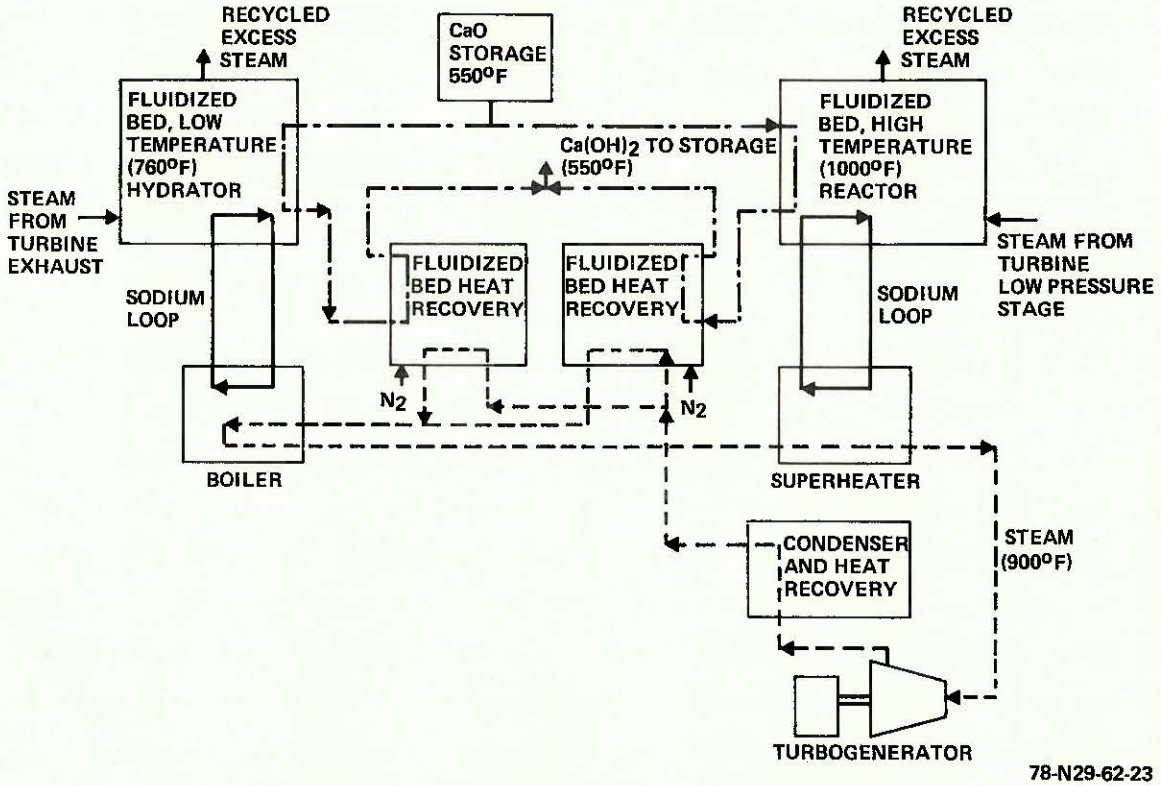

Figure I-3. Central Solar Power Station With CaO - $Ca(OH)_2$ Heat Storage, Night Operation

In the rotating drum system, drums replace the fluidized-bed reactors, and fluidizing nitrogen is not used.

b. Alternate System Evaluation, Assessment, and Ranking

The performance and economics determined for the two moving solids thermal storage systems in this investigation were compared with previous determinations for a fixed-bed CaO - $Ca(OH)_2$ and an HT-43, hot rocks storage system.[I-12] These latter two systems, however, were sized for 70 MWe nighttime load, so that an extrapolation had to be applied for comparison at the same level as the other two systems.

The rotating drum reactor concept proved to be significantly (3 to 5%) lower in overall station efficiency and ~50% more costly (8.60¢/kWhe versus 5.80¢/kWhe) to operate than the other systems. Consequently, this concept is not recommended for this application.

Station Efficiency

Figure I-4 shows the efficiency as a function of nighttime operating hours at 70 MWe for the fixed-bed, the fluidized-bed, and the HT-43 and hot rocks systems. For the reference 6 h storage, the fixed bed has the highest efficiency (33.7%), HT-43 and hot rocks the lowest (31.1%), and fluidized bed, intermediate (31.7%). All efficiencies decrease with increasing storage time, but the hot rocks system decreases much faster.

Levelized Busbar Cost of Electricity ($\overline{BBEC}$)

In Figure I-5, $\overline{BBEC}$ values are plotted against duration of nighttime storage for these three systems, and for two different annual makeup rates for the heat storage media — 0, and 15%. At 6 h of storage (the reference value), and with zero makeup, the fixed bed has the lowest value, 5.8¢/kWhe. The hot rocks system $\overline{BBEC}$ is 5.91¢/kWhe, while the fluidized bed is 6.06¢/kWhe. For shorter storage (4 h), the HT-43 and hot rocks system is the same as the fixed

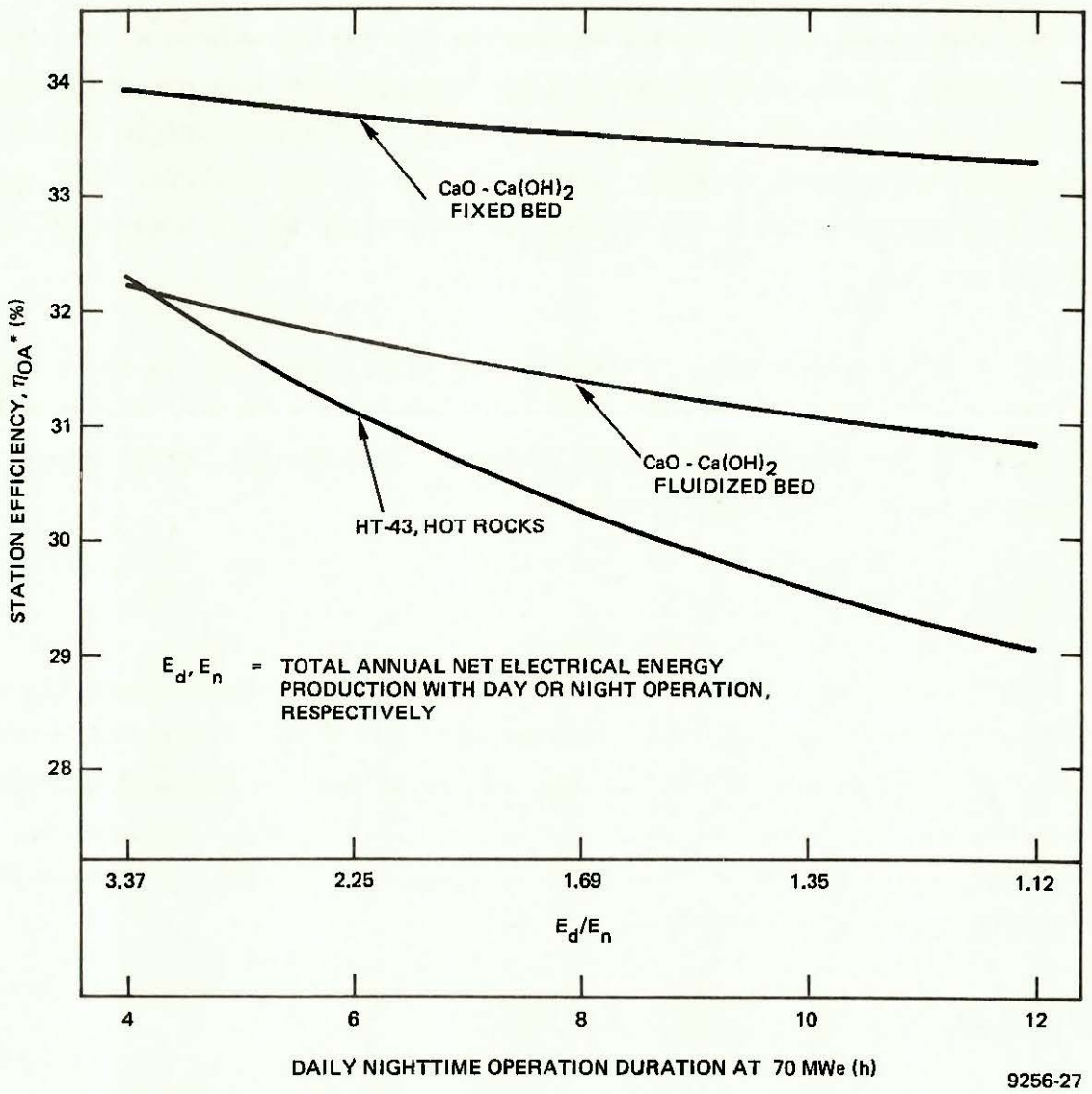

*SEE PAGE III-41 FOR DEFINITION OF η_{oA}

Figure I-4. Overall Station Thermal Efficiency vs Hours of Nighttime Operation at 70 MWe (E_d is constant at 311.4 x 10^6 kWh/year)

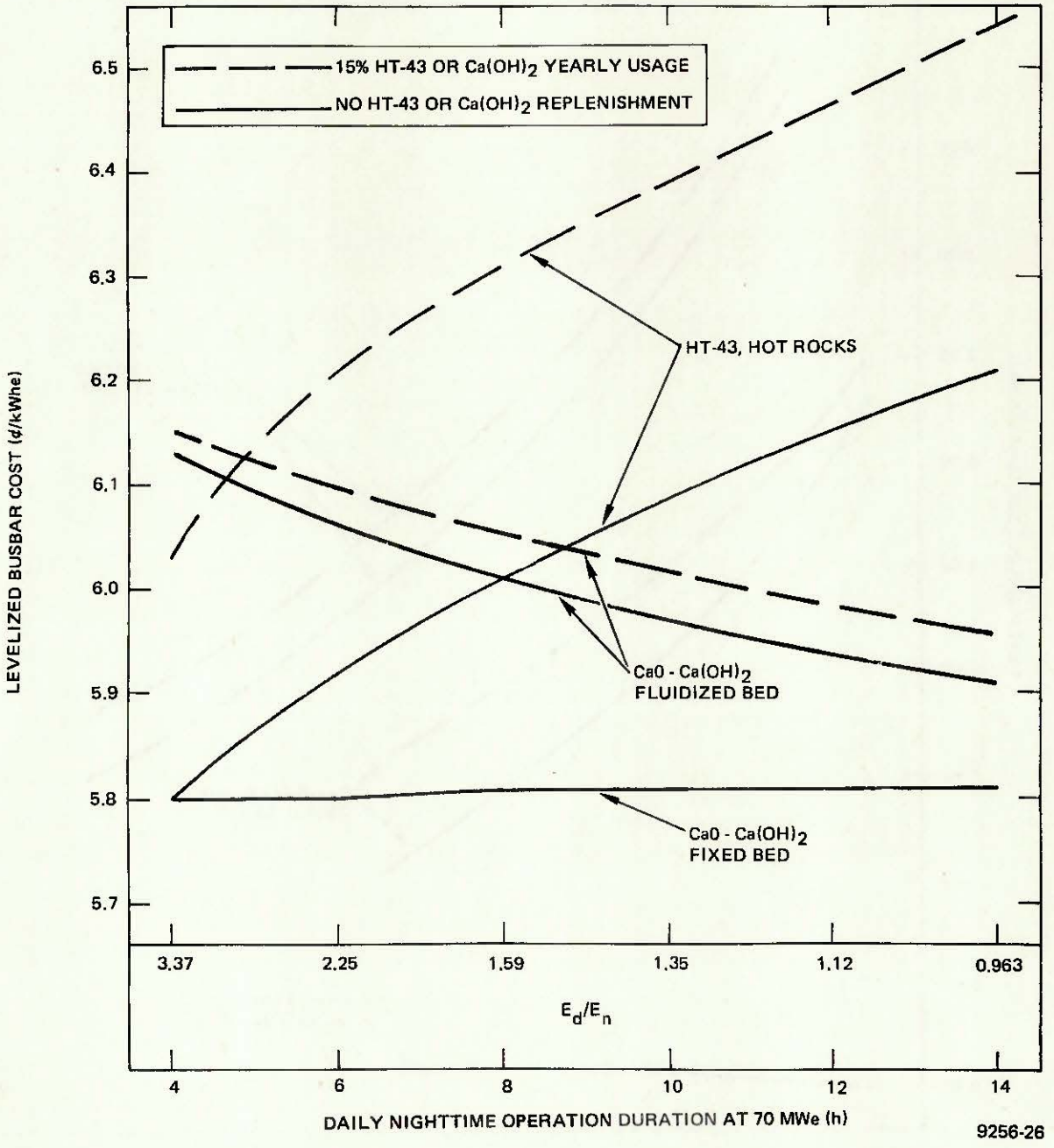

Figure I-5. Levelized Busbar Cost of Electricity, $\overline{BBEC}$
(70-MWe Night and 100-MWe Day Operation,
E_d constant 311.4 x 10^6 kWh/year)

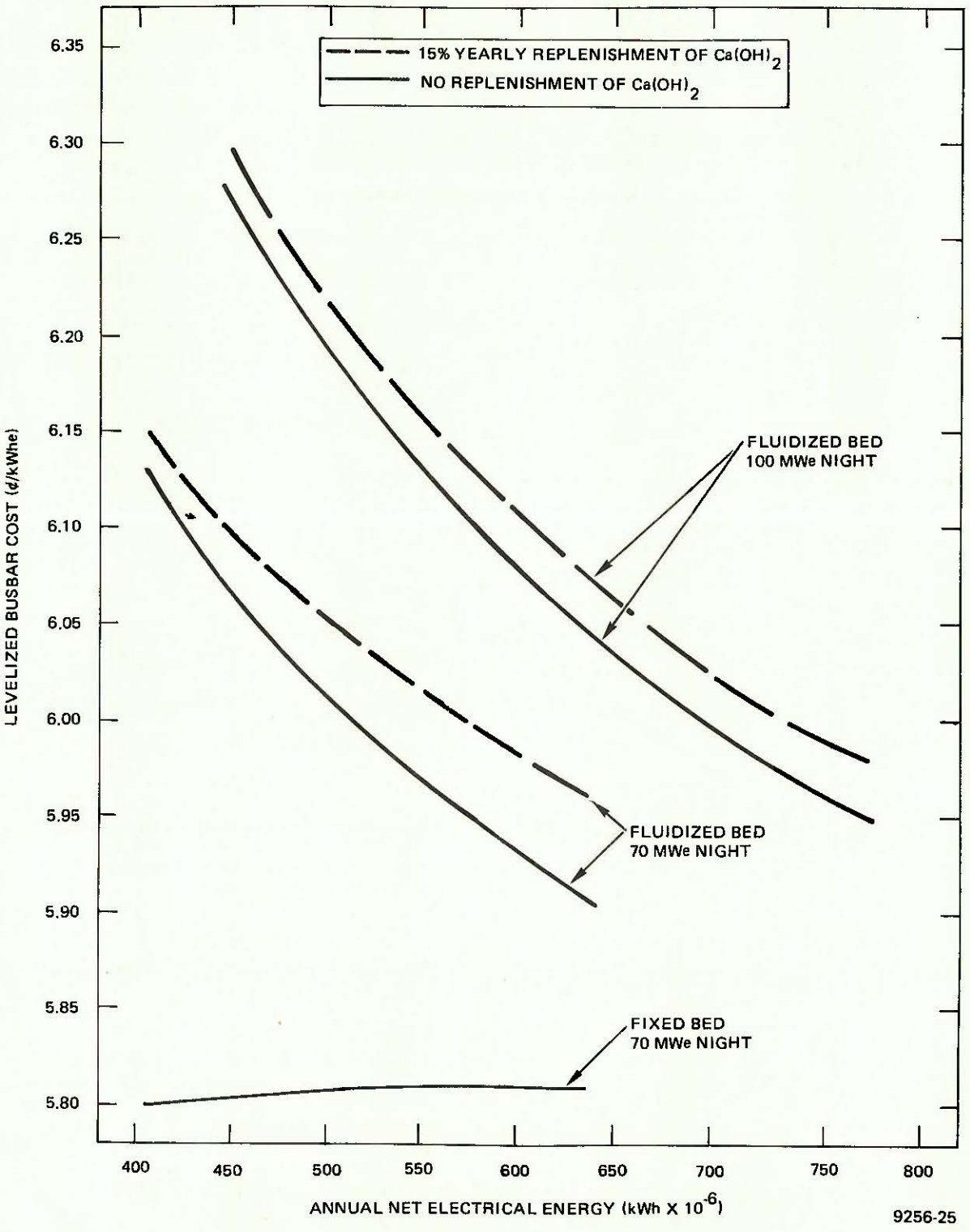

Figure I-6. Levelized Busbar Cost vs Total Annual Net Electrical Energy
(E_d is constant at 311.4 x 10^6 kWh/year)

bed, about 5.8¢/kWhe. Beyond 12 h of storage, the $\overline{\text{BBEC}}$ derived from the fluidized-bed system will eventually reach and then become less than that of the fixed bed. At 15% annual makeup, both HT-43 and hot rocks and fluidized-bed energy cost increase, but the HT-43 increase is considerably greater. (A comparable value for the fixed bed was not calculated.)

$\overline{\text{BBEC}}$ costs are plotted for the three systems against total annual energy in Figure I-6 for a fixed daytime annual energy and variable nighttime energy, and two levels of fluidized bed nighttime power, 70 and 100 MWe. Operation is more costly at 100 MWe than at 70 MWe for the fluidized bed. Even at 70 MWe, its costs are generally higher than for the fixed-bed system; but a combination of long storage time (as in Figure I-5), low $Ca(OH)_2$ makeup rate, and low nighttime power would bring costs below the fixed-bed system.

Effect of Higher Operating Temperatures

The HT-43 and hot rock system has a serious limitation in that the HT-43 oil is limited to a maximum temperature of about 600°F. Therefore, relatively low pressure (500 psia) and temperature (550°F) steam is generated during operation of the storage system. This situation results in an inherently low thermodynamic efficiency and necessitates the use of a complex dual admission turbine. The CaO - $Ca(OH)_2$ system does not have this temperature limitation, and its efficiency can be improved by operating at higher temperatures.

A brief study was made of the effect of increasing the operating temperature level by 100°F for the fluidized-bed system operating at 70 MWe from the storage system. The sodium temperature was increased from 950 to 1050°F, and the steam temperature and pressure were increased from 900 to 1000°F and from 1300 to 1800 psia. The results indicated a significant improvement in station efficiency (2.1%) and a 6.4% reduction in the $\overline{\text{BBEC}}$.

Assessment and Ranking

Since the fixed-bed system is by far the simpler to operate and, for the application considered, is theoretically the better performer, it is the most

promising candidate for development. The rotating drum reactor concept does not merit further work. The fluidized-bed system should be considered when large storage capability (~12 h operation time) is a requirement. The difference in busbar cost between the fixed bed and fluidized bed is 2% at 12 h storage. This difference may well be eliminated by fluidized-bed design improvements. Above about 20 h storage, the fluidized-bed system is less expensive than the fixed-bed system. Since the operational characteristics have not been demonstrated for either system, it is impossible to conclusively decide which is better or, indeed, if either system will perform satisfactorily under required operating conditions. For both systems, experimental data from tests in scaled-down equipment would provide needed information to judge performance and guide design. For the fluidized bed, data are particularly needed on particle characteristics (sizes and attrition rates), fluidizing gas velocity effects, and achievable heat transfer and reaction rates. For the fixed bed, measurements of reaction rates and heat transfer over long path lengths and the determination of cycling behavior when there are temperature gradients in the bed are some of the data required.

There will likely be applications where the fluidized-bed system would be more advantageous than the fixed-bed system and vice versa. Further system studies of other fluidized-bed configurations are likely to disclose additional design features that will improve the fluidized bed performance and reduce its complexity. For example, storage of the material at higher temperatures and mechanical conveying of solids are such potential improvements. Different operating conditions would be advantageous, especially higher reactor temperatures, higher handling temperatures, transport of materials (well above 580^{o}F), and higher sodium temperatures (above 950^{o}F). These improvements could lead to simplification of operation and higher efficiencies. More detailed design studies with conceptual plant layout and major component drawings are needed to refine system operational concepts and cost data.

REFERENCES

I-1. G. Ervin, Jr. and R. L. McKisson, "Energy Storage for a Proposed 100-MWe Solar Power Plant" (May 4, 1973) (Rockwell Proprietary)

I-2. U.S. Patents 3,973,552 dated August 10, 1976, "Method of Storing and Releasing Thermal Energy," and 4,054,126 dated October 18, 1977, "System for Storing and Releasing Thermal Energy," G. Ervin, Jr. (assigned to Rockwell International)

I-3. G. Ervin, Jr., D. K. Chung, and T. H. Springer, "A Study of the Use of Inorganic Oxides for Solar Energy Storage for Heating and Cooling of Buildings," AI-75-63, October 1975 (Final Report June 1, 1974-July 31, 1975, Grant AER74-09069-A01)

I-4. G. Ervin, Jr., "Experimental Test of Gas Heat Transfer System for Hydroxide Heat Storage," AI-ERDA-13176 (October 29, 1976)

I-5. D. K. Chung, "Effect of Presence of Noncondensibles on the Rate of Hydration and Dehydration of Spherical $MgO/(OH)_2$ Pellets," AI Internal Document No. N162TI130002 (March 5, 1976)

I-6. R. J. Bratton and G. W. Brindley, Trans. Faraday Soc. 62 (10) 2909 (1966). This is cited as Reference 9 of the paper by Ervin and others (see Reference I-3 of this report).

I-7. G. Ervin, Jr., "Hydration-Dehydration Cycling of MgO - $Mg(OH)_2$ for Application to Solar Heat Storage Systems," AI-ERDA-13178 (September 30, 1976)

I-8. D. K. Chung, "Application of MgO - $Mg(OH)_2$ and CaO - $Ca(OH)_2$ as a Daily and Seasonal Heat Storage System for Heating and Cooling of Buildings," AI Internal Document No. N162TI130004 (October 27, 1976)

I-9. D. K. Chung, "Application of Seasonal Solar Heat Storage for Crop Drying, Process Steam Generation, Electrical Power Generation, and Water Pumping," AI Internal Document No. N162TI130006 (October 25, 1976)

I-10. G. P. Hajela, "Application of MgO - $Mg(OH)_2$ Storage System for Electric Power Generation," AI Internal Document No. N162TI130005 (June 18, 1976)

I-11. J. Guon, "Economic Comparison of Calcium Oxide and 'Hot Rocks' Storage Systems," AI Internal Document N162TI160001 (January 27, 1977)

I-12. D. K. Chung, "An Economic Assessment of the Application of a CaO - $Ca(OH)_2$ Thermal Energy Storage System Applied to a Commercial Solar Power Station," AI Internal Document N162TI120008 (September 19, 1977) (to be released)

II. EXPERIMENTAL INVESTIGATIONS

The experimental studies conducted in this project were partially directed toward the further understanding of the intrinsic chemical properties of the CaO - $Ca(OH)_2$ system — properties that are required for the design of fixed-bed as well as moving solids reactors — and partially directed toward the acquisition of operating data specifically for a fixed-bed configuration. In the latter regard, it was a goal of this project to verify that a fixed-bed configuration of CaO - $Ca(OH)_2$ can be chemically cycled many times without degrading in terms of water utilization and rate of reaction.

The scope of the experimental studies also included the characterization of the reactant (in terms of chemical and physical properties) during and after such a long-term, cyclic operating period.

Kinetic reaction studies were made using a pressure differential scanning calorimeter (PDSC). The PDSC was also used to determine heats of reaction and equilibrium properties. Thus, the experimental portion of the project consisted of three tasks: (1) cycling studies on CaO - $Ca(OH)_2$, (2) calorimetry and kinetics, and (3) materials characterization.

A. CYCLING TESTS

The overall goal of this task was to verify that a fixed-bed configuration of calcium oxide-hydroxide can be chemically cycled many times without degrading in terms of bed utilization and rate of reaction. The target duration for the tests was 1000 or more cycles.

1. Equipment and Procedure

Because of the relatively short duration of the program, it was necessary to design the cycling reactor so that each cycle could be completed in as short a period as practicable. The basic reactor used earlier for study of the MgO - $Mg(OH)_2$ system[II-1] was adapted to the present project.

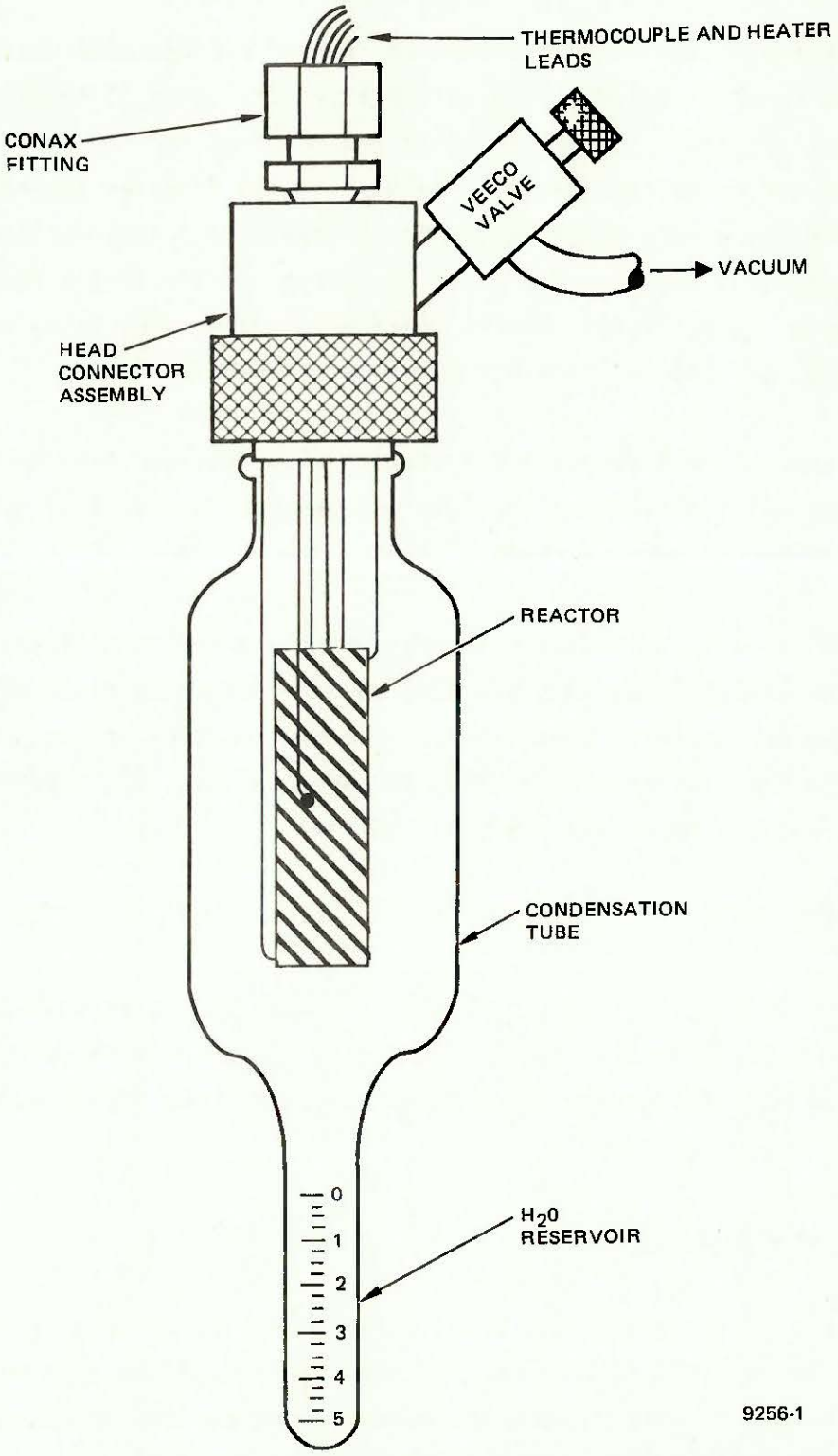

Figure II-1. Cycling Test System Schematic

Figure II-1 is a schematic drawing of the reaction apparatus. The reactor itself was suspended by the thermocouple and heater-lead bundle inside a Pyrex vacuum shell. At the bottom of the shell, a volumetric water reservoir was fused to the outer envelope (condensation tube). The thermocouples passed through a Conax gland fitting attached to a high-vacuum quick-connect. Details of the head assembly are shown in Figure II-2. The vacuum fitting was attached to a Kovar junction at the top of the glass envelope.

The reactor itself is shown schematically in Figure II-3. The sample charge was contained in the 0.13-in. annulus between the outer shell and a wire screen central retainer. The sheathed, Nichrome heater cable extended beyond the sample zone to maintain reasonably constant longitudinal temperature uniformity. At any selected temperature, the various thermocouples showed no more than a $2^{o}C$ deviation during periods in which reaction was not taking place. A fifth thermocouple (not shown) was attached diametrically opposite Position 1 and was used for heater control. A thermocouple was also wired to the bottom of the calibrated water tube.

The heater coil was attached with a thin strap to the reactor shell, as shown in Figure II-4. The inner wire-cloth tube is shown in Figure II-5. All parts of the reactor, including the heater sheath, were constructed of Type 304 stainless steel. The thermocouples were Inconel sheathed.

Figure II-6 shows a typical reaction apparatus. A heating tape was wrapped around the top of the assembly and maintained at $200^{o}C$ to prevent condensation of water in the upper part of the system.

The blower at the bottom of the water reservoir was used to air-cool the condenser during dehydration half-cycles, while the reactor heater was energized (nominally to $550^{o}C$). Heatup time of the reactor heater was approximately 1 min.

During hydration half-cycles, the reactor heater was de-energized and the reactor was allowed to cool ballistically. The heating coil at the blower (visible in Figure II-6) was energized to heat the water in the tube as well as

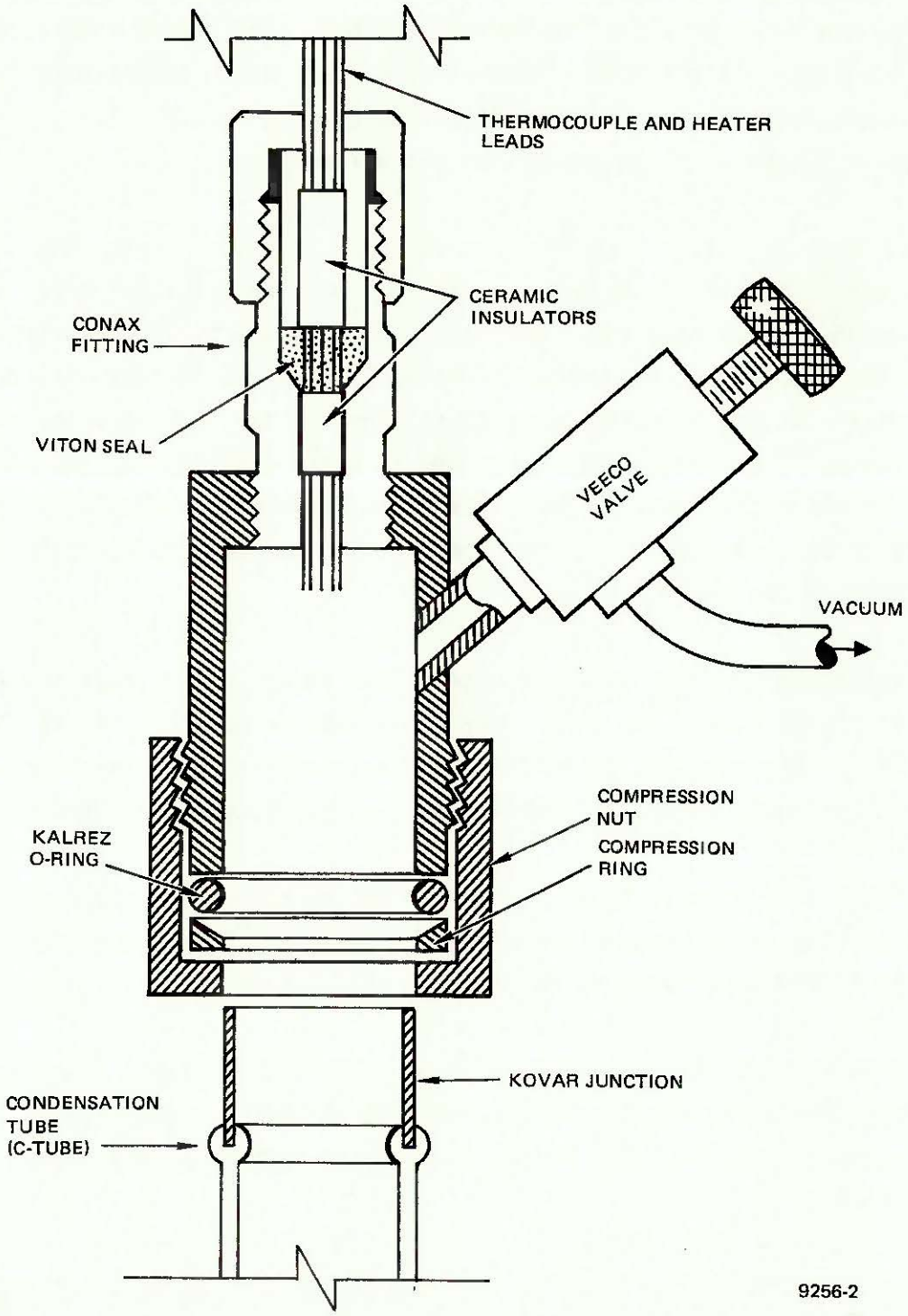

Figure II-2. Upper Section of Test System

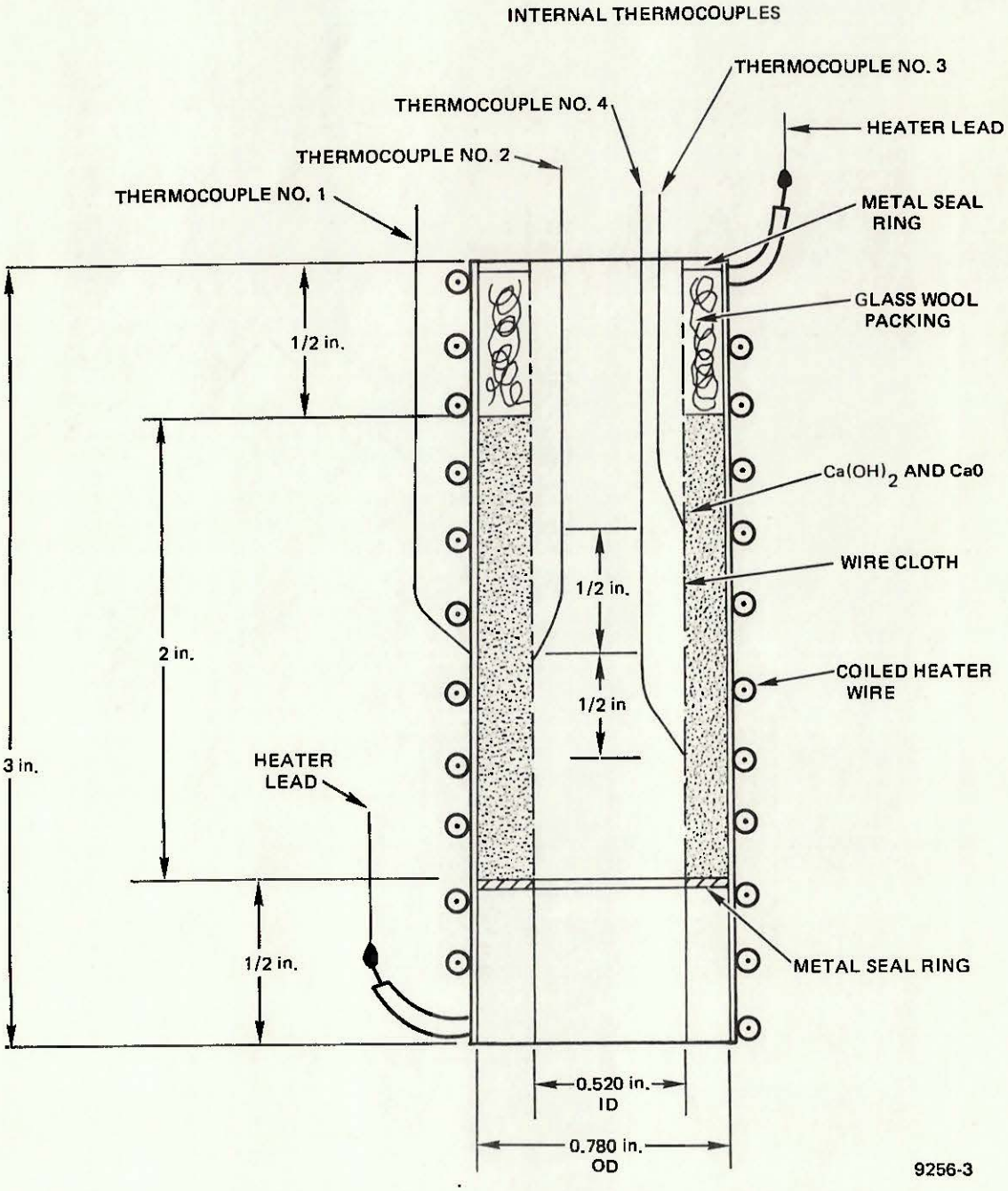

Figure II-3. Sketch of Reaction Tube

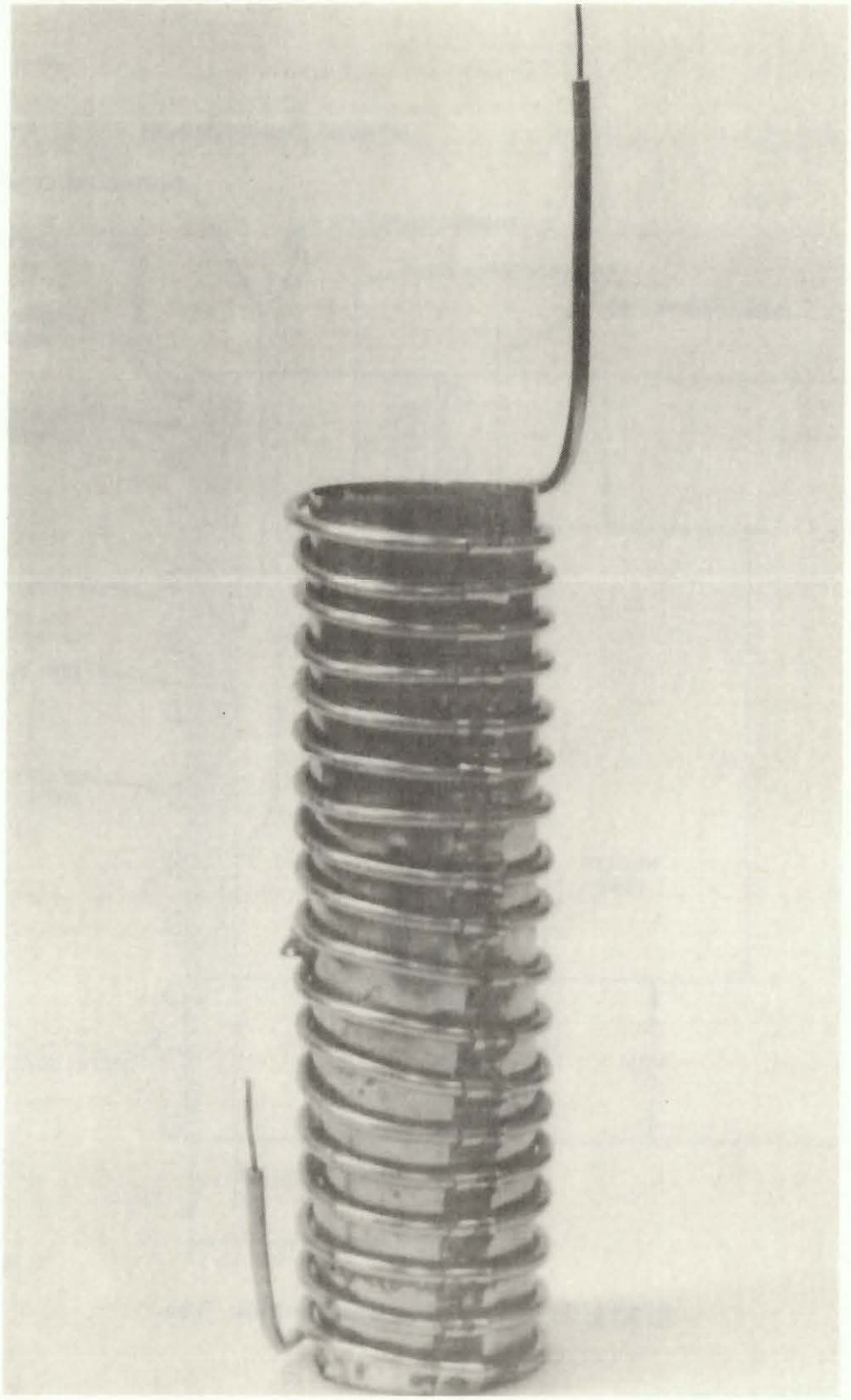

40443-9

Figure II-4. Typical Reactor Assembly

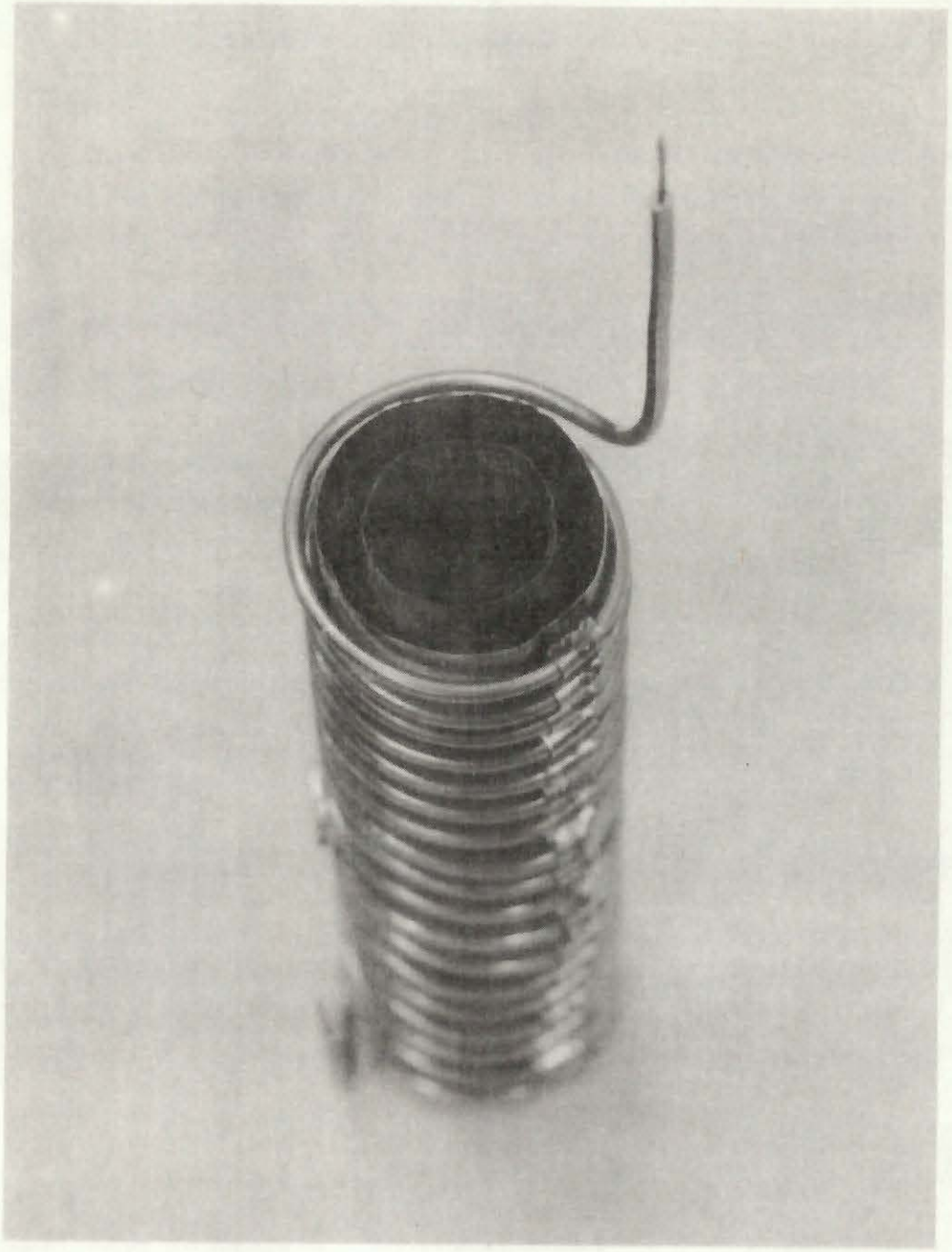

40443-8

Figure II-5. Reactor Showing Internal Retainer Screen

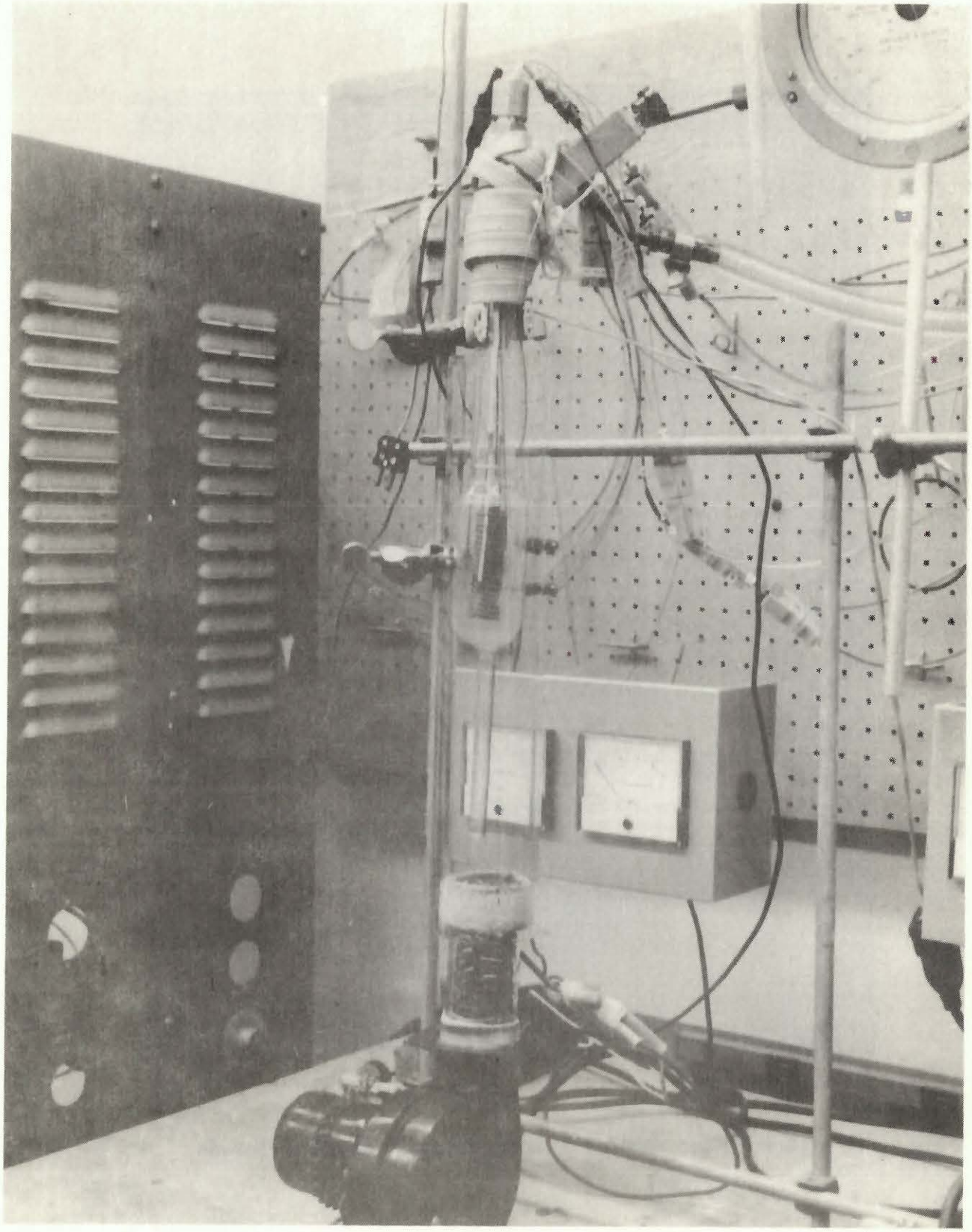

Figure II-6. Assembled Test Apparatus

40443-6

the condensation tube walls (thereby retarding condensation on the latter). Typically, hydration began when the sample temperature had fallen to about 350°C. At that time, the water reservoir was essentially still at room temperature. The blower heater current was set so that final water tube temperature was about 110°C.

Since it was desirable, but not practical in view of the small charge involved, to characterize the material after intermediate periods of cycling, three cycling systems were assembled to enable sample characterization at different lifetimes. One of the test rigs (Unit I) was loaded with $Ca(OH)_2$ powder (nominally 7.2 g) and subjected to a short series of dehydrations and hydrations (six cycles) using manual operation of the heaters in order to degas the sample and establish conditions for later automatic cycling. This test was terminated after six cycles as a result of excessive loss of water during the conditioning steps (see Section II-A-2). Subsequently, all three test rigs were loaded and subjected to continuous automatic cycling. A multipole electrical clock timer energized the heaters at the appropriate times. The following schedule was employed: 44 min for dehydration at 550°C, 1 min from reactor heater turnoff to steam generator (blower) heater on, 14 min for hydration with the reactor ballistically cooling and the water tube eventually reaching 110°C, and then 1 min between water tube heater turnoff to reactor heater on.

Thermocouple signals were continuously recorded throughout the test program on multipoint recorders. Records of water level as a function of time (rate of reaction) were prepared during the course of at least one complete cycle each day. In addition, more frequent checks of final water level (utilization) at the conclusion of several half-cycles were made throughout the work day. These checks were not made on any rigid schedule; rather, the data were taken dependent on the availability of an operator at the known time of day at which half-cycles were terminated (e.g., on the hour for the end of hydration and 44 min later for the end of dehydration).

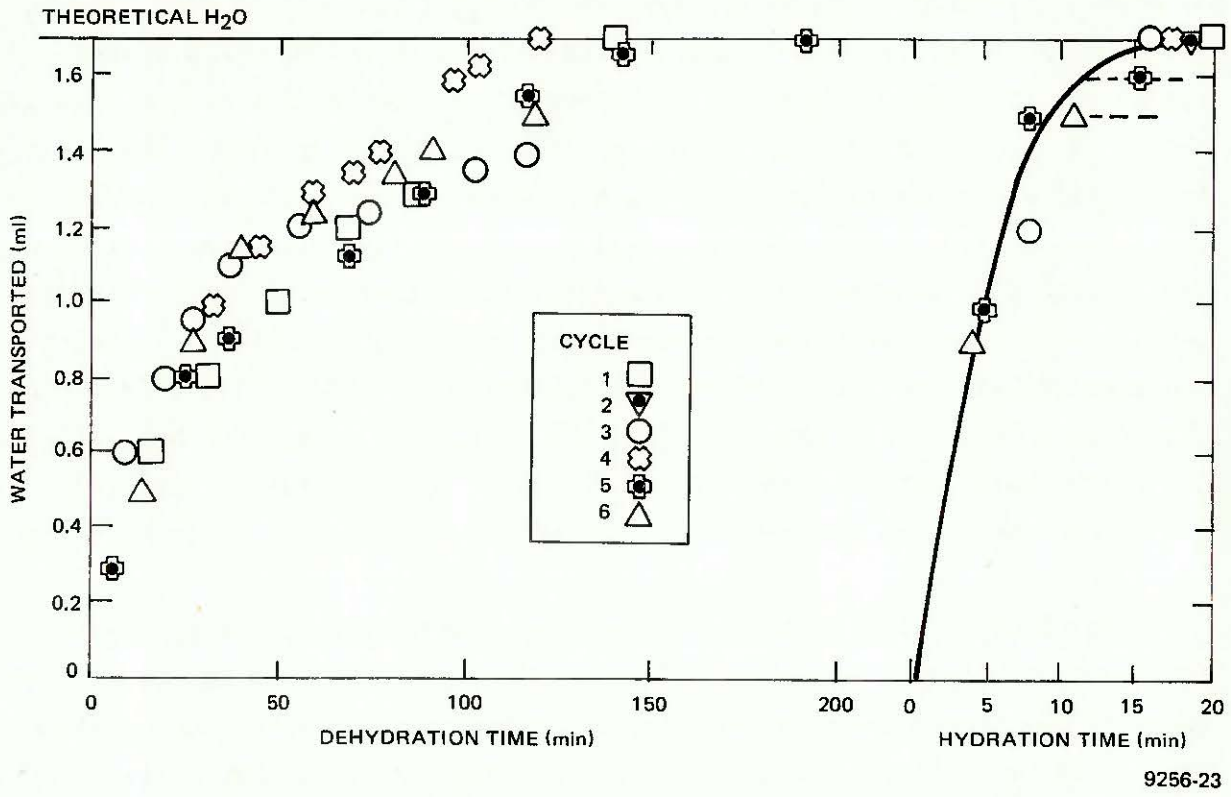

Figure II-7. Water Transport in Six-Cycle Test

2. Results and Discussion

Normally, prior to initiation of the automatic cycling, a few manually controlled cycles were performed. This procedure was used to completely degas the sample through several extended dehydrations at 550°C. Periodic evacuation of the assembly (to the point of vigorous boiling of the water in the collection tube) enabled removal of inert gases.

The starting material was reagent-grade $Ca(OH)_2$ in all tests. The water evolved during the initial dehydration was thus added to that initally placed in the tube. Characterization of the material is summarized in Section C.

In the initial six-cycle test with Unit I, a small amount of water (2 ml) was originally placed in the tube to allow for some water loss during the evacuations. It was originally intended that, after several cycles, the unit would be put on automatic operation. After several evacuations, as previously described, the remaining water was not sufficient to completely hydrate the charge. In subsequent startup operations, the entire collection tube was prefilled with boiled, distilled water to prevent recurrence of the water loss problem.

Figure II-7 summarizes the results of the six-cycle, manually controlled test. Typically, hydration commenced at about 375°C (after cooling from 550°C), and the reactor temperature rose to and stabilized for up to about 10 min at 400°C. After hydration was essentially complete, the reactor again cooled.

It can be seen in Figure II-7 that after five dehydration half-cycles, there was insufficient water in the reservoir to complete subsequent hydrations. The relatively long period of time for hydration (2 h or more) was of some concern. Much shorter reaction times had been required in earlier tests with $Ca(OH)_2$.[II-2]

Reaction Units I (after refilling), II, and III were started up with a considerable excess of water in the tubes. It was found that with all three

units much shorter dehydration times were required to attain complete utilization than in the six-cycle test, even in the initial manual cycles. As much as 95% dehydration occurred in as little time as 16 min. Since the startup procedure was identical for the six-cycle test and for Units I and II (in fact, with Unit III, initial manual cycles were not employed; the unit was put on automatic operation from the start and degassed as required), no explanation has been apparent for the relatively long dehydration periods required in the short test. Hydration was essentially complete in 10 to 15 min in early cycles with all units indicating that, once dehydrated, all sample charges were equally active.

In general with the three test units, hydration occurred at the fastest rates when the reaction was initiated at about 375°C (reactor temperature then rose to 400°C or higher). Interestingly, 375°C corresponds to an equilibrium vapor pressure of about 23 mm over the $Ca(OH)_2$; such a pressure is available with a generator temperature of only about 25°C. At initiation of reaction, the generator is essentially at room temperature, indicating that reaction occurs at conditions not far removed from equilibrium (i.e., no cutout phenomenon as with MgO).

Occasionally, the sharp temperature rise did not occur on hydration. Left unattended, the system would usually revert to normal, "active" operation in a few cycles. In some cases where recovery was not apparent in several cycles, the more active operation could be brought about by quickly evacuating the system (for 10 s or less) while in the latter stages of dehydration (i.e., when water partial pressure was at a minimum to avoid excessive boiloff).

Tables II-1, II-2, and II-3 summarize the utilization data. (More extensive logs of water transfer, temperatures, and times have been accumulated, as well as a continuous record of all temperatures.) The column headings are the percentages of theoretical water transferred in the time limitations of the automatic cycles.

TABLE II-1

CYCLING RECORD FOR UNIT I
(Sheet 1 of 2)

Cycle	Dehydration (% in 44 min)	Hydration (% in 14 min)
1	>95	>95
2	>95	>95
3	>95	>95
4	>95	>95
5	>95	~95
6	>95	~95
7	>95	~95
8	100	100
26	100	-
27	95	100
48	92	100
119	-	88
165	91 (vac)*	100
166	100	88
188	96	94
212	95	82
281	- (vac)	-
288	100	91
353	- (vac)	100
354	100	100
381	-	91
382	84	-
449	-	48
450	45	-
496	51	-
521	-	32
522	32	-
616	-	30
617	- (vac)	94
618	-	100
641	-	95
642	82	82
669	76	76
689	-	59
712	60	72†
784	-	52
815	-	56
832	-	31
956	-	25

TABLE II-1

CYCLING RECORD FOR UNIT I
(Sheet 2 of 2)

Cycle	Dehydration (% in 44 min)	Hydration (% in 14 min)
1000	-	39
1001	39	39§
1002	73	88
1003	87	-
1023	-	63
1055	-	64
1119	-	61
1148	-	57§
1149	85	65**
1150	-	66
1151	66	100
1167	89	89
1171	-	85

*(vac) indicates that a 5 to 15 s evacuation was applied near the end of dehydration

†Tapping the reactor after about 7 min of hydration with very little water transfer initiated vigorous boiling

§Cold evacuation — 10 s with reactant and water reservoir below 50°C

**Generator tube malfunction; temperature was only 88°C. Corrected prior to Hydration 1151.

TABLE II-2

CYCLING RECORD FOR UNIT II

Cycle	Dehydration (% in 44 min)	Hydration (% in 14 min)
1	-	100
2	100	-
3	44 (vac)*	100
4	100	100
5	100	100
6	100	100
7	100	-
8	100	100
26	100	100
47	100	100
119	51	30
141	34	34
165	58 (vac)	100
166	100	78
188	95	60
212	26	26
213	26	26
287	- (vac)	100
288	100	100
353	- (vac)	69†
354	94	100
381	-	100
382	100	-
449	-	76
450	75	-
496	73	-
501	81	-
521	-	63
522	56	-
616	-	61
618	74	-
641	-	84§
642	45	44
669	31	78§
670	-	68
689	-	36
690	36	81§
784	-	66
815	-	32
832	-	44
833	40	48
837	-	29

*(vac) indicates that a 5 to 15 s evacuation was applied near the end of dehydration

†100% in 40 min

§Tapping the reactor after about 7 min of hydration with very little water transfer initiated vigorous boiling

TABLE II-3

CYCLING RECORD FOR UNIT III

Cycle	Dehydration (% in 44 min)	Hydration (% in 14 min)
1	88 (vac)*	98
2	90 (vac)	100
3	100 (vac)	75
4	69 (vac)	71
5	63 (vac)	100
6	100	92
22	-	100
23	100	100
25	-	98
26	100	-
27	94	-
47	-	66
49	- (vac)	-
50	96	98
54	-	88
119	71 (vac) (tightened head)	99
143	-	94
172	-	60
191	- (vac)	56
192	76	72
216	-	83
287	-	51
288	- (vac)	100
289	100	-
317	-	79
335	-	65
459	44	-
480	-	41
482	-	40†
483	93	93
484	93	93

*(vac) indicates that a 5 to 15 s evacuation was applied near the end of dehydration.

†Cold evacuation — 10 s with reactant and water reservoir below 50°C

As seen in all three tables, gradual activity loss occurred with time. Quick evacuation of the systems near the end of a dehydration half-cycle, as mentioned, invariably restored activity.

Two of the most plausible reasons for the observed activity recovery by evacuation are:

1) A general, gradual "sintering" action occurs, causing the material to develop into a less permeable "plaster." Evacuation during heated dehydration causes residual water to erupt and creates fissures in the bed, or even in individual agglomerates of crystallites, facilitating subsequent water transport.
2) The presence of noncondensibles retards either the hydration or dehydration steps, or both. In either case, the noncondensibles will diffuse to the zone of importance (i.e., to the reactor on hydration or to the condenser on dehydration), causing a decrease in the overall rate. During hydration, noncondensibles will lower the partial pressure of H_2O at the reacting surface. During dehydration, the noncondensibles will accumulate in the condenser; again, the partial pressure of H_2O is lowered and, in this case, leads to condensation rate control of the process. That is, the dewpoint can be lowered to the extent that the heat dissipation rate to the external atmosphere at the condenser controls the process.

The evacuations applied near the end of the dehydration half-cycles may have worked to overcome both resistance effects listed above. For instance, it was observed that during the "hot" evacuations, reactant temperature dropped, sometimes as much as $75^{o}C$ during the 15-s bursts, indicating very rapid decomposition of a considerable amount of residual $Ca(OH)_2$. Invariably, a sharp increase in the rate of condensation simultaneously occurred in the receiver tube in the remaining portion of the dehydration half-cycle after these evacuations. It could not be certain, however, whether (1) the water was locked up in impervious plaster or large crystallites, or (2) noncondensibles had simply inhibited transfer of water to the condenser, keeping the reactant predominantly

in the hydroxide state. In either case, the evidence inferred that the apparent degradation was related to incomplete dehydration steps. It may well be that on the hydration half-cycles, the water utilization was close to stoichiometric for the available amount of CaO.

It was considered that a meaningful test to assist in discriminating between the two possible mechanisms listed previously would be to evacuate the system under conditions such that $Ca(OH)_2$ decomposition would not occur to any appreciable extent. To accomplish this, Unit III was evacuated for 15 s after the entire system (except for the head-fitting heater) was cooled below 50°C. The unit was evacuated following a hydration half-cycle.

As seen in Table II-3, hydration in Cycle 482 immediately before the evacuation corresponded to only 40% of theoretical water. As noted before, this amount of water may well have been stoichiometrically complete for the available CaO (the remainder was already in hydroxide form). In Cycles 483 and 484, the water utilization was sharply improved. Unit III was shut down with the material in this active state.

The cold evacuation technique was again tested with Unit I, which had degraded to 39% (of theoretical) utilization (Cycle 1001). As seen in Table II-1, significant recovery again occurred. It may be inferred that the accumulation of noncondensibles plays the more significant role in the degradation of the systems.

Unit II was shut down with the material in the "degraded" state for subsequent characterization. Prior to shutdown, a sample of the gas in the glass envelope was obtained and analyzed by gas chromatography. Table II-4 lists the analysis obtained.

The $N_2/(O_2 + Ar)$ ratio, 4.1, is reasonably close to atmospheric conditions (3.6). The slight discrepancy easily can be associated with differences in in-leakage diffusion rates (e.g., argon versus nitrogen) or the consumption of oxygen (e.g., oxidation of the heater coils or reactor walls). The CO_2/N_2

TABLE II-4

GAS ANALYSIS FROM UNIT II

Species	Vol % (or ppm) (Dry Basis)
N_2	60.6
O_2/Ar	14.7
CH_4	0.3
CO_2	0.2
C_2H_6	(200)
C_3H_8	(100)
H_2	24.2

ratio is about ten times that in the atmosphere. It is not known if CO_2 continued to be evolved from the sample for the 800+ cycles, was a product of oxidation of the hydrocarbons present, or came from another source.

On Cycle 1148, Unit I was rejuvenated from low utilization using the "cold" evacuation technique. In this case, however, activity did not recover immediately. It was subsequently found that the steam generator heater was not operating at the normal temperature level (88^{o} compared with 110^{o}C). After readjusting the Variac controller, 100% utilization was achieved and remained above 85% until shutdown. Unit I was shut down after 1171 cycles.

During the evacuation step on Cycle 1148, a sample of the gas in the glass envelope was analyzed to determine if H_2 was present as discovered in Unit II. Table II-5 summarizes the dry gas analysis.

The fraction of H_2 in the noncondensible gases was about twice that found in Unit II. Methane and CO_2 levels were about the same. In Unit I, no hydrocarbons higher than C_1 were found. The O_2 level in Unit I was very much lower than in Unit II.

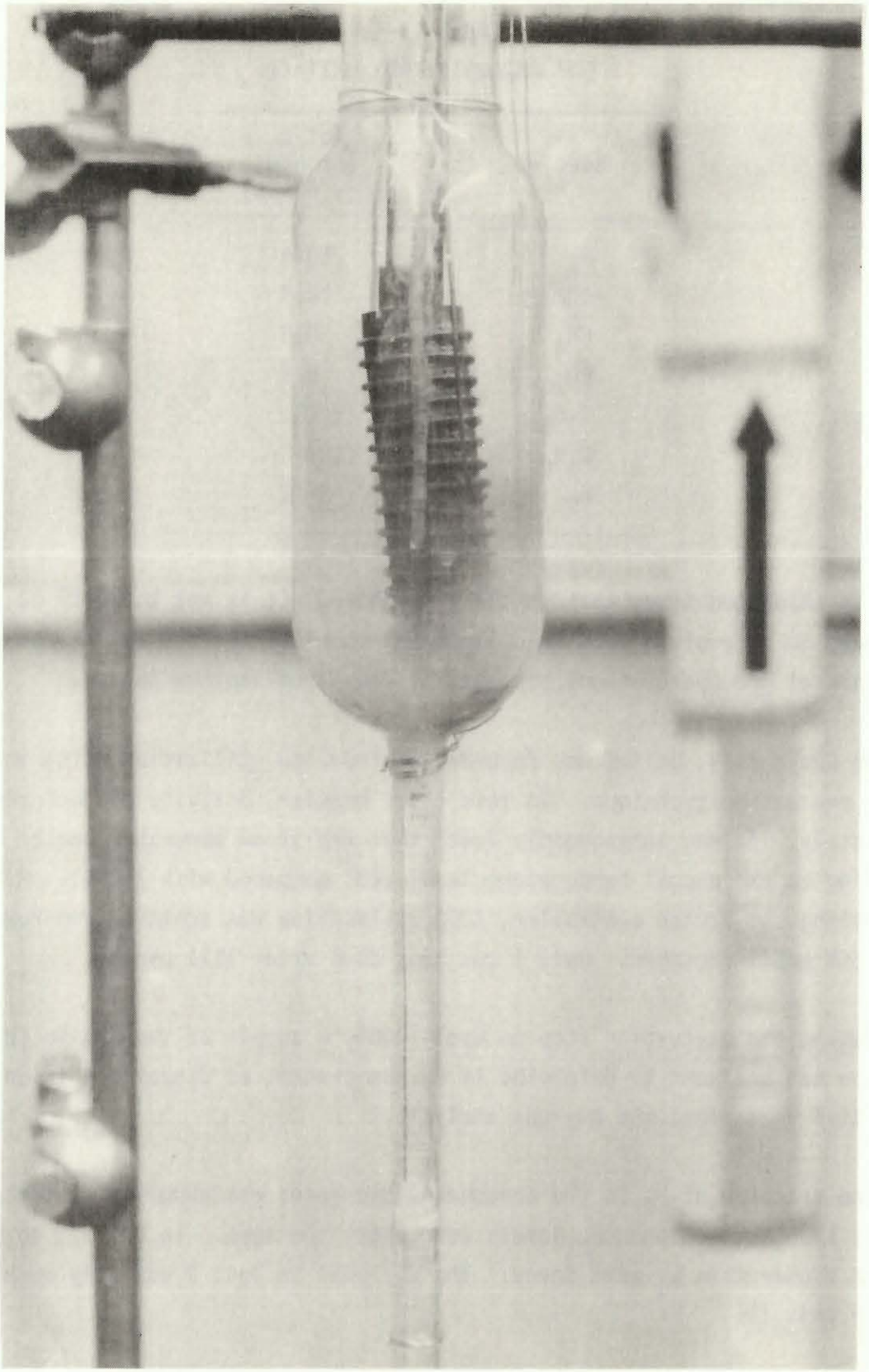

Figure II-8. Post-Test Appearance of Unit I

40443-12

TABLE II-5

GAS ANALYSIS FROM UNIT I

Species	Vol % (Dry Basis)
H_2	49.8
N_2	47.8
O_2 + Ar	1.6
CO_2	0.4
CH_4	0.4

The following figures show the general appearance of each unit at shutdown.

Figures II-8 and II-9 are views of the reactor-envelope assembly for Units I and II, respectively. Notice the cocked attitude of the reactor in Unit I. Discoloration in Unit I in the lower portion of the glass envelope was dark, resembling a deposited metal film. Also present were granules of white material adhering to the walls. A precipitate was present on the walls and in the bottom of the volumetric condenser tube. In Unit II (Figure II-9), the material deposited in the tube and in the larger diameter portion of the envelope was white. This material was probably deposited in the upper locations, after having fallen from the reactor, by being blown out of the generator tube during more violent boiling periods in hydration half-cycles.

Figure II-10, showing Unit III, reveals no deposits or precipitates.

Figure II-11 is a photograph taken through the window of the glovebox during disassembly of Unit I. Notice the extreme distortion to the left of the inner retaining screen. Figures II-12, II-13, and II-14 are sketches of the three reactor assemblies at shutdown, indicating the distortion of the screens and the disposition of the material.

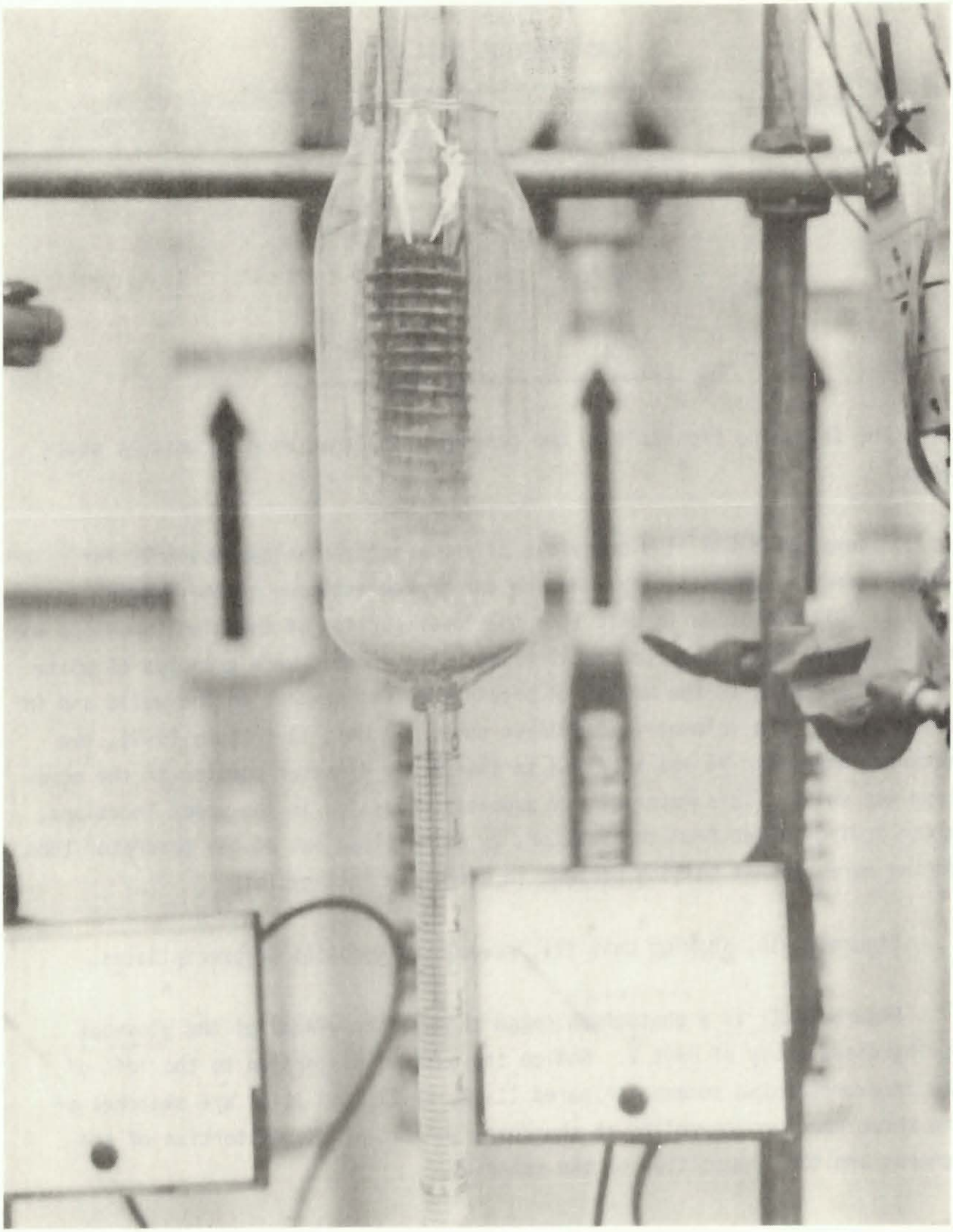

40443-10

Figure II-9. Post-Test Appearance of Unit II

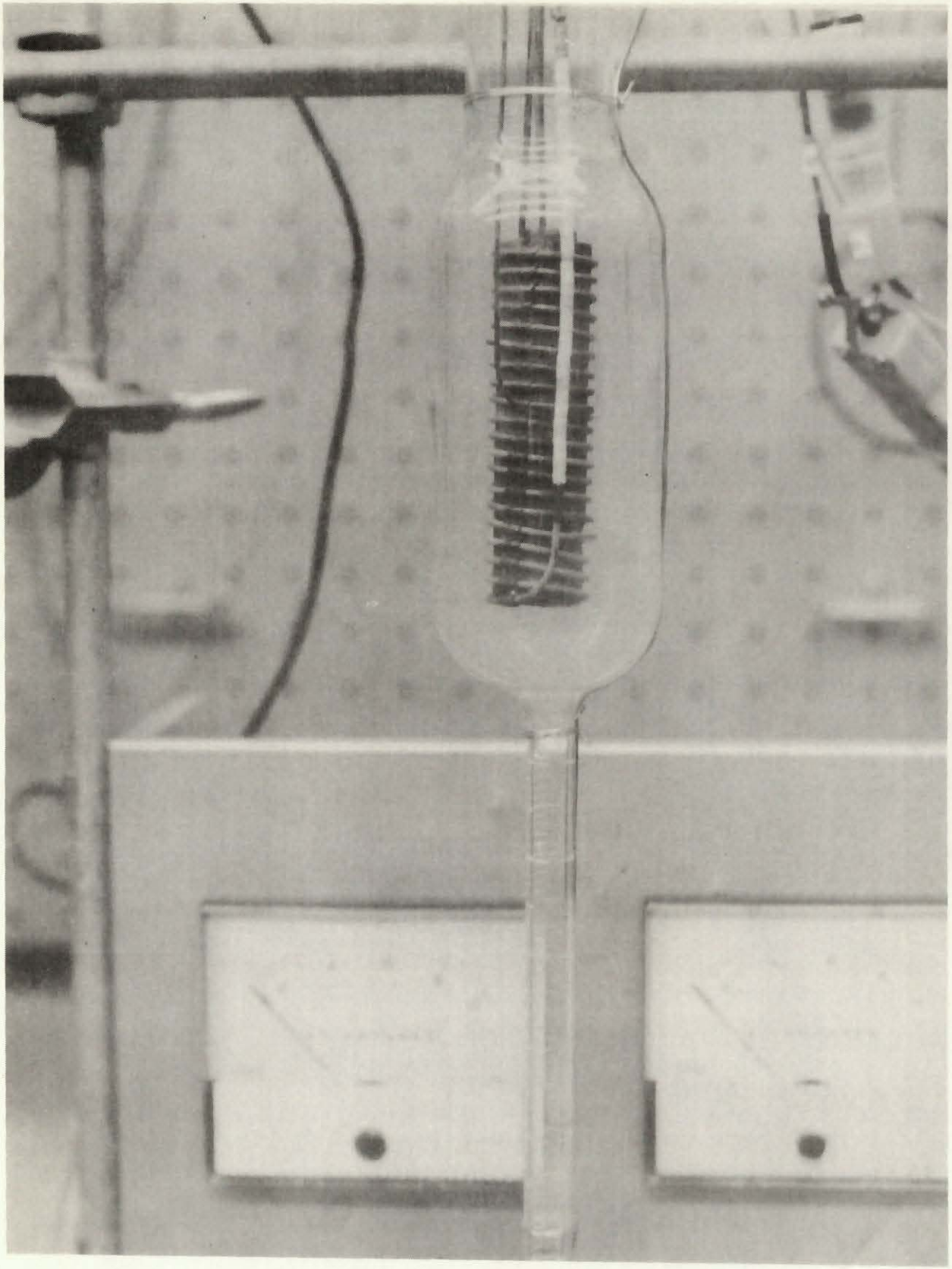

Figure II-10. Post-Test Appearance of Unit III

40443-11

Figure II-11. View of Distorted Retainer Screen in Unit I Reactor

40443-2

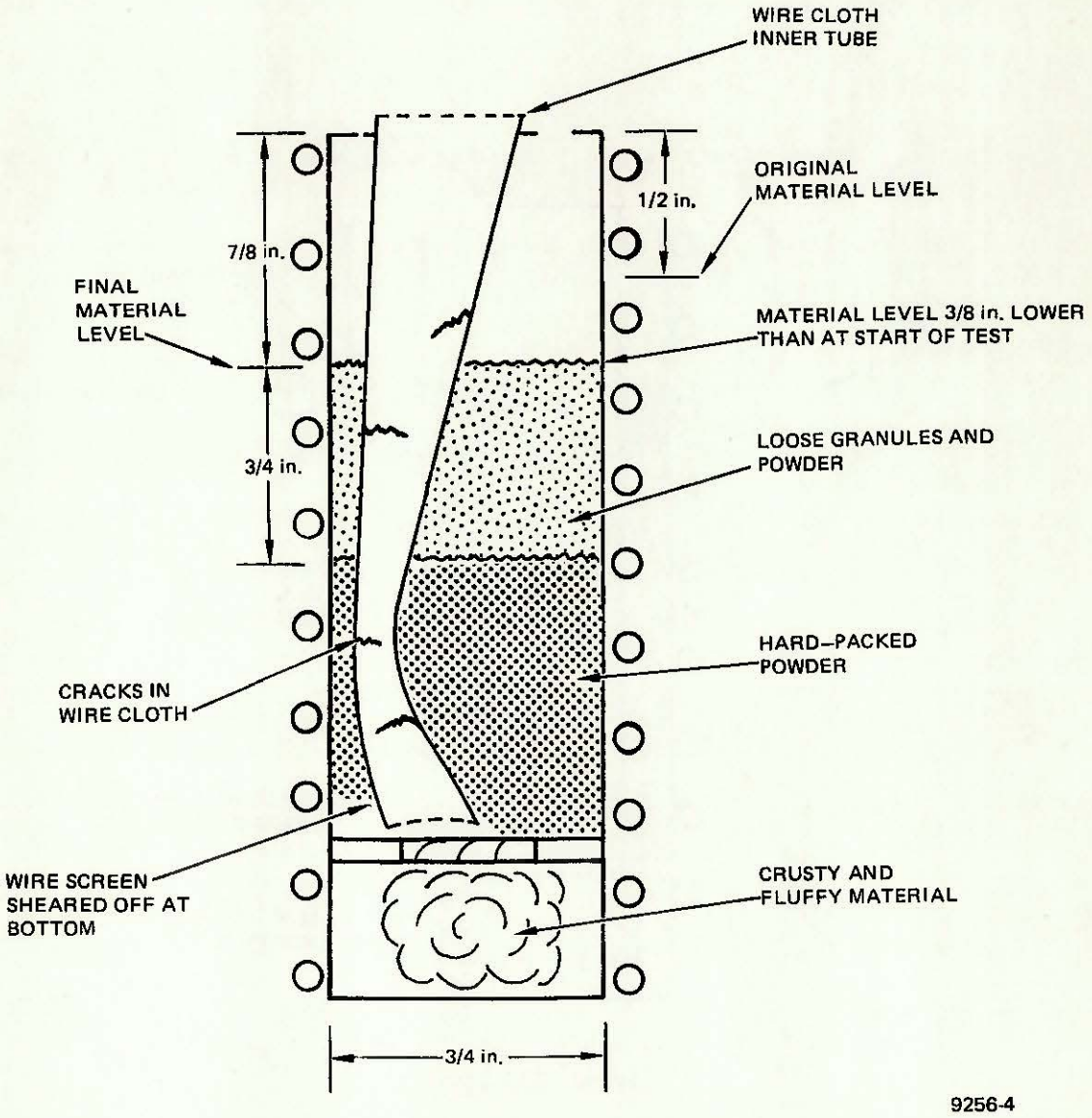

Figure II-12. Sketch of Unit I Reactor at Shutdown (After 1171 cycles)

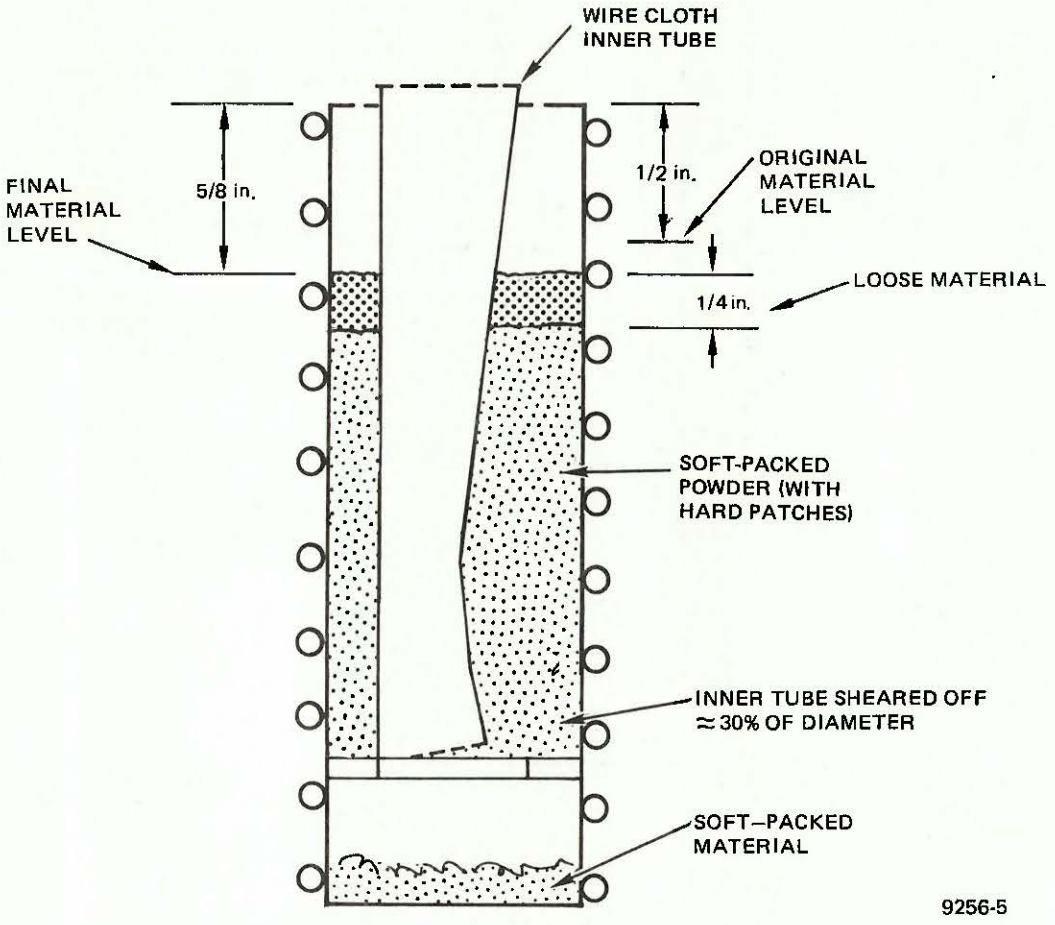

Figure II-13. Sketch of Unit II Reactor at Shutdown (After 837 cycles)

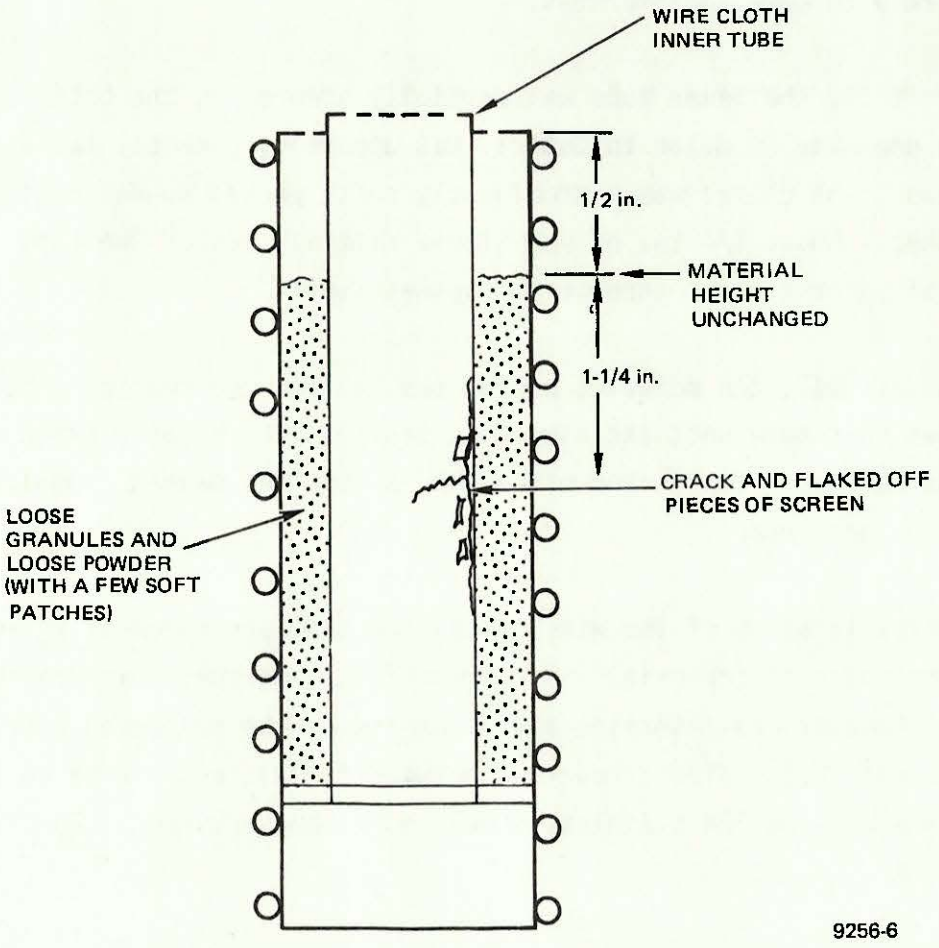

Figure II-14. Sketch of Unit III Reactor at Shutdown (After 489 cycles)

With Unit I, the inner screen was pushed to one side and almost pinched shut. Several cracks were apparent in the wire cloth, and the entire screen was sheared from the bottom "washer"-shaped floor. Considerable material had fallen through the floor opening and was also present inside the wire-cloth tube. The upper level of material was about 3/8 in. lower than at the start. The material in the bottom was a mixture of fluffy powder and "crusty" flakes. The lower half of the charge and the upper layer of material were in loose powder form with some agglomerates.

In Unit II, the inner tube was partially sheared at the bottom. A pinched effect to one side, similar to Unit I, was apparent, probably having just begun at shutdown. The charge was predominantly soft, packed powder containing a few hard patches. About 1/4 in. of very loose material was at the top. A small quantity of material fell through the washer floor.

With Unit III, the material poured easily from the reactor except for a few patches that were soft and dislodged easily. There was a crack in the screen, as well as a few flaked-off segments, but the welded connection to the washer floor was intact.

The deterioration of the wire screen and the appearance of H_2 in the cell suggest some type of corrosion. A thorough metallographic examination has not been made, however, to determine the mechanism of the suspected corrosion. It is conceivable that a direct reaction between $Ca(OH)_2$ and one or more of the constituents of Type 304 stainless steel could have occurred. For instance, the reaction

$$2\ Cr + 3\ Ca(OH)_2 \longrightarrow Cr_2O_3 + 3\ CaO + 3\ H_2$$

has a free energy on the order of -70 kcal/mole (Cr_2O_3) in the 425 to 525°C range. A similar reaction of Fe to Fe_2O_3 has a small positive ΔG at low temperatures, becoming negative above about 525°C.

3. Conclusions

1) $Ca(OH)_2$ can be cycled repeatedly to oxide form and rehydrated at least 1000 times, while still maintaining utilization of H_2O of 85% or better.
2) Apparent losses of activity in the present tests were undoubtedly related to inert gas buildup in the "dead-end" type of reaction system used. The inert gases apparently prevented rapid condensation of water during dehydration and possibly blanketed the oxide surface on hydration. It is not expected that presence of minor amounts of inert gases will seriously affect a moving solids type of reactor.
3) Careful consideration should be given to the methods and materials of containment of the charge in a fixed-bed reactor in view of the severe distortion of parts of the reactor, as well as the apparent corrosion.

B. CALORIMETRY AND KINETICS

In previous studies, only global hydration and dehydration rate expressions representative of the individual reactors employed had been developed for oxide-hydroxide systems. Attempts to utilize these expressions as intrinsic surface rate expressions were not successful, suggesting that mass and/or heat transfer limitations influenced the original kinetic experiments.[II-3]

For proper process design of heterogeneous reaction systems, it is essential that intrinsic surface reaction rate expressions be developed in order to provide a data base for fully evaluating thermal or mass transfer limitations. In many cases, it is found that similar transport restraints exist at all levels of application (e.g., heat transfer always controls from laboratory experiment to full scale), obviating the necessity for precise chemical kinetic information for design use. However, the realization that such chemical kinetics data are not necessary for design usually follows from a fundamental analysis in which either the intrinsic surface rate expression is available, or it

is analytically well established that mass or heat transfer must control the type of process in question.

In the present case ($CaO - Ca(OH)_2$), it was realized (see above) that some kinetic restraints existed even in early, small-scale, scoping studies; however, the actual rate-limiting step was not known. Thus, it was desirable that an experimental study be carried out to develop intrinsic rate expressions for the dehydration and hydration steps.

Typically, two approaches are frequently used to provide intrinsic kinetic expressions for heterogeneous processes. In one case, the reaction is studied in relatively simple systems to provide a global rate expression and a series of conversion-experimental condition data. Then, the laboratory experiment itself is modeled, incorporating fundamental relationships for mass (e.g., bulk and intraparticle diffusion) and heat transfer. Various assumed mechanistically possible or empirical intrinsic rate expressions are combined with the fundamental transport relationships to calculate conversion for comparison with (and eventual minimization of deviation from) the experimental conversions. This approach is frequently used for heterogeneous catalysis studies.(II-4 - II-7)

A second approach used for the development of intrinsic rate expressions is to design the experiments such that mass and heat transfer limitations are negligible. This approach, of course, involves considerably less data manipulation, but the design of and the carrying out of the experiment itself may be quite complex. Such an approach for the $CaO - Ca(OH)_2$ system, based on previous work, would seem to involve the following requirements:

1) Intimate contact of the maximum amount of the solid reagent with heat transfer surfaces
2) Minimum reactant bed thickness
3) Very small particle size (to minimize intraparticle diffusion effects)
4) Maximum area for contact with the bulk gaseous phase

5) A convenient means for determining the extent of conversion when only a very small quantity (as implied by requirements 1 through 4) of reactant is used.

Differential scanning calorimetry (DSC) was seen to be a potentially powerful technique for studying heterogeneous reactions (fulfilling requirements 1 through 5) and for the possible direct determination of intrinsic reaction kinetics. In the following sections, a brief description of DSC and its potential application in the current project is given, followed by the results obtained to date by the Energy Systems Group of Rockwell International in adapting DSC for kinetic study of the CaO - $Ca(OH)_2$ system. At the publication time of this report, the DSC has been successfully used for the determination of the heat of dehydration of $Ca(OH)_2$, for the determination of the activation energy for dehydration into an inert atmosphere, and for the preliminary establishment of the mechanism of solid phase change.

1. Differential Scanning Calorimetry

Differential scanning calorimetry is a thermal analysis method in which the dependent variable observed at a given time or temperature is the differential heat flow into or out of a sample relative to an inert reference material. In practice, a small sample of test material (0.5 to 100 mg) and the reference are subjected to a specific temperature program (either isothermal or variable as a known function of time). The differential heat flux (recorded as millicalories per second) is continuously monitored, and at points of either endothermic or exothermic activity in the sample, deviations from the baseline for zero differential heat flux occur. The area under the curve of differential heat flux (from departure-from to return-to baseline) on a time abscissa is directly proportional to the quantity of heat absorbed or rejected.

Typically, DSC has been widely used to determine specific heats, heats of phase changes, thermal and oxidative stability, curing phenomena with resins, and a variety of other thermal and chemical properties. Since the area under a thermal activity curve is directly related to the heat involved, DSC can be used for purity determination; for instance, for a melting endotherm of an

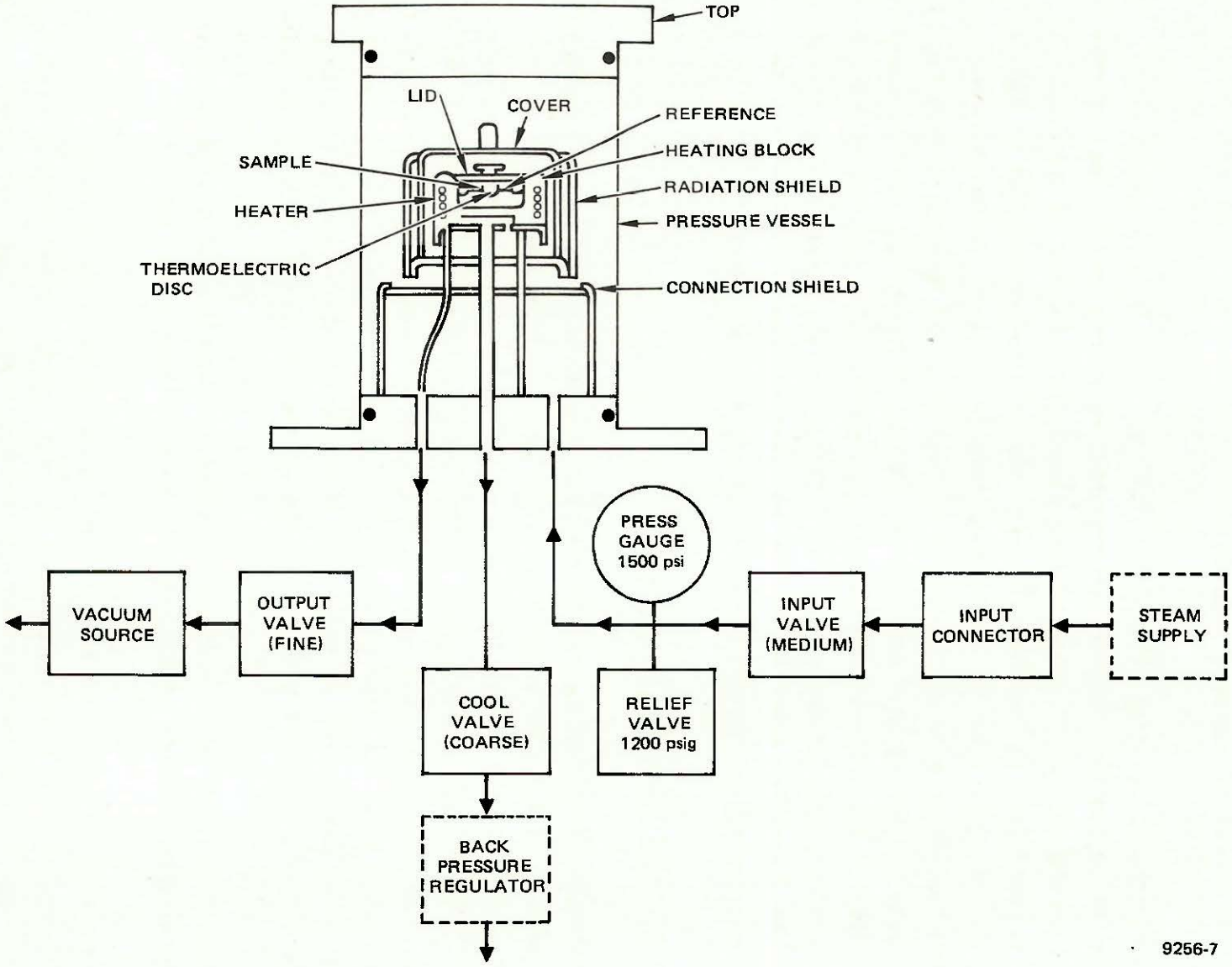

Figure II-15. Block Diagram of PDSC Cell

alloy, the heat absorbed can be compared with the theoretical amount for the pure parent metal. Similarly, for a chemical reaction, the heat evolved or absorbed can be used to determine initial purity of a given weight of sample. Knowing initial and final sample weights, the actual heat of the reaction may be determined. Finally, and constituting the most useful property of DSC for kinetic work, the percentage conversion at any time can be determined by taking partial areas under the thermal curve (up to various times into the reaction). Details of the methods of processing such DSC data will be given in a later section.

2. Equipment and Procedure

A duPont 990 thermal analyzer equipped with a pressure differential scanning calorimeter (PDSC) cell was used in this phase of the study. The PDSC cell was selected rather than a standard DSC cell because of the capability to maintain preselected pressures from 0.01 torr to 1000 psig in the cell. In addition, the duPont PDSC cell is mounted on a small satellite base and the cell and base can be detached from the main base and enclosed in an oven to maintain any desired ambient temperature around the cell (up to about $125^{o}C$, as initially recommended by the manufacturer).

This latter capability was a very important feature in the development of the present test plan. By flowing steam through the cell at pressures up to slightly over 1 atm, the elevated ambient temperature would prevent condensation in the cell, thus enabling kinetic studies of both dehydration and hydration. Figure II-15 is a sketch of the PDSC cell.

An outline of the steps in the overall test plan for the development and use of the PDSC for determination of heat effects and reaction kinetics is as follows:

1) Heat of reaction by direct measurement
2) Equilibrium constant and vapor pressure of $CaO - Ca(OH)_2$ as functions of temperature
3) Dehydration kinetics in inert atmosphere

a) Activation energy
b) Solid phase mechanism

4) Dehydration kinetics in steam atmosphere
5) Hydration kinetics in steam atmosphere

In all tests conducted to date, reagent-grade $Ca(OH)_2$ was used (see Section II-C for material characterization). Approximately 2.8 mg of the hydroxide was used in each run. Samples were contained in a hermetically sealed pan with a pinhole in the lid (~0.002 in. diam).

3. Results and Discussion

The PDSC cell was calibrated in both the "normal" (constant amplifier gain) and the "DSC-calibrated" (constant cell coefficient) modes over the temperature range of 50 to 600°C, using the heats of fusion of indium, tin, and zinc, and the specific heat of sapphire. The calibration was conducted at various pressure levels (in N_2) from 0.1 to 2 atm.

a. Heat of Reaction by Direct Measurement

The heat of a reaction is calculated using the following formula:

$$\Delta H = \frac{A}{M} (60\ BEq) \qquad ...(1)$$

where

ΔH = heat of reaction (mcal/mg)
A = area of peak ($in.^2$)
M = sample mass (mg)
B = time base setting (min/in.)
E = PDSC cell calibration coefficient (calculated from Equation 1 using a suitable material with a known ΔH of reaction or phase change)
q = Y-axis sensitivity (mcal/s-in.)

Samples of $Ca(OH)_2$ were dehydrated in N_2 atmospheres at 302, 540, and 831 mm Hg abs. A hermetic pan with a pinhole lid was used to retard loss of water into the water-free atmosphere until the equilibrium temperature was approached. Figure II-16 is a typical PDSC record for decomposition at 540 mm.

Practice has shown that extrapolation of the linear leading edge of the endothermic peak (dotted line in Figure II-16) to the baseline is representative of the equilibrium temperature. Notice that a portion of the area under the peak is to the left of the extrapolation, indicating some loss of water by diffusion through the pinhole. For the run depicted in the figure, the intercept with the baseline is at 505°C (pens are offset about 0.15 in. for clearance), as indicated by the simultaneous temperature (emf) curve. This temperature is in agreement with published JANAF[II-8] data for equilibrium at 540 mm Hg.

The areas under the endothermic peaks were determined planimetrically for use with Equation 1. Table II-6 summarizes ΔH measurements conducted at the three pressures. The observed values for ΔH were corrected for actual weight loss (actual conversion of $Ca(OH)_2$) after deducting the known amount of free moisture (~0.7% – see Section II-C for characterization of sample $Ca(OH)_2$) that was driven off of the samples by holding the PDSC isothermally for a period at 150°C. Agreement with values for ΔH were within 10% of the JANAF data; the agreement was excellent under nonvacuum conditions, indicating possible loss of sensitivity at the lower pressures.

TABLE II-6
HEAT EFFECT DETERMINATION WITH PDSC

Pressure (mm Hg)	Observed Temp. (°C)	Theor. Temp. (°C)	Observed ΔH (cal/gm)	Theor. ΔH (cal/gm)	% of Theor. ΔH*	Wt Loss (%)	% of Theor. Wt Loss
302	470	474	281	324	93	22.54	93.5
540	505	505	293	322	91	24.31	101
831	528	528	313	321	99	23.67	98.2

*Corrected for actual weight loss and moisture content

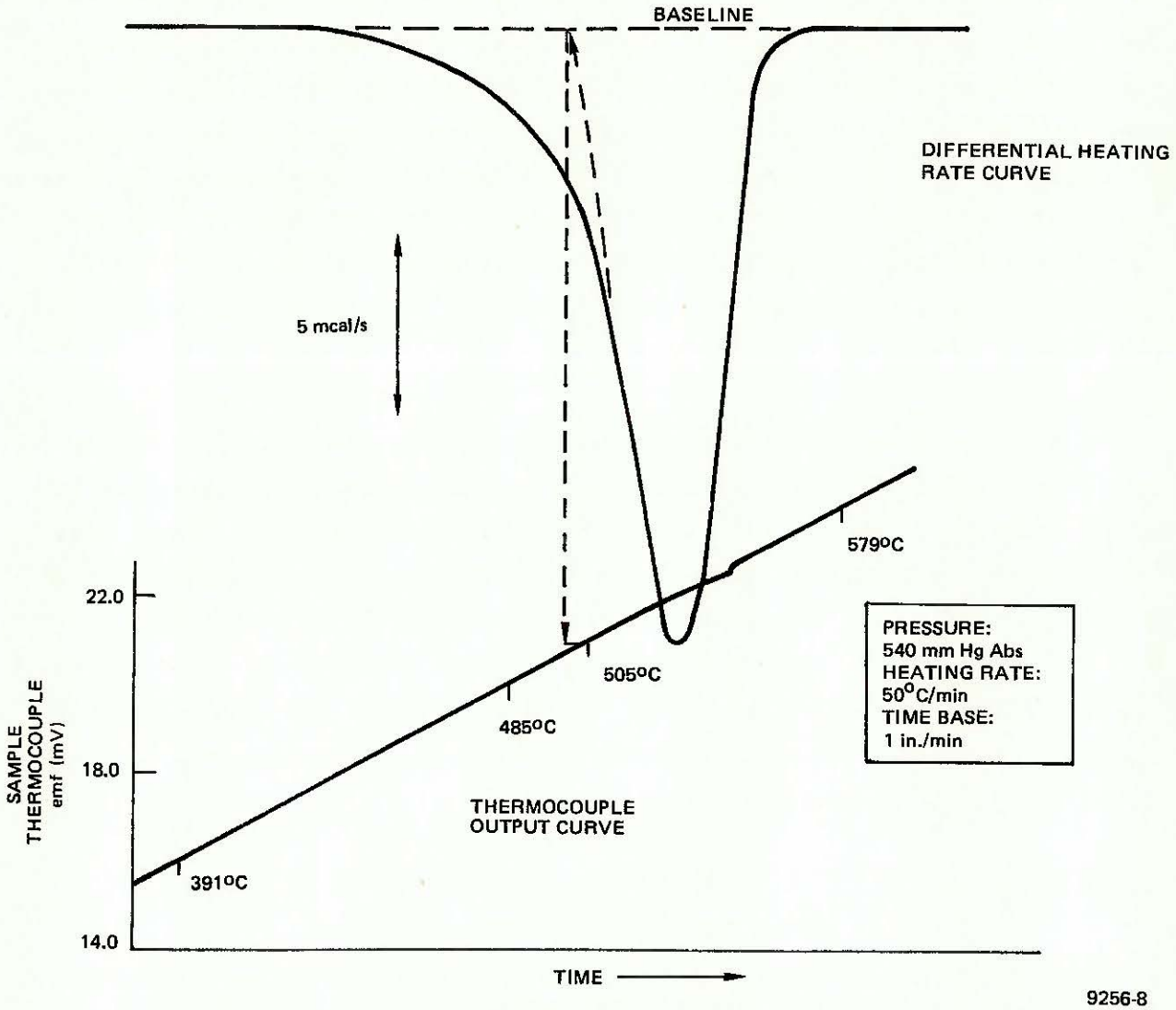

Figure II-16. Typical PDSC Record for Decomposition of $Ca(OH)_2$

b. Equilibrium Constant and Vapor Pressure of CaO - $Ca(OH)_2$ as Functions of Temperature

A series of runs was made at various pressures of N_2 ranging from 0.12 to 3.1 atm using the pinhole-lid technique mentioned earlier. Scan rate was $50^{o}C$/min in each test. The leading edges of the endothermic peaks were extrapolated to the baselines to give decomposition temperatures, as before. The data are shown in Figure II-17, along with a solid line representative of JANAF equilibrium data.

In general, the experimentally determined temperatures were within $5^{o}C$ of the JANAF data for corresponding pressures.

Since for the reaction

$$Ca(OH)_2 \longrightarrow CaO + H_2O,$$

the equilibrium constant is equivalent to the water vapor pressure (assuming unit activity for the solid phases and a perfect gas), the slope of the curve of Figure II-17 is $-\Delta H/R$, as indicated by the integrated form of the van't Hoff equation:

$$\ln K_p = -\Delta H/RT + C \qquad ...(2)$$

From the slope of the line, a value for ΔH of 23,770 cal/mole was obtained. Values for ΔH from the JANAF tables range from 23,215 to 24,139 cal/mole over the same temperature range.

c. Dehydration Kinetics in Inert Atmosphere

A series of tests of the decomposition of $Ca(OH)_2$ was made again in an inert atmosphere (N_2) to establish a kinetic data base for later, planned kinetic studies in steam atmospheres. In such a swept, water-free atmosphere, the dehydration rate at a given temperature is probably the maximum rate attainable. Both temperature-programmed and isothermal runs were made. The basis

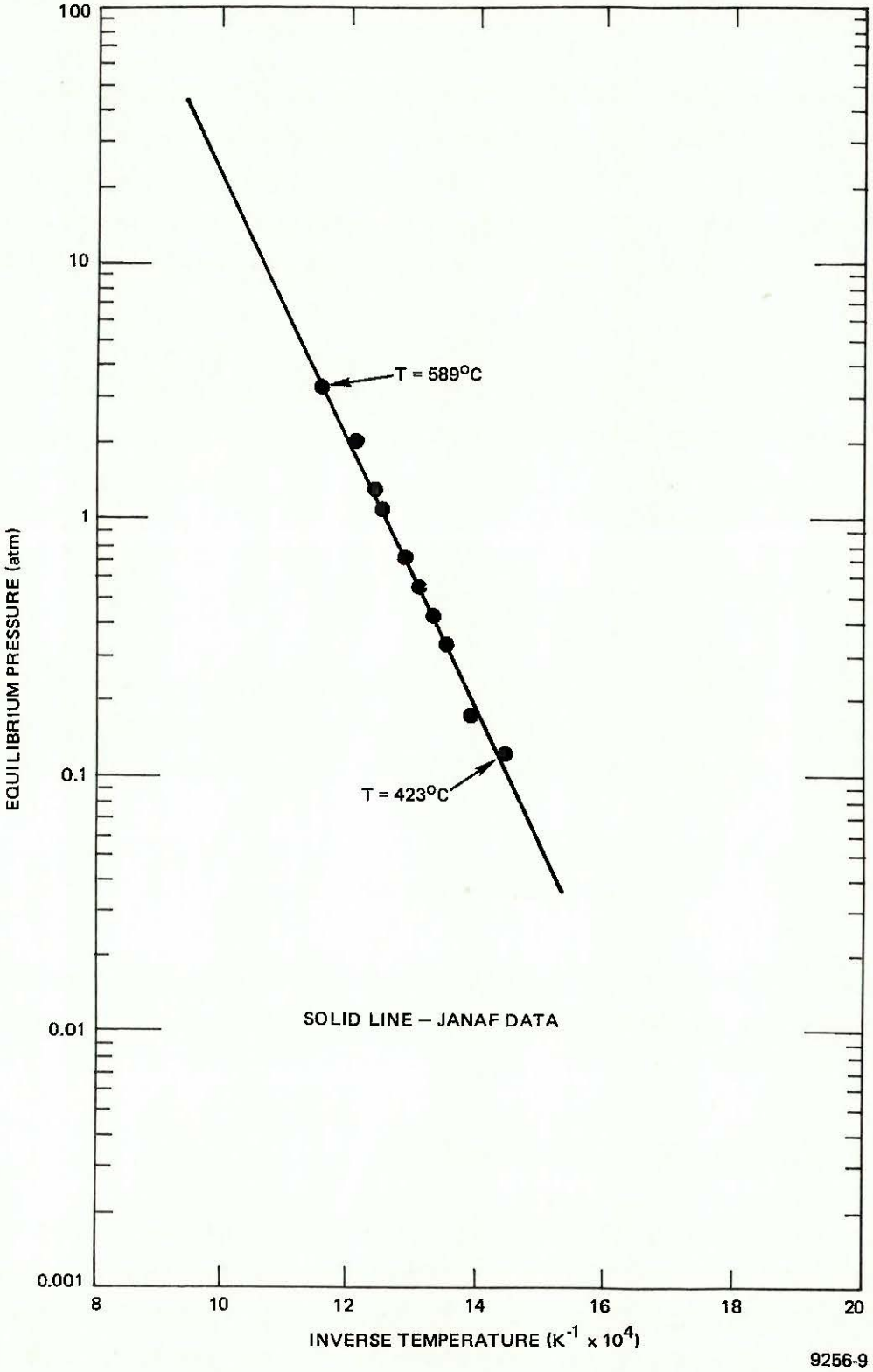

Figure II-17. Vapor Pressure - Temperature Relationship for $Ca(OH)_2$

for the experimental procedure of and the data analysis for the linear-temperature scan tests follows.

It is assumed that the rate of conversion of a solid reactant can be represented by

$$\frac{d\alpha}{dt} = kf(\alpha)g(p) \qquad ...(3)$$

where α is the fraction of material converted, k is a temperature-dependent rate constant, and $f(\alpha)$ and $g(p)$ are temperature-independent functions of conversion and external driving force terms, respectively. The latter term is written, for the present development, as a general function of pressure (possibly involving total pressure, partial pressure, and the equilibrium vapor pressure of the $CaO - Ca(OH)_2$).

At a constant rate of heating, $\beta = dT/dt$, assuming $f(\alpha)$ and $g(p)$ are independent of temperature, Equation 3 may be integrated to obtain:

$$F(\alpha) = \frac{1}{g(p)} \int_0^{\alpha} \frac{d\alpha}{f(\alpha)} = \frac{1}{\beta} \int_{T_0}^{T} k \, dt = \emptyset \qquad ...(4)$$

where T is the temperature and T_0 is the initial temperature.

If k is assumed to follow the standard Arrhenius temperature dependency, it can be shown that

$$F(\alpha) = \emptyset = \frac{A}{\beta} \int_{T_0}^{T} \exp\,(-E/RT)\, dT$$

$$= \frac{AE}{\beta R} \left\{ -\frac{e^x}{x} + \int_{-\infty}^{x} \frac{e^x}{x}\, dx \right\} = \frac{AE}{\beta R}\, p(x), \qquad ...(5)$$

where $x = -E/RT$.

The function $P(x)$ has been tabulated for limited ranges and has been approximated by various expansions.[II-9] A good approximation is given by Doyle:[II-10]

$$\log P(x) = -2.315 + 0.457\,x \qquad \ldots(6)$$

For $-20 \geq x \geq -60$, Equation 6 is accurate to ±3%. Substituting Equation 6 into Equation 5 and taking common logarithms,

$$\log F(\alpha) = \log \frac{AE}{R} - \log \beta - 2.315 - 0.457\,\frac{E}{RT} \qquad \ldots(7)$$

Then at constant conversion levels (i.e., for $F(\alpha)$ = constant at each α) for several heating rates, a plot of log α versus 1/T (inverse temperature at which the reference α occurs) should have a slope of

$$\frac{d \log \beta}{d(1/T)} = -0.457\,E/R \qquad \ldots(8)$$

or

$$E = -4.35\,\frac{d \log \beta}{d(1/T)} \quad (\alpha = \text{constant}) \qquad \ldots(9)$$

A series of $Ca(OH_2)$ decomposition runs was made in the PDSC, using a flowing N_2 cover gas at 835 mm Hg abs, and at heating rates of 5, 10, 20, 50, and 100°C/min.

Typical PDSC data were in the form of bell-shaped curves of the differential heating rate (between sample and reference) versus time. The curves were similar to the example given in Figure II-16. A second pen recorded sample temperature emf. The area under the curve (up to a given temperature) divided by the total area is the fraction converted, α.

A computer program was developed to determine percentage conversion as a function of time using displacement from the PDSC recorder baseline as the dependent variable. The derived conversion curves were all sigmoid in shape, indicating an accelerating rate at the beginning of the reaction. Mikhail, et al.,[II-11] attribute the early accelerating rate to the combination of lateral spread of the reaction interface from isolated nuclei at the surface combined with radially inward movement. Eventually, there is only radial inward movement of the interface.

Figure II-18 is a plot of log β versus 1/T, which shows good linearity for heating rates above 10^{o}C/min. It is not clear why the data for a 5^{o}C/min heating rate appear to be displaced to higher temperatures. Typically, such nonlinearity occurs at the higher heating rates, at which point thermal lags begin to be apparent (i.e., actual temperature is slightly lower than the measured temperature). The values for activation energy at the various levels of conversion are:

Conversion (%)	E (kcal/mole)
80	34.1
50	35.1
30	36.8
20	37.0
10	37.7

A slight trend toward decreasing activation energy is indicated as conversion nears completion, but the deviation may be within experimental error.

For gas-solid reactions proceeding radially inward, if there is no resistance to gas transport through the product layer, the residual fraction is related to time, t, for equiaxed particles by:[II-11]

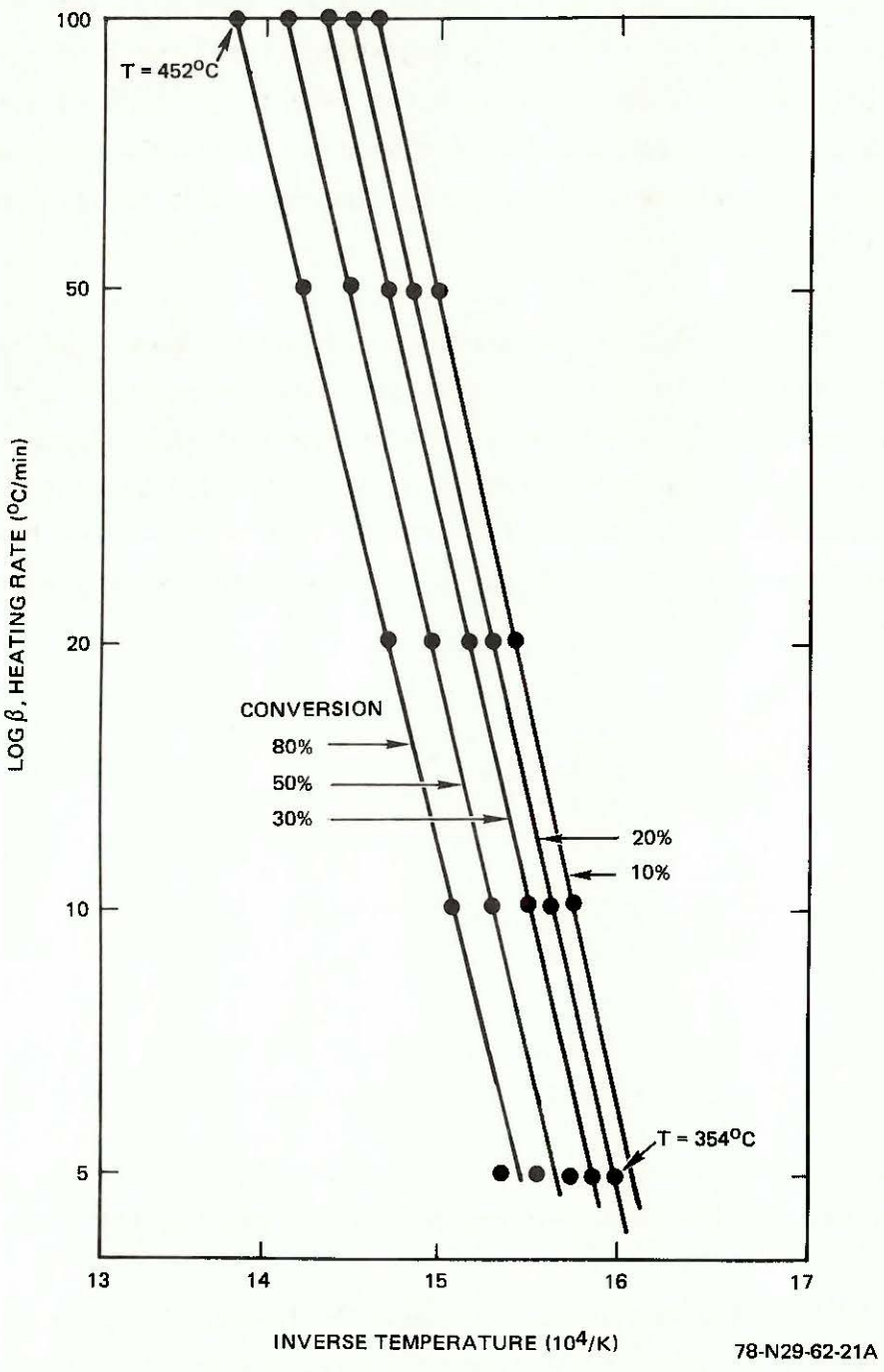

Figure II-18. Heating Rate - Temperature Correlation for $Ca(OH)_2$ Decomposition

$$\left[\frac{w}{w_o}\right]^{(1-m)/3} = 1 - kt \qquad \ldots(10)$$

where w_o is initial weight. The residual fraction is, of course, related to conversion, α, by:

$$\alpha = 1 - w/w_o \qquad \ldots(11)$$

The constant, m, is included in Equation 10, as suggested in Reference II-11, to account for possible nonconstant movement of the reaction front as a function of radius, r:

$$-\frac{dr}{dt} = k'r^m \qquad \ldots(12)$$

Consequently,

$$\frac{dw}{dt} = Cr^2 \frac{dr}{dt} \qquad \ldots(13)$$

where C is a constant. By simple geometric consideration:

$$\frac{dw}{dt} = -k'w^{(2+m)/3} \qquad \ldots(14)$$

which integrates to Equation 10 as given.

For a gas-solid reaction following a general shrinking core mechanism, a plot of the left-hand side of Equation 10 versus t should be a straight line, provided that the proper value for m is selected. For the classical shrinking core model for an equiaxed particle, the inward radial velocity is constant (m = 0). Thus, a plot of $(w/w_o)^{1/3}$ (or $(1 - \alpha)^{1/3}$, $1 - (1 - \alpha)^{1/3}$, etc.) should be a straight line with a slope whose absolute value is equal to k.

In Reference II-11, the authors reported that an exponent of 1/3 was not applicable, and that an exponent of 1/4 ($\frac{1 - m}{3} = \frac{1}{4}$) was needed to provide a linear plot for decomposition of $Ca(OH)_2$ into vacuum. An order less than 1/3

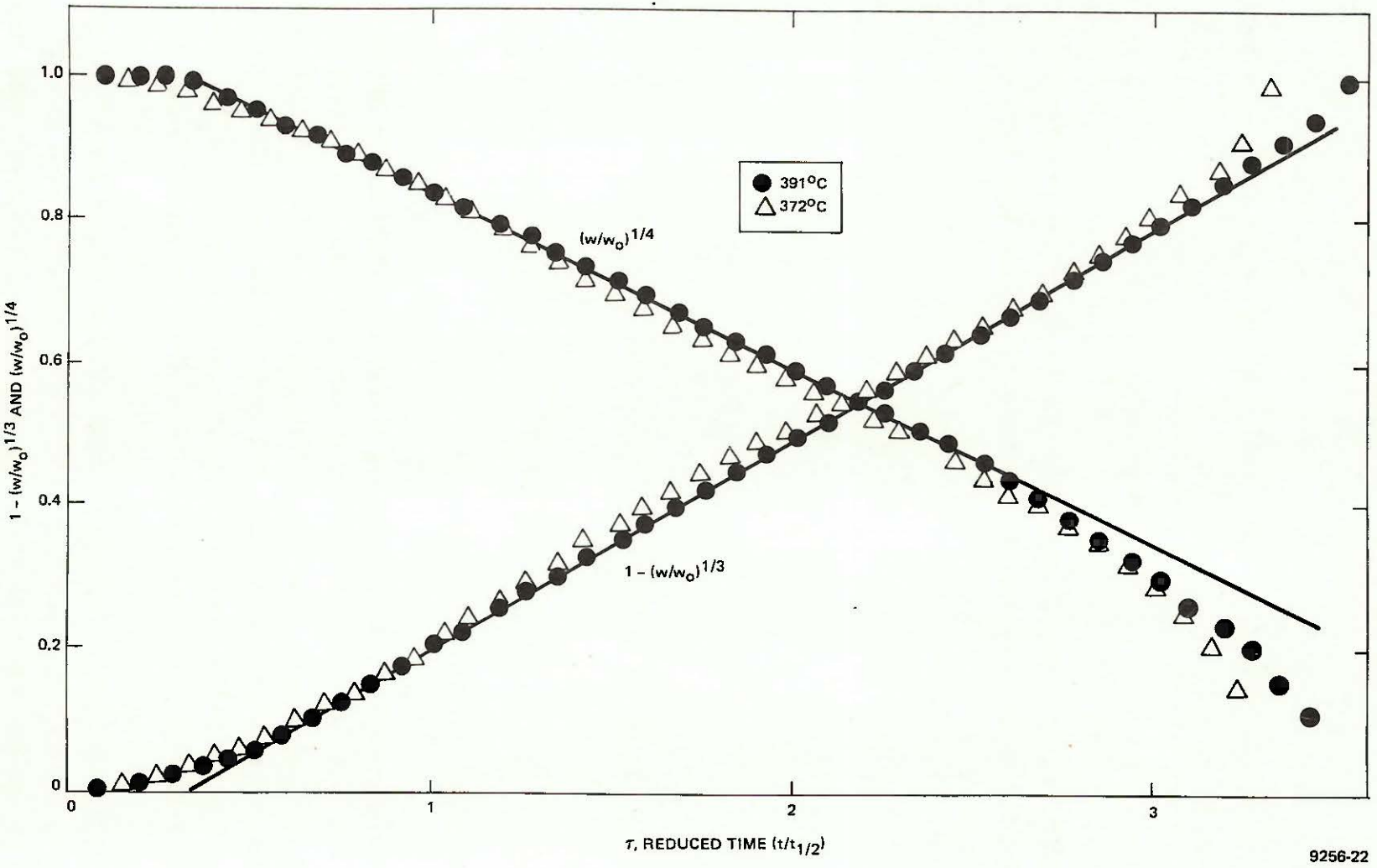

Figure II-19. Linearized Isotherms for Decomposition of $Ca(OH)_2$

is impossible for a constant radial velocity. Thus, the constant, m, in Equation 12 was 0.25 in the referenced work, indicating a decreasing inward velocity during the reaction.

A test of the mechanism could not be applied to the nonisothermal runs used earlier to obtain E. It was found, however, that the PDSC could be heated rapidly and held constant in a limited range of temperatures in which measurable reaction rates could be followed and in which the calorimeter was able to equilibrate before significant reaction occurred. This temperature band was from about 365 to 400°C.

Figure II-19 is a plot, for runs at 391 and 372°C, of the functions, $1 - (\frac{w}{w_o})^{1/3}$ and $(w/w_o)^{1/4}$, versus reduced time, τ, which is defined as:

$$\tau = t/t_{1/2} \qquad \ldots(15)$$

where $t_{1/2}$ is time to 50% conversion. The reduced time parameter is used to normalize the plots. It can be seen that the present data follow a linear relationship with time for a somewhat longer period for the 1/3 exponent than for the 1/4 exponent, although both show linearity beyond 90% conversion (to 99% with the 1/3 exponent and to 94% with the 1/4 exponent). For the data taken, it is not necessary to postulate a diminishing velocity during the reaction, and a constant-velocity, shrinking-core model fits well.

Strong downward concavity should be evident in a curve of $1 - (w/w_o)^{1/3}$ versus τ if there is appreciable resistance to gas movement through the CaO mantle. Thus, it appears in the present case that the CaO does not impede water movement.

The data from the isothermal runs can be used to provide a cross-check of the activation energy determined in the temperature scans. Note that for a reaction following the mechanism given in Equation 10, when $w/w_o = 0.5$ (i.e., at $\tau = 1$),

$$(0.5)^{(1-m)/3} = 1 - kt_{1/2} = \text{Constant} \qquad \ldots(16)$$

or

$$k = \frac{1 - (0.5)^{(1-m)/3}}{t_{1/2}} = \frac{\text{Constant}}{t_{1/2}} \qquad \ldots(17)$$

If the Arrhenius dependence of k with T is followed,

$$\ln (\text{Constant}) + \ln 1/t_{1/2} = \ln A - E/RT \qquad \ldots(18)$$

Thus, a plot of the logarithm of the "half-life" versus 1/T should give a straight line of slope, E/R. Such a plot for runs at 367, 372, and 391°C gave a straight line with an indicated activation energy of 37.8 kcal/mole, indicating good agreement with the nonisothermal approach.

It is of interest that the energy of activation is definitely higher than the endothermic heat of reaction as would be expected for a single-step reaction. In Reference II-11, it was postulated that the decomposition must occur by a two-step reaction (viz)

$$Ca(OH)_2 \longrightarrow CaO \cdot H_2O \text{ and}$$

$$CaO \cdot H_2O \longrightarrow CaO + H_2O(g),$$

in view of the low apparent activation energy measured (~14 kcal/mole and, thus, much lower than the heat of reaction). In the referenced work, the materials used were rather large single crystals of pure $Ca(OH)_2$; while in the present study, very thin layers (weighing about 2.8 mg) of $Ca(OH)_2$ powder of 1.8-μm diameter were used. In addition, a "hard" vacuum was applied in the work of Reference II-11, while a sweeping N_2 cover gas was used in this work.

In a recent study by Fujii and Tsuchiya,[II-12] an activation energy of 32 kcal was found for dehydration at temperatures of 500°C and less into air. At higher temperatures, however, the data indicated a trend toward lower activation energy. Under vacuum (10 mm Hg abs.) an activation energy of about 18 kcal/mole is indicated from the Japanese data. Relatively large samples were used by Fujii.

In an earlier study, Dave and Chopra[11-13] found that the activation energy varied from 45 kcal/mole for 18 to 20 U.S. mesh samples to 38.5 kcal/mole for 240 to 270 mesh samples. Precipitated $Ca(OH)_2$ had an activation energy of 36.5 kcal/mole, and lime hydrated at atmospheric pressure and 295 psi had activation energies of 35.2 and 36.7 kcal/mole, respectively. Only 1-g samples were used in the latter work, using thermogravimetric analysis for kinetic evaluation. In this study as well as in the present project, dehydration kinetics were performed at or near atmospheric pressure.

It is obvious that the apparently simple reaction of the dehydration of hydrated lime is still not well understood. The apparent effect of total pressure, in some studies, as opposed to obtaining equivalently low partial pressures of water vapor by sweeping the sample chamber with dry, inert gas has yet to be resolved. It is felt that the scale of the current study, involving 2 to 3 mg of finely divided sample, represents potentially the closest approach to date to the kinetic measurement of $Ca(OH)_2$ dehydration devoid of heat transfer control and effects of intraparticle diffusion. It remains to be determined if the apparent difference in activation energies obtained by maintaining low H_2O partial pressure by either evacuation or inert gas exchange is related to bulk diffusion effects.

d. Dehydration Kinetics in Steam Atmospheres

This task, as well as the subsequent planned series, "Hydration Kinetics in Steam Atmospheres," was not completed within the short time frame of this project. Modification of the PDSC cell by the manufacturer to correct some deficiencies discovered during initial scoping runs with the cell at 125°C and containing an atmosphere of steam were still under way at the close of the project.

In short, the problems found were that various parts of the cell had to be upgraded to accept the 125°C ambient temperature. These parts included valve packings and stems and insulation of some of the internal wiring. It is not surprising that, for such a unique application in such a severe environment,

the capabilities of the original cell were not fully understood by either Rockwell or the manufacturer. The efforts by duPont to upgrade the cell to meet the present requirements are gratefully acknowledged.*

4. Conclusions

1) Differential scanning calorimetry is an effective means for determining the heat of reaction of CaO + H_2O, either directly or through the use of equilibrium considerations.
2) Direct measurement gave a heat of reaction within 10% of published (JANAF) values.
3) Equilibrium constants were determined to be in excellent agreement with published values. For given pressures, the equilibrium temperatures were within 5°C of JANAF data.
4) The activation energy for decomposition of $Ca(OH)_2$ into an inert atmosphere was on the order of 34 to 38 kcal/mole, in agreement with at least two independent works.
5) A search of the literature has shown that for decomposition into a vacuum, the activation energy may be considerably smaller. It is not known at present if a mechanism change exists between high vacuum and atmospheric pressure conditions.
6) The solid phase appears to follow a shrinking core mechanism, at least for the very small particles employed in this study. No hinderance by the CaO mantle to the passage of H_2O seems to exist.

C. MATERIALS CHARACTERIZATION

The purpose of this task was to determine specific chemical and physical properties of material used in the various experimental studies. Such

*The cell has been rebuilt and has been operated under Rockwell funding for over 100 h at 125°C ambient temperature. The next phase of checkout will be runs with live steam in the cell. Successful completion of this phase will enable continuation of the development of intrinsic rate expressions for both hydration and dehydration.

characterization studies were made on each starting material and, where possible, the material removed from the system at the end of the test. The data obtained in the characterization studies then provided a potential means for relating performance (e.g., utilization in the cycling tests) with the various chemical and physical properties.

1. Experimental Procedure

The following characterization tests and the procedures used in each are described below.

a. Chemical Analyses

Analyses for Si, Al, Ca, Mg, Fe, Ni, and Cr were made by atomic absorption spectrophotometry. Sulfur was determined as sulfate by gravimetric, barium precipitation methods. Free water was determined by weight loss on heating at $110^{o}C$. Carbon dioxide was determined by absorption in Ascarite of gases evolved on acidification of the sample. Chemical (hydrate) water was determined by weight loss on ignition (at $900^{o}C$), correcting for CO_2 content, as determined above.

b. Surface Area and Particle Size

The surface area of samples was determined using a Micromeritics surface area analyzer, which uses the single point BET method. The average particle size of powdered samples was measured using a Fischer Subsieve Sizer.

c. Gas Evolution on Heating

In addition to the gas-phase analyses performed on two of the fixed-bed cycling systems at about the time these units were shut down, a sample of the starting material used in the cycling tests was heated in a small, stainless steel (Type 304) pipe bomb, and a sample of the gases evolved was analyzed by gas chromatography.

TABLE II-7

CHEMICAL ANALYSIS OF STARTING MATERIALS

Constituent	Concentration [wt % (or ppm)]			
	Reagent Bottle 1	"Stored" Reagent Bottle 1*	Reagent Bottle 2	"Aged" Reagent Bottle 2†
CO_2	0.60	1.09	0.76	0.78
H_2O (free)	0.70	1.04	0.68	1.19
H_2O (combined)	23.40	N.A.§	22.03	N.A.
Si	0.22	N.A.	0.25	N.A.
Mg	0.29	N.A.	0.43	N.A.
Fe	(420)	N.A.	(400)	N.A.
Ni	(37)	N.A.	(65)	N.A.
Cr	(27)	N.A.	(50)	N.A.
Al	(448)	N.A.	N.A.	N.A.
S	N.D.**	N.D.	N.D.	N.D.
Ca	N.A.	47.76	50.77	46.50

*Bottle 1 was stored in a desiccator about 2 months over Drierite with house vacuum maintained at all times

†A sample from Bottle 2 was exposed to air in a shallow pan for 2 h

§N.A. = not analyzed

**N.D. = none detected

d. ESCA and SEM Studies

Electron spectroscopy for chemical analyses (ESCA) and scanning electron microscopy (SEM) were used to determine surface elements and morphological properties of fresh, reagent $Ca(OH)_2$ and $Ca(OH)_2$ cycled 5 and 11 times. This work was conducted at the Rockwell International Science Center. Cycling was accomplished in a small glass reactor fitted with fritted glass discs to retain the sample. The reactor had to be cut apart for partial sample removal after five cycles; thus, total exclusion of air was not possible. Some chemical analyses were performed on the final (11 cycles) material.

In all tests described in Sections II-A and II-B, the starting material was reagent $Ca(OH)_2$ taken from two bottles of J. T. Baker Lot 608363, analytical-grade $Ca(OH)_2$. The material from Bottle 1 was also used in the ESCA and SEM studies described above, and the material from Bottle 2 was used in all PDSC studies.

2. Results and Discussion

a. Chemical Analyses

Table II-7 summarizes chemical analyses of starting materials taken from the two supply bottles. Also shown are analyses for the material in Bottle 1 stored for 2 months over Drierite under house vacuum, and a sample from Bottle 2 purposely exposed to the air for 2 h in a shallow pan. The purpose of the latter test was to determine the extent of H_2O and CO_2 pickup that is possible during, for example, the cycling rig-loading sequence.

It can be seen that the exposed sample picked up some free water but did not show an appreciable change in CO_2 content, indicating that short-term exposure to air was acceptable for typical loading operations in the various experiments. The "stored" reagent picked up a small amount of water and CO_2.

Table II-8 summarizes measurements for cycled materials, comprising the materials from Units I, II, and III, the 11-cycle study made at the Science

TABLE II-8

ANALYSIS OF CYCLED MATERIALS

Constituent	Concentration [wt % (or ppm)]				
	6 Cycles in Unit I*	11 Cycles At Science Center†	Unit I (1171 cycles)*	Unit II (837 cycles)*	Unit III (484 cycles)†
CO_2	1.84	5.50	5.02	0.65	3.54
H_2O (free)	0.70	0.93	Nil	Nil	Nil
H_2O (combined)	21.37	19.72	18.08	22.95	20.46
Si	0.28	0.45	0.31	0.32	0.24
Mg	0.49	0.41	0.30	0.25	0.27
Fe	(491)	(685)	(730)	(870)	(540)
Ni	(67)	(55)	(184)	(157)	(107)
Cr	(50)	(50)	(59)	(100)	(38)
Al	N.A.§	N.A.	(560)	(1,800)	(530)
S	N.D.**	N.D.	N.D.	N.D.	N.D.

*Starting material was from Bottle 1, Lot 608363, Baker analytical-grade $Ca(OH)_2$, shortly after opening

†Starting material was from Bottle 2, same Baker lot, immediately after opening

§N.A. = not analyzed

**N.D. = not detected

Center, and the short 6-cycle test. It can be seen in comparison with data of Table II-7 that all cycled materials exhibited an increase in CO_2 content. The increase was quite large for material cycled in Units I and III and at the Science Center.

The material from the three fixed-bed units showed increases in Fe, Cr, and Ni, probably because of the incorporation of corrosion products of the metal parts. No explanation for the sharp indicated increase in aluminum in the Unit II sample can be given; the amount reported is probably in error.

Table II-9 summarizes the probable material composition, based on the elemental CO_2 and H_2O analyses, and compares typical starting $Ca(OH)_2$ with samples withdrawn from the three cycling units. It was assumed for material balance calculations that the CO_2 was present as $CaCO_3$ and that the trace metals were as their most stable oxides.

The amounts of $Ca(OH)_2$ shown as "equivalent $Ca(OH)_2$" in Table II-9 are calculated from the measured amount of combined H_2O available after deducting a portion for Mg (assumed to be present as $Mg(OH)_2$). Note that for the three cycled samples, the sums of the equivalent $Ca(OH)_2$ and the contaminant amount (subtotal) are not as close to 100% as for the reagent $Ca(OH)_2$. In the case of the reagent $Ca(OH)_2$, it is likely that only a very small portion of the CO_2 was not removed during the loss in weight determination at the minimum 900°C firing temperature. Thus, in subtracting CO_2, as determined by acidic evolution and absorption in Ascarite, from the measured ignition weight loss, the chemical water value tends to be only slightly low.

It was found, however, that the muffle furnace used for the ignition weight loss, with samples from Units I, II, and III, had stabilized at only 750°C (instead of 900°C or higher). In these cases, considerable CO_2 was undoubtedly retained in the sample. Thus, weight loss less the known CO_2 quantity would result in low indicated chemical water concentrations. A material balance on the ignition process shows that if the $Ca(OH)_2$ values at the bottom of the table (as calculated by difference) are correct, only between 35 and 50% of the

TABLE II-9

CONTAMINANT CONTENTS AND MATERIAL COMPOSITIONS

Contaminant	Starting Material (Reagent $Ca(OH)_2$, wt %)	Cycled Materials		
		Unit I (wt %)	Unit II (wt %)	Unit III (wt %)
$CaCO_3$	1.36	11.41	1.48	8.05
H_2O (moisture)	0.70	0	0	0
SiO_2	0.47	0.66	0.68	0.51
$Mg(OH)_2$	0.69	0.72	0.60	0.65
Fe_2O_3	0.06	0.10	0.12	0.08
NiO	0.00	0.02	0.02	0.01
Cr_2O_3	0.00	0.01	0.01	0.01
Al_2O_3	0.08	0.11	0.34	0.10
Subtotal*	3.36	13.03	3.25	9.41
Constituent				
Combined H_2O†	23.40	18.08	22.95	20.46
H_2O in $Mg(OH)_2$	0.21	0.22	0.19	0.20
H_2O for $Ca(OH)_2$	23.19	17.86	22.76	20.26
Equivalent $Ca(OH)_2$	95.44	73.50	93.67	83.38
$Ca(OH)_2$ + Subtotal	98.80	86.53	96.92	92.79
$Ca(OH)_2$ by difference (100% ≅ Subtotal)*	96.64	86.97	96.75	90.59

*Subtotal of measured contaminants

†By ignition loss less CO_2 content determined by acidic evolution of CO_2 and gravimetric absorption in Ascarite

CO_2 evolved on ignition with Samples I and III. It is therefore assumed that the $Ca(OH)_2$, determined by difference, is the more accurate figure for the cycled materials.

It is recalled that Units I and III were shut down in an active state, and Unit II was shut down with low utilization. Final utilizations reported for Units I and II were 85% and 93%, respectively. By using the Table II-9 calculated amounts for $Ca(OH)_2$ by difference, the theoretical water amounts available for Units I and III were only 90% and 94%, respectively, of the water transferred at the start of cycling. Thus, utilization of water by available lime in Units I and III (94% and 99%, respectively) is actually greater than reported in Section II-A-2. The reason is that the earlier values were based on initial $Ca(OH)_2$ present.

b. Surface Area and Particle Size

Table II-10 summarizes the specific surface area of reagent $Ca(OH)_2$, as well as areas for partially and nearly totally dehydrated samples.

TABLE II-10

SURFACE AREA OF $Ca(OH)_2$ AND $Ca(OH)_2$ - CaO SAMPLES

Sample	Specific Surface Area (m^2/g)	Percentage Dehydrated*
$Ca(OH)_2$ (as received)	16.5	0
Dehydrated 30 min	26.0	4
Dehydrated 2-1/2 h	62.4	42
Dehydrated 56 h	91.2	96.5
$Ca(OH)_2$ heated to 400°C in closed tube	10.1	1.5

*Based on total initial weight and not corrected for actual $Ca(OH)_2$ content

TABLE II-11

SURFACE AREA AND PARTICLE SIZE MEASUREMENTS

Sample	Specific Surface* Area (m^2/g)	Average Particle† Size (μm)(at 44% theoretical density)
Feed Bottle 1 (new)	16.5	1.83
Feed Bottle 1 after§ 3-month storage	17.0	1.71
Feed Bottle 2**	16.9	1.65
Aged sample from Feed Bottle 2††	15.4	1.68
Material from Unit I (1171 cycles)	6.42	1.70
Material from Unit II (837 cycles)	5.33	2.68
Material from Unit III (484 cycles)	7.16	20.5
Material cycled six times	13.40	1.06

*Measured with a Micrometric Model 2200 Surface Area Analyzer
†Measured with a Fisher Subsieve Sizer
§Bottles 1 and 2 were from Lot 608363, J. T. Baker Analytical-Grade $Ca(OH)_2$. Storage of Sample 1 was under house vacuum. $Ca(OH)_2$ from Bottle 1 was used as the starting material for cycling Units I and II and recent PDSC studies and for the early ESCA, SEM, and cycling studies performed at the Science Center. Material from Bottle 2 was used with cycling Unit II and recent PDSC work.
**Sample from Bottle 2 when it was first opened
†† Open in shallow pan for 2 h

The dehydration operation was performed under vacuum (<1 mm Hg) at 400°C in the BET sample tubes (equilibrium pressure is about 46 mm Hg at 400°C). A sharp increase in surface area occurred as the dehydration continued. This result is consistent with earlier data that showed that samples of bonded $Mg(OH)_2$ underwent a sharp increase in porosity upon dehydration.

Since the samples had been thoroughly dried and degassed for the BET measurements, the final weight loss (96.5% of theoretical) is considered to be an accurate indication of minimum chemical water in the reagent material (0.2345 g H_2O/g material where 0.2430 g/g is theoretical). This figure agrees well with the percentage of $Ca(OH)_2$ determined by difference for the starting material (Table II-9).

The final entry in Table II-10 is for a sample heated overnight at 400°C in N_2 in a closed tube. The slight dehydration weight loss is the result of the combination of water vapor loss on venting the tube and a small amount of condensed water observed in the cooler regions at the top of the tube. The prolonged heating operation caused a 39% decrease in surface area of the $Ca(OH)_2$, possibly indicating crystal growth or sintering of the equilibrated sample.

Table II-11 summarizes surface area and particle size data for the feed materials and the materials cycled in the fixed-bed endurance studies. Also included are data for the material subjected to six cycles prior to switching to automatic operation.

It can be seen that storage of Bottle 1 under house vacuum caused an insignificant change in surface area and particle size and that the production lot is uniform with respect to these properties. The materials cycled in Units I, II, and III all exhibited a decrease in specific surface area. Units I and III were shut down with the material in active form (85% for Unit I and 93% for Unit III), and Unit II was shut down in inactive form (29%). With Units I and II, the decrease in surface area is primarily due to pore closure in view of the relatively small change in average particle size. For spherical

particles of 1.7 and 2.7 μm diameter with no internal pores, the geometric surface areas are theoretically calculated to be about 3.4 and 2.1 m^2/g, respectively, indicating that internal pore surface area had dropped from about 80% to about 50% of the total surface area.

A relatively large particle size was measured for the material from Unit III. With the sample from Unit III, the outer surface area of nonporous spherical particles of the indicated size is calculated to be only about 0.3 m^2/g, indicating that this sample had a considerably higher percentage of area attributed to internal pores (95% of the total) than the starting material (80%). It is more likely in this case that the 20-μm particles are agglomerates of basic particles similar in size to those from Units 1 and II with similar internal pore structure.

It appears, from the data for the six-cycle sample, that surface area starts to decrease early upon cycling. The particle size data also indicate particle breakdown. It is possible that this breakdown is followed by formation of agglomerates and by further refracturing, possibly in a cyclic fashion. The growth and fracturing may be related to the reactor structural failures noted with Units I and II.

c. Gas Evolution on Heating

The appearance of H_2 and hydrocarbons in the cycling reactors has been described earlier. As a part of the characterization studies, a much larger sample of $Ca(OH)_2$ was subjected to a single, extended dehydration to provide gases for analysis.

A 49-g sample of $Ca(OH)_2$ was heated to 550°C overnight in a helium atmosphere in a closed, Type 304 stainless steel tube fitted with an external, valved gas lock equipped with a silicone rubber septum. The sample was cooled to 350°C and vented in several steps to purge the sample lock. Hypodermic syringe samples were then withdrawn through the septum for analysis. Noncondensible gases evolved on heating were analyzed by gas chromatography

(molecular sieve 13X and Porapak Q columns). Species found in measurable quantity were hydrogen, argon and oxygen (not separated), nitrogen, carbon dioxide, methane, and water. Trace amounts of three additional species were found and were tentatively identified as acetylene, ethane, and propane. The calculated concentrations are given in Table II-12.

TABLE II-12
NONCONDENSIBLE GAS ANALYSES*

Component	Mole % (Dry Basis)
H_2	0.234
O_2/Ar	0.094
N_2	0.429
CO_2	0.084
CH_4	0.506

*Reactor at 350^{o} cooling ballistically with 30 psig at time of sampling.

The ratio of nitrogen to oxygen plus argon (4.56) is somewhat higher than in air (3.56), implying that if complete exclusion of air had not been accomplished (assume as a limiting case that all the oxygen can be ascribed to a leak or residual air), nitrogen may have been initially preferentially adsorbed. The ratio of CO_2 to O_2 (0.89) is about 400 times larger than in air, indicating strong evolution of CO_2 from the sample or combustion of some of the hydrocarbons.

The origin of hydrogen and the hydrocarbon species is not known, but it is suspected that, again, corrosion of the stainless steel parts occurred. It is shown later that ESCA determinations revealed the presence of both paraffinic and carbide carbon bonds, the latter disappearing as the material was repeatedly dehydrated and hydrated. The origin of the hydrocarbons may well have been during one of the $Ca(OH)_2$ production steps (e.g., furnace-roasting of limestone).

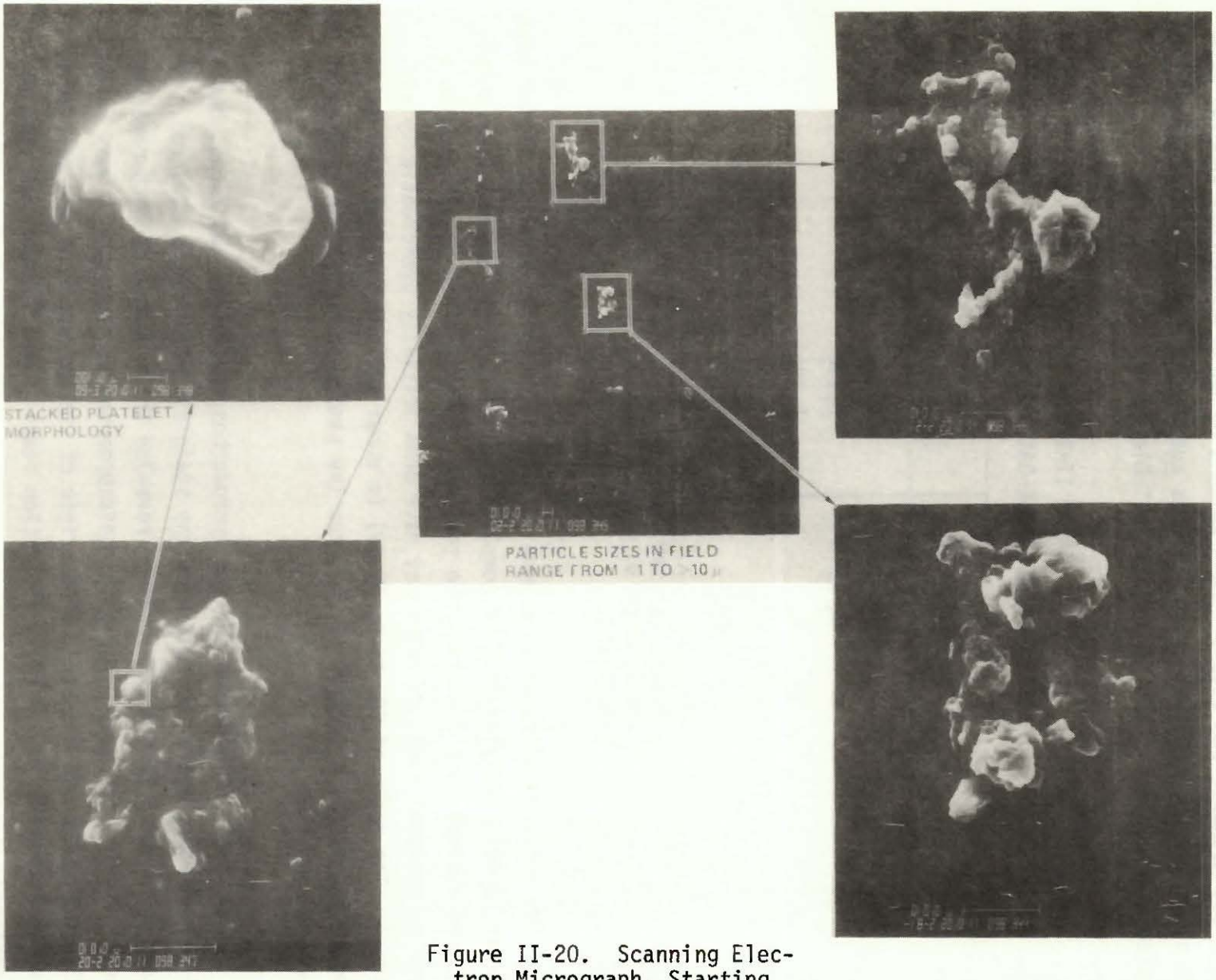

Figure II-20. Scanning Electron Micrograph, Starting $Ca(OH)_2$ Powder

9256-10

All of the components, if it is assumed that they were all irreversibly desorbed from the sample, amount to a total weight percentage of the original sample of only about 0.003%. Nevertheless, the consequences of the presence of the noncondensibles during hydration and dehydration in a fixed-bed reactor are significant. They total 1.35% (by volume) at 3 atm, corresponding to a total partial pressure of about 31 mm Hg. Thus, it is not surprising that repeated degassing of the cycling apparatus was necessary, particularly since it is unlikely that the materials are completely and irreversibly desorbed in a single heating operation.

d. ESCA and SEM Studies

Electron spectroscopy for chemical analysis (ESCA) has been used to determine surface elements in particles of reagent $Ca(OH)_2$. The records obtained showed the presence of very small amounts of carbide and carbonate carbon. The oxygen-to-calcium ratio was determined to be 2.03/1. ESCA was also applied to samples cycled for 5 and 11 times in a reaction tube fitted with fritted glass discs to retain the sample charge. Water utilization was 80% or better in the cycles. The surface analysis revealed the disappearance of carbide carbon and an increase in carbonate carbon with cycling. At the surface, the O/Ca ratio was 2.16 and 2.5 after 5 and 11 cycles, respectively. Air was not totally excluded from the apparatus; thus, the surface formation of $CaCO_3$ is not unexpected. The main intent of these material cycles was to prepare samples for morphological investigation using scanning electron microscopy (SEM).

Figure II-20 is a reproduction of several SEM photographs obtained with the reagent $Ca(OH)_2$. Many particles appear to be made up of stacked plates and are on the order of 5 μm in diameter. Many smaller pieces ($<2\,\mu$m), which appear to have been formed by fracture of the larger particles, as well as large agglomerates of the 5-μm structures, are present. In each case, a plate-like appearance with distinct angularity is visible.

A sponge-like particle, which was apparent in the SEM field after 11 cycles, was examined more closely (see right-hand photograph in Figure II-21).

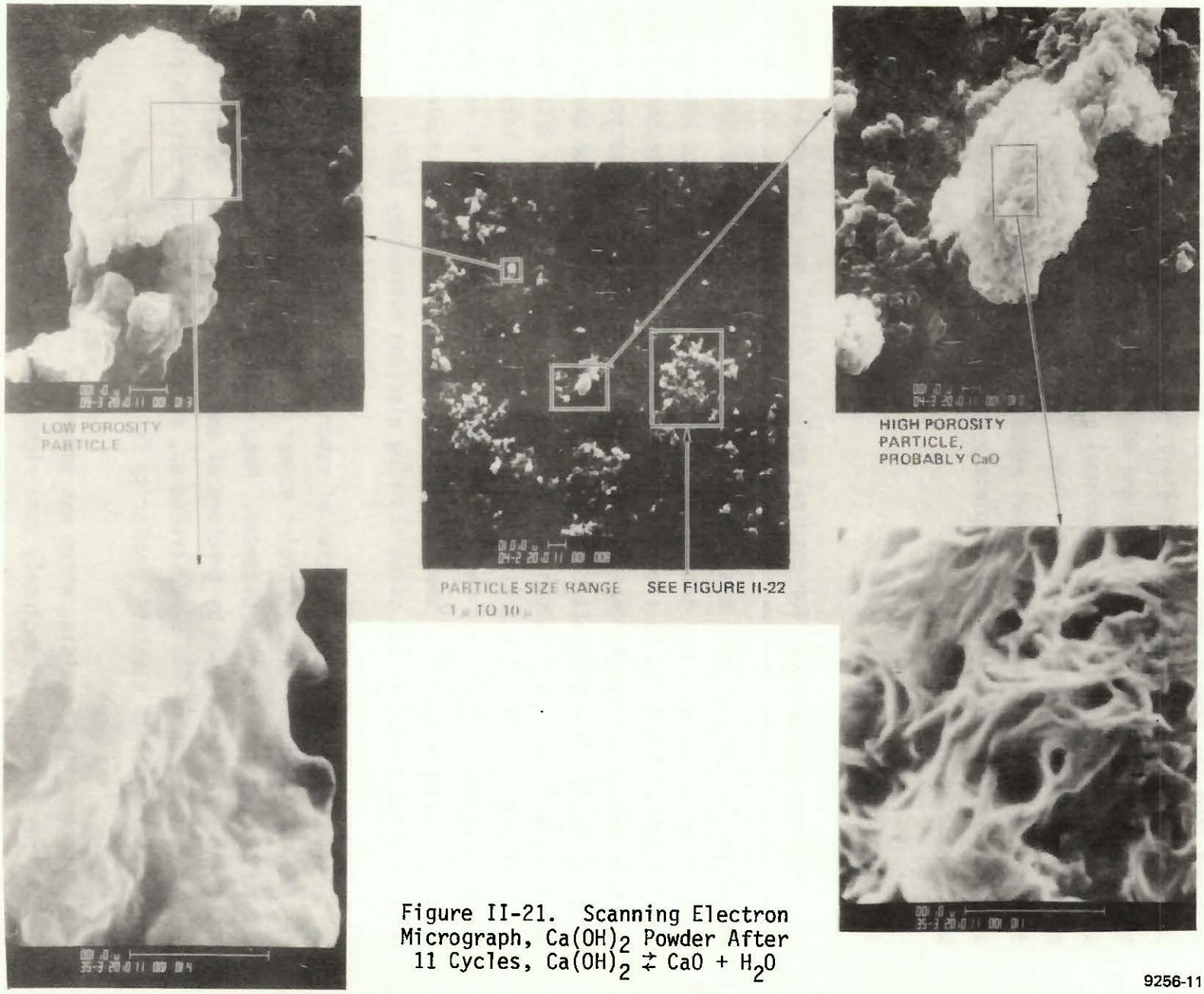

Figure II-21. Scanning Electron Micrograph, $Ca(OH)_2$ Powder After 11 Cycles, $Ca(OH)_2 \rightleftarrows CaO + H_2O$

9256-11

It is postulated that these isolated high-area structures are particles of CaO which, at least in freshly dehydrated form, have very high surface area as previously established by BET techniques.

The relatively large single crystal in Figure II-22 is of interest, and shows a distinct departure from the plate-like agglomerates. The leading edge of the crystal appears to exhibit hexagonal angularity. ($Ca(OH)_2$ is hexagonal, similar to the CdI_2 arrangement.) It is likely that this crystal grew throughout the cycles (none was found in the sample of starting material), which were not 100% complete in terms of water utilization.

3. Conclusions

The following conclusions are related to data presented in this section, and relationships with performance data are given, where applicable.

1) Even though $CaCO_3$ was continuously formed during the extended cycling tests (due at least in part to leakage of air), its presence did not seem to inhibit the reactions. Utilization remained high for available CaO. In a commercial application, consideration will be given to conducting the dehydration periodically at about $900^{o}C$ to decompose the carbonate (or adding a separate periodic calcination step).
2) Corrosion of the stainless steel parts and appearance of H_2 in the vapor space was consistent with increases in the presence of Fe, Cr, and Ni in the solid charge. Careful consideration of materials containment must be given to advanced designs of reaction and transport equipment.
3) Surface area of the $Ca(OH)_2$ appears to decrease with cycling; however, all charges leveled off at about 6 m^2/g (from 17 m^2/g for materials cycled from 484 to 1171 times).
4) Average particle size appears to fluctuate during cycling, a situation that indicates possible alternating agglomeration and fracturing (not the same cycle period).

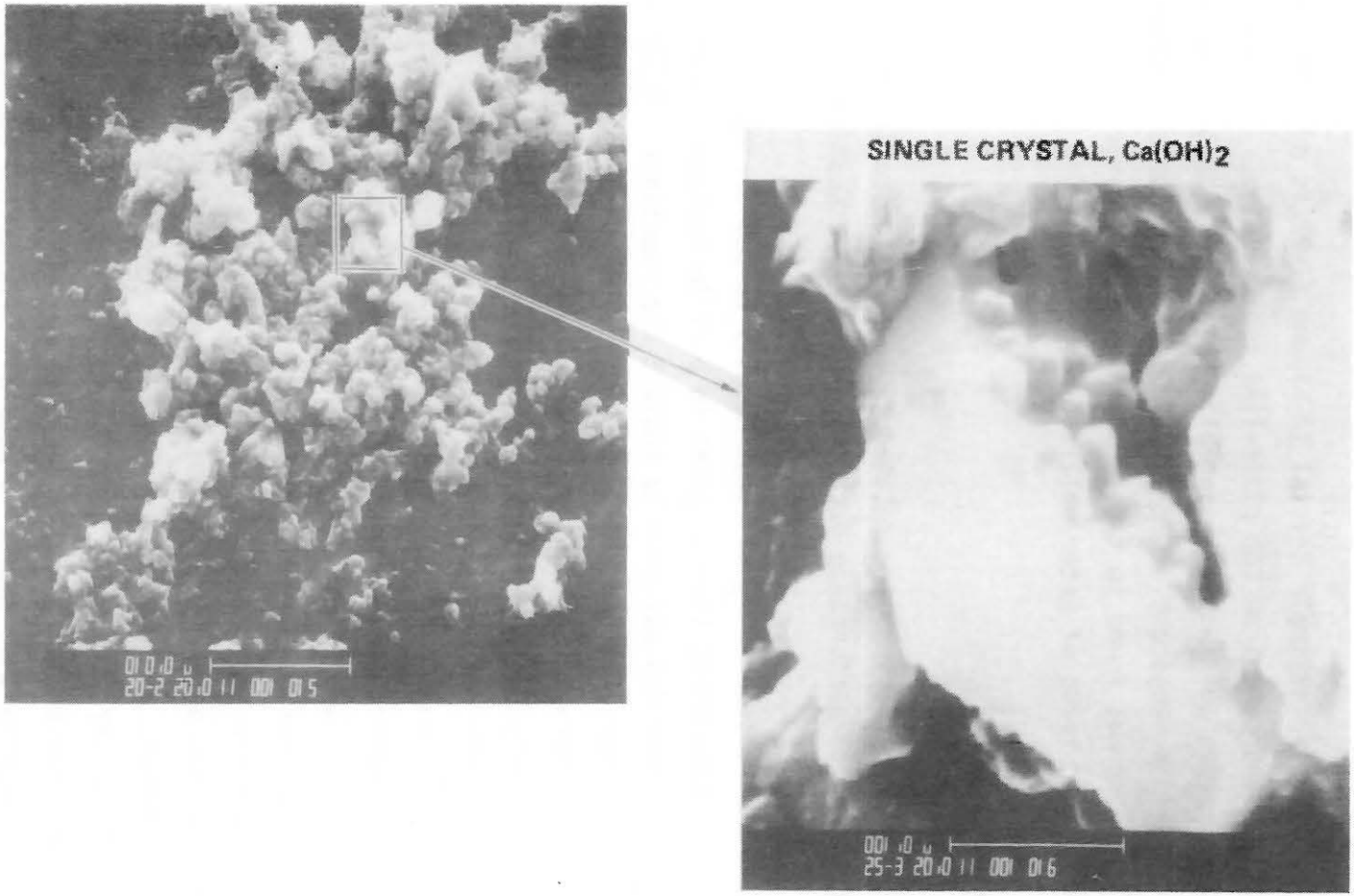

Figure II-22. Detail, $Ca(OH)_2$ Powder After 11 Cycles

9256-12

5) Freshly formed CaO has a much higher surface area than the parent $Ca(OH)_2$ as a result of pore formation as the water discharges.

6) Residual hydrocarbons from the original limestone burning may have been the source of hydrocarbons found in the gas phase of the cycling reactors. Carbide carbon bonds were found on the material using ESCA, and this material may constitute another potential source of hydrocarbons.

REFERENCES

II-1. G. Ervin, "Hydration-Dehydration of MgO - $Mg(OH)_2$ for Application to Solar Heat Storage Systems," ERDA Research and Development Report, AI-ERDA-13178 (September 30, 1976)

II-2. T. H. Springer and G. Ervin, "Solar Energy Storage System for Heating and Cooling of Buildings," Paper presented at ERDA Thermal Energy Storage Program Information Exchange Meeting, Cleveland, Ohio, September 8-9, 1976

II-3. D. K. Chung, Private Communication (1977)

II-4. J. M. Smith, Chemical Engineering Kinetics, 2nd Edition, McGraw-Hill, New York (1970)

II-5. L. S. Caretto and K. Nobe, "Effects of Pore Diffusion in the Catalytic Oxidation of Ethylene," A.I.Ch.E.J., 15, 18-24 (1969)

II-6. G. L. Bauerle, S. C. Wu, and K. Nobe, "Parametric and Durability Studies of NO_x Reduction with NH_3 on V_2O_5 Catalysts," I&EC Prod. Res. Develop., 17, 117-22 (1978)

II-7. G. L. Bauerle, S. C. Wu, and K. Nobe, "Parametric and Durability Studies of NO_x Reduction with NH_3 on Fe-Cr Oxide Catalysts," I&EC Prod. Res. Develop., 17, 123-8 (1978)

II-8. D. R. Stull and H. Prophet, JANAF Thermochemical Tables, Nat. Stand. Ref. Data Serv., Nat. Bur. Stand., 37 (June 1971) and supplements for 1974 and 1975

II-9. J. H. Flynn and L. A. Wall, "General Treatment of the Thermogravimetry of Polymers," Journal of Research, U. S. Nat. Bur. Stand., 70A, 487-523 (1966)

II-10. C. D. Doyle, J. Appl. Polymer. Sci., 6, 639 (1962)

II-11. R. S. Mikhail, S. Brunauer, and L. E. Copeland, "Kinetics of the Thermal Decomposition of Calcium Hydroxide," J. Colloid and Interface Sci., 21, 394-404 (1966)

II-12. I. Fujii and K. Tsuchiya, "Experimental Study of Thermal Energy Storage by Use of Reversible Chemical Reactions," Paper presented at International Conference on Alternative Energy Sources, Miami, Florida, December 5-7, 1977

II-13. N. G. Dave and S. K. Chopra, "Preparation and Thermal Decomposition of Calcium Hydroxide Crystals," J. Am. Ceram. Soc., Disc. and Notes, 575 (October 1966)

III. APPLICATION STUDY AND EVALUATION

A. INTRODUCTION AND SCOPE

The intermittent characteristics of solar energy make it necessary to store some portion of the solar energy collected during hours of sunshine for a continuously functioning solar thermal system. In addition, the solar heat storage system can provide power station load leveling. The thermal power collected from the mirror field varies as a function of the time of day and as a function of the season of the year, while the demand of electric power varies independently from solar insolation. Therefore, a practical solution is to store the excess solar heat during a peak thermal collection period, while a properly sized turbine-generator unit operates simultaneously to meet the electrical demand.

Since early in 1973, the Energy Systems Group of Rockwell International has been investigating solar energy storage using reversible chemical reactions of inorganic salts. The systems work described herein studied the application of $CaO - Ca(OH)_2$, the most promising of the inorganic materials that have previously been investigated.

The fundamental advantages of the $CaO - Ca(OH)_2$ heat storage applied to a solar power station are:

1) High Energy Storage Density — The energy storage density of $CaO - Ca(OH)_2$ heat storage is approximately 40,000 Btu/ft^3 of vessel, while that of hot rock storage is approximately 4000 Btu/ft^3 of vessel in the temperature range at which the power cycle operates.
2) Isothermal Heat Release at a High Temperature — The energy is stored and released at essentially constant temperature; this feature results in a relatively high thermal efficiency during night operation.
3) Inexpensive Noncorrosive Material — CaO or $Ca(OH)_2$ is plentiful, inexpensive, relatively noncorrosive, and safe to handle.

4) Recovery of Latent Heat – Approximately two-thirds of the energy supplied to the $Ca(OH)_2$ for storage is stored as energy of chemical reaction ($Ca(OH)_2 \longrightarrow CaO + H_2O$), while one-third of the energy leaves with the released water vapor. The water vapor is condensed in the condenser, and thus about one-third of the energy applied to the heat storage is lost as latent heat of water. Most of this latent heat can be recovered by using the exhaust steam from the steam turbine as a water-vapor source for the hydration ($CaO + H_2O \longrightarrow Ca(OH)_2$) during night operation.

In this study, 100-MWe commercial solar power stations coupled to two different CaO - $Ca(OH)_2$ heat storage systems were evaluated. One storage system used a fluidized-bed reactor to carry out the hydration-dehydration reaction, and the other system used a rotating drum reactor concept. Both systems use relatively low-cost storage bins to contain the bulk of the CaO or $Ca(OH)_2$, and higher-cost reactors in which to carry out the exothermic hydration reaction and the endothermic dehydration reaction. The reactors also include internal heat exchangers to transmit the generated or absorbed heat to or from an intermediate fluid (sodium). Both systems require a solids conveying subsystem to transfer the solids from storage to the reactors. A pneumatic conveying system was selected for this study.

To provide equipment size information for pricing purposes, a plant point design was studied in detail. The main system characteristics of the 100-MWe solar power station studied were as follows:

1) The station is located in the desert area of New Mexico (north 35^{o}).
2) Overall plant size is 100 MWe net for both direct operation and operation off of the stored energy supply.
3) Thermal storage is to be sized to provide 100 MWe net for 6 h of night operation.
4) The intermediate heat transfer fluid for the CaO - $Ca(OH)_2$ heat storage is liquid sodium.

5) The maximum temperature of the heat transfer fluid from the central receiver is 950°F. (A brief study also considered 1050°F.)
6) The mirror field is sized so that 6 h of 100-MWe net night (extended) operation capability can be charged during a winter solstice day.
7) All days are clear except for 35 days in which the sun is completely obscured and no energy is collected. These days are uniformly distributed throughout the year.
8) The system operates in the direct (daytime) generation mode during all periods when the sun is >15 degrees above the horizon.
9) The turbine generates a constant 100 MWe net during its period of operation. All other solar energy collected during the day is stored up to the maximum storage capacity.
10) Maintenance downtime coincides with the 35 cloudy days of the year.
11) The thermal energy collected during the day is completely expended the same evening.

The above assumptions are identical to those used in References III-1 and III-2, with the exception that those studies used a nighttime power level of 70 MWe. The tabulated assumptions result in a total annual production of 311.4×10^6 kWhe net by direct generation, E_d, and 198.0×10^6 kWhe net by thermal storage generation, E_n, or a ratio E_d/E_n of 1.573. For the studies of References III-1 and III-2, the resulting values are:

$$E_d = 311.4 \times 10^6 \text{ kWhe (same as this study)}$$
$$E_n = 138.6 \times 10^6 \text{ kWhe}$$
$$E_d/E_n = 2.247$$

The results of the point designs for the rotating drum concept and the fluidized-bed concept are compared at the 100-MWe nighttime power level. The fluidized-bed concept, however, was re-evaluated at the 70-MWe nighttime power level and compared with the fixed-bed CaO - $Ca(OH)_2$ system and the HT-43 and hot rock system presented in Reference III-1.

It is not practical to use CaO - $Ca(OH)_2$ heat storage with a water-steam cooled solar receiver, since the temperature level required for the decomposition of $Ca(OH)_2$ is higher than the critical temperature of the steam (705^oF); only the sensible heat carried by the superheated steam leaving the solar receiver can be utilized as a heat source for charging the CaO - $Ca(OH)_2$ heat storage system. Hence, a high flow rate of heat transfer fluid (superheated steam) through the CaO - $Ca(OH)_2$ reactor is required during daytime operation. Since this steam flow rate is much larger than the required throttle steam flow rate of the steam turbine, some portion of the steam has to be pumped back to the solar receiver through a separate riser pipe, thereby avoiding two-phase flow conditions in a single riser pipe. This is a principal reason for using liquid sodium as an intermediate heat transfer fluid for the CaO - $Ca(OH)_2$ system. In addition, a sodium-cooled solar receiver system has other advantages over a steam-cooled solar receiver system. For example, the high heat transfer capability and the low operating pressure of the liquid sodium simplifies the design of the solar receiver and results in a higher collection temperature with less potential burnout problems on the receiving tubes.

The fluidized-bed and rotating drum reactor concepts offer several advantages over the fixed-bed CaO - $Ca(OH)_2$ reactor concept.

1) The heat transfer coefficients for the fluidized-bed and rotating drum reactors are approximately 100 and 10 times, respectively, greater than the fixed-bed reactor.
2) The fluidized-bed and rotating drum concepts use a single, relatively complex, high-temperature, high-cost reactor combined with a solids transport system and relatively low-cost, simple storage bins, whereas the fixed-bed system uses many complex, high-cost, reactor-storage vessels.
3) The fluidized-bed and rotating drum reactors provide continuous agitation and mixing of the reactants, thereby promoting fast reaction times and uniform solids temperature, and preventing agglomeration of solids. The reaction rate in a fixed-bed reactor is controlled by heat and mass diffusion through a

relatively large thickness (on the order of 3 ft) of packed stationary solids.

The principal reason for conducting this study with other CaO - $Ca(OH)_2$ storage system concepts was the feeling that the fixed-bed CaO - $Ca(OH)_2$ storage system studied in Reference III-1 was costly, because each storage vessel was itself a high-temperature reactor requiring costly materials of construction and complex internal heat exchange equipment. The two systems studied herein consist of large, low-cost solids storage vessels and a relatively few high-temperature reactors to generate the required power level. This study does indeed indicate that there is a theoretical point at which it is more economical to use the separate reactor and storage bin concept.

B. SYSTEM DESCRIPTION

Figure III-1 shows the flow diagram (with operating conditions indicated) for a 100-MWe solar power plant, coupled with a fluidized-bed CaO - $Ca(OH)_2$ heat storage system and operating directly off of solar energy (daytime operation). Figure III-2 shows the flow diagram and operating conditions for the plant operating off of the stored energy supply. Because the initial assumption of energy flow from storage was high, the nighttime plant output determined in the detailed material and energy balance calculations came out to be approximately 115 MWe net, instead of the target value of 100 MWe net. However, since all flows and powers are directly proportional to the net power generated (for nighttime operation), flow and power requirements for a 100-MWe plant may be determined by applying the ratio 100/114.59 to the corresponding value shown in Figure III-2. The 115-MWe plant is shown, because detailed sizing and pricing were based on these flows and auxiliary power requirements and were then scaled to the 100-MWe (nighttime operation) size. The rotating drum reactor system layout is identical to those shown, except that the fluidized-bed reactors and heat recovery vessels are replaced by rotating drums. Figure III-3 shows the overall plant system layout, which indicates the commonality of components and piping for day and night operation.

During daytime operation, liquid sodium is heated in the central receiver to 950°F. A small portion of the flow goes to the superheater of the steam turbine power generation loop, and the remaining flow goes to the dehydration reactor where a portion of the sensible heat of the liquid sodium is used to drive off water vapor in the dehydration of $Ca(OH)_2$ (charging process). The two streams of liquid sodium recombine and enter the shell side of the steam generator. The liquid sodium is cooled to 729°F and is pumped back to the central solar receiver located at the top of a 1000-ft high tower.

$Ca(OH)_2$ is pneumatically conveyed from its storage bin to an intermediate feed bin. From there, it is fed at a controlled rate (through a rotary valve) to the fluidized-bed dehydration reactor. The bed is maintained in a fluidized state by a recirculated stream of nitrogen saturated with water vapor. The dehydration occurs at a uniform bed temperature of 800°F and a total pressure of 1.9 psia (1.86 water vapor pressure). Some of the sensible heat carried by the steam leaving the reactor is recovered in Heaters H2 and H1. The condensate is reheated to 220°F and stored for nighttime use. The moist nitrogen from the condenser is recirculated back to the dehydration reactor.

The solids at 800°F overflow from the reactor to a heat recovery fluidized bed. Here boiler feedwater is heated from 415°F to 450°F, while the solids are reduced in temperature to 550°F. The solids flow used was the total charge required for 6 h of nighttime operation at 100 MWe, averaged over a 12.2-h charging period. The heat recovery fluidized bed operates at a low pressure of 4.0 psia in order that the solids can flow by gravity from the low pressure reactor into the heat recovery vessel. The heat recovery bed is fluidized by recirculating nitrogen.

The CaO flows by gravity into one of two alternately evacuated receiving bins. The receiving bins are alternately evacuated to accept CaO from the heat recovery vessel (HRV) and pressurized to transport the CaO to a storage vessel.

The steam generator produces 983,630 lb/h of steam at 650°F, which is further superheated to 900°F. The steam pressure to the turbine is 1300 psia.

This steam produces 112.27 MWe (gross) at a 37.95% gross thermal efficiency, and 99.78 MWe net for a net efficiency of 33.09%.

For the rotating drum concept, the same gross thermal efficiency was used in lieu of doing a detailed design. For this valid assumption, the total generated power required to give 100 MWe net was 124.31 MWe gross. This resulted in a net thermal efficiency of 29.95.

During nighttime operation (see Figure III-2), the heat of hydration released in the high-temperature reactor (not used in charging process) is supplied to the superheater by the circulation of liquid sodium with a 148-kW circulating pump. The heat released in the low-temperature hydration reactor (the same reactor used for dehydration during charging) is supplied to the steam by a 726-kW sodium circulating pump.

In order to obtain a high thermal efficiency, a small high-temperature ($1000^{o}F$) reactor, which uses 24-psia turbine steam, is used only to supply the higher level heat requirement for the steam superheater. The low-temperature ($760^{o}F$) hydrator is supplied with low-pressure (2.5 psia) turbine exhaust steam, and provides heat at a level sufficient for boiler operation. A total of 179,900,000 Btu/h are released to the superheater from the high-temperature reactor, and 837,800,000 Btu/h to the boiler from the low-temperature reactor. The low-temperature and high-temperature heat recovery units supply 126,860,000 Btu/h and 70,960,000 Btu/h, respectively, to the boiler feedwater. Approximately 62% of the turbine exhaust steam (44% of the total turbine inlet flow) is supplied to the low-temperature reactor. Approximately 11% of the total turbine inlet flow is supplied to the high-temperature reactor at 24 psia.

Approximately 1.5% excess steam at 1.04 psia leaves the low-temperature hydration reactor. It is mixed with 5% excess steam (at 19.6 psia) from the high-temperature reactor in an ejector where the pressure is raised to 1.9 psia. The resulting steam (at $871^{o}F$) is passed through heat exchangers H2 and H1 to lower its temperature to $175^{o}F$ before being condensed in an air-cooled condenser.

The condensate is reheated to 220°F and returned to the water storage tank. The hot water stored in this tank during daytime operation is supplied directly to the boiler feedwater loop by a condensate pump.

CaO is supplied from a storage bin to both the high-temperature reactor feed bin and the low-temperature reactor feed bin through a diverter valve. The required flow to the reactors is metered through rotary valves. The hydration temperature is 760°F in the low-temperature reactor and 1000°F in the high-temperature reactor. $Ca(OH)_2$ flows by gravity from the reactors to the heat recovery vessels, where its temperature is reduced to 550°F by boiler feedwater. Both heat recovery vessels operate as fluidized beds and use recirculated nitrogen. The high-temperature heat recovery vessel operates at atmospheric pressure, whereas the low-temperature heat recovery vessel operates at below atmospheric pressure (4.5 psia). $Ca(OH)_2$ flows to an evacuated receiving bin, which is subsequently pressurized to transfer the $Ca(OH)_2$ to storage. Two receiving bins are required to maintain a continuous flow of solids from the low-temperature heat recovery vessel. Since the high-temperature heat recovery vessel operates at atmospheric pressure, only one intermediate receiving bin is required. Solids from this bin are continuously conveyed to the $Ca(OH)_2$ storage vessel by a separate nitrogen blower system.

Since the throttle steam condition of the steam turbine cycle during night operation is the same as that during day operation, a relatively high thermal efficiency of 34.61% is achieved. During night operation, 1,011,300 lb/h of throttle steam (900°F, 1300 psia) produces 123.28 MWe busbar power. The system net thermal efficiency is 32.17%, with a net power production of 114.59 MWe. The thermal efficiencies referred to in this study pertain to (1) the total heat transferred from the solids to the steam turbine loop via the reactors and the heat recovery units during night operation, and (2) the total solar heat supplied directly to the superheater and steam generator by liquid sodium and indirectly to the boiler feedwater via the solids (CaO) heat recovery unit during daytime operation. The sensible heat recovery from the process steam during day and night operation were not included in the thermal efficiency calculations. The heat losses involved in the CaO - $Ca(OH)_2$ heat storage system operation, however, were taken into account in the calculation of the overall

(combined night and day operation) power station efficiency. In other words, the overall station efficiency is based on the total solar energy input.

When using the rotating drum reactor concept for the night operation similar to that shown in Figure III-2, the resultant net power output was only 95.74 MWe because of extremely high parasitic power requirements (27.54 MWe) to drive the rotating drum reactors and rotating drum heat recovery units.

The nighttime flow rate requirements shown in Figure III-2 were used as a basis for sizing and pricing the total heat storage system, since these requirements proved to be more severe than for daytime operation.

C. REACTOR DESIGN

Considerable effort was devoted to the design of the fluidized-bed reactors. The literature was reviewed to some extent, and several telephone discussions were held with Conoco Coal Development Company in Library, Pennsylvania, and Dorr-Oliver Corporation in Stamford, Connecticut. Conoco is the developer of the CO_2-Acceptor process for coal gasification. This process circulates CaO to a fluidized-bed coal gasifier in which $CaCO_3$ is formed. The $CaCO_3$ flows from the gasifier to a fluidized bed where CaO is regenerated, and then flows back to the gasifier. This process has been successfully developed on a large pilot plant scale. The Dorr-Oliver Corporation has produced fluidized-bed $CaCO_3$ calciners since 1946. They also produce other fluidized-bed processes for regenerating lime sludge from wastewater treatment facilities into active CaO spherical particles in the 200 to 3000 μ size range. They also assisted Conoco Company in regenerating inactive CaO formed in the CO_2-Acceptor process.

For the rotating drum concept, the reactor and heat recovery units were sized and priced by the Stansteel Corporation (a division of Allis-Chalmers) of Los Angeles, based on the operating conditions, total flows, and heat loads supplied by the Energy Systems Group. Stansteel Corporation is a leading manufacturer of large steam-tube-heated rotating drum calciners, and recently supplied 10 high-pressure (300 psig) steam-tube units, each 100 ft long by 12 ft

in diameter, to a user in Trona, California. The requirements for this application were thoroughly reviewed with them in a meeting at their office.

1. Physical and Thermodynamic Properties

The thermodynamic properties of CaO, $Ca(OH)_2$, and water vapor used in determining the heat of reaction and the equilibrium dissociation pressure for the reaction

$$CaO\ (solid) + H_2O\ (gas) \longrightarrow Ca(OH)_2\ (solid)$$

were obtained from the Joint Army, Navy, Air Force (JANAF) Thermochemical Tables. The data used were the heat and free energy of formation of the compounds from their elements, and the corresponding equilibrium constant and the heat capacities of the compounds. From this information, the heat of reaction and the equilibrium dissociation pressure were calculated as a function of temperature. The results are shown in Figures III-4 and III-5.

A consideration of particle density leads to a determination that three densities must be defined. The first is the pure crystallite density, ρ_{th}, which is the theoretical material density with no voids or gas pockets within the mass. The second is the macroscopic or actual density, ρ_p, of a single particle with internal voids whose magnitude depends on the process used in forming the particle. The third density, ρ_B, is the bulk density of a relatively large collection of particles, which introduces additional voidage between the individual particles. Corresponding with these definitions of density are three definitions of voidage, ϵ.

$$1)\quad \epsilon_f = \frac{V_B - V_p}{V_B} = 1 - \rho_B/\rho_p$$

$$2)\quad \epsilon_B = \frac{V_B - V_{th}}{V_B} = 1 - \rho_B/\rho_{th}$$

$$3)\quad \epsilon_p = \frac{V_p - V_{th}}{V_p} = 1 - \rho_p/\rho_{th}$$

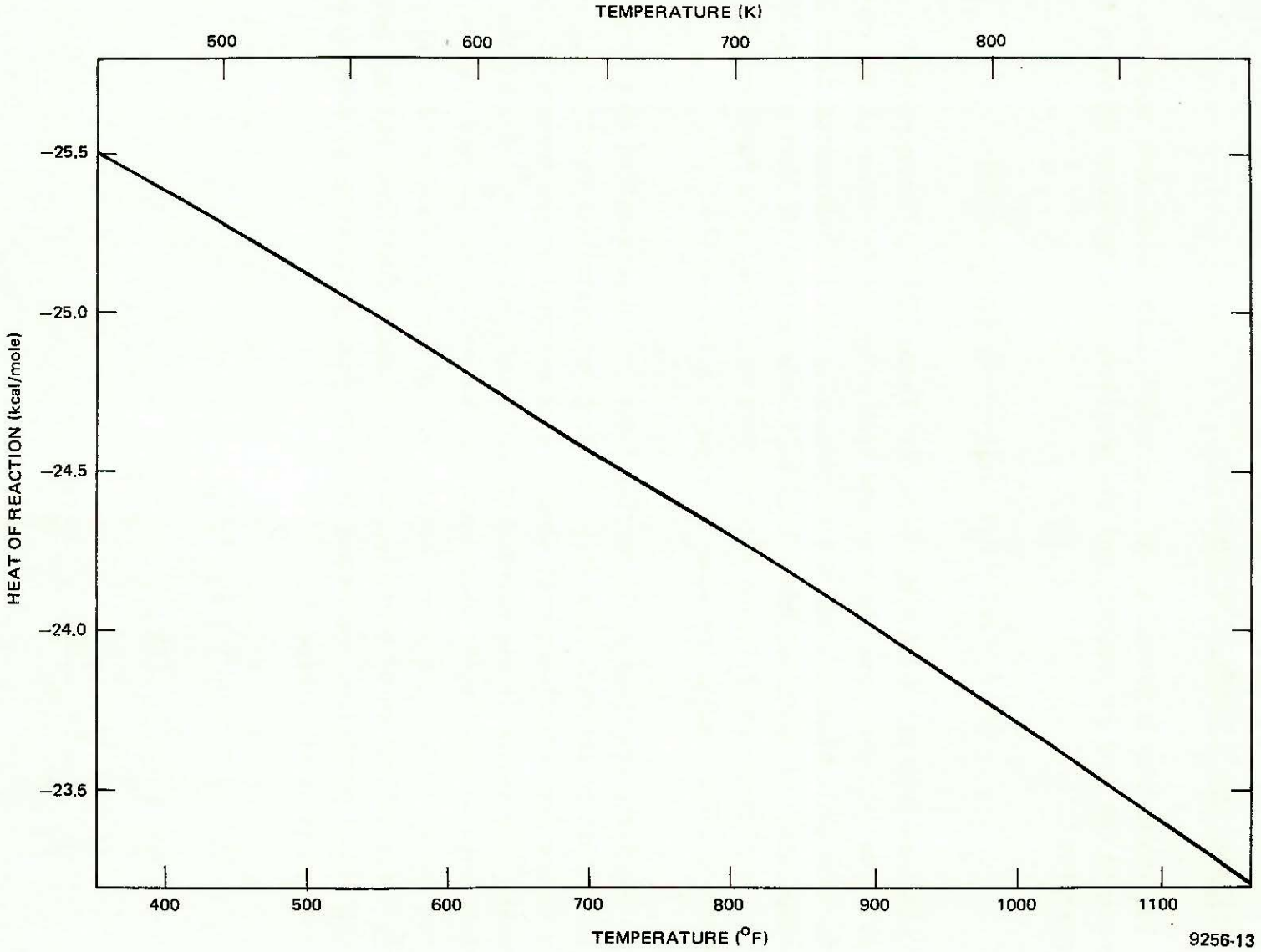

Figure III-4. Heat of Reaction vs Temperature, $CaO(c) + H_2O(g) \rightarrow Ca(OH)_2(c)$

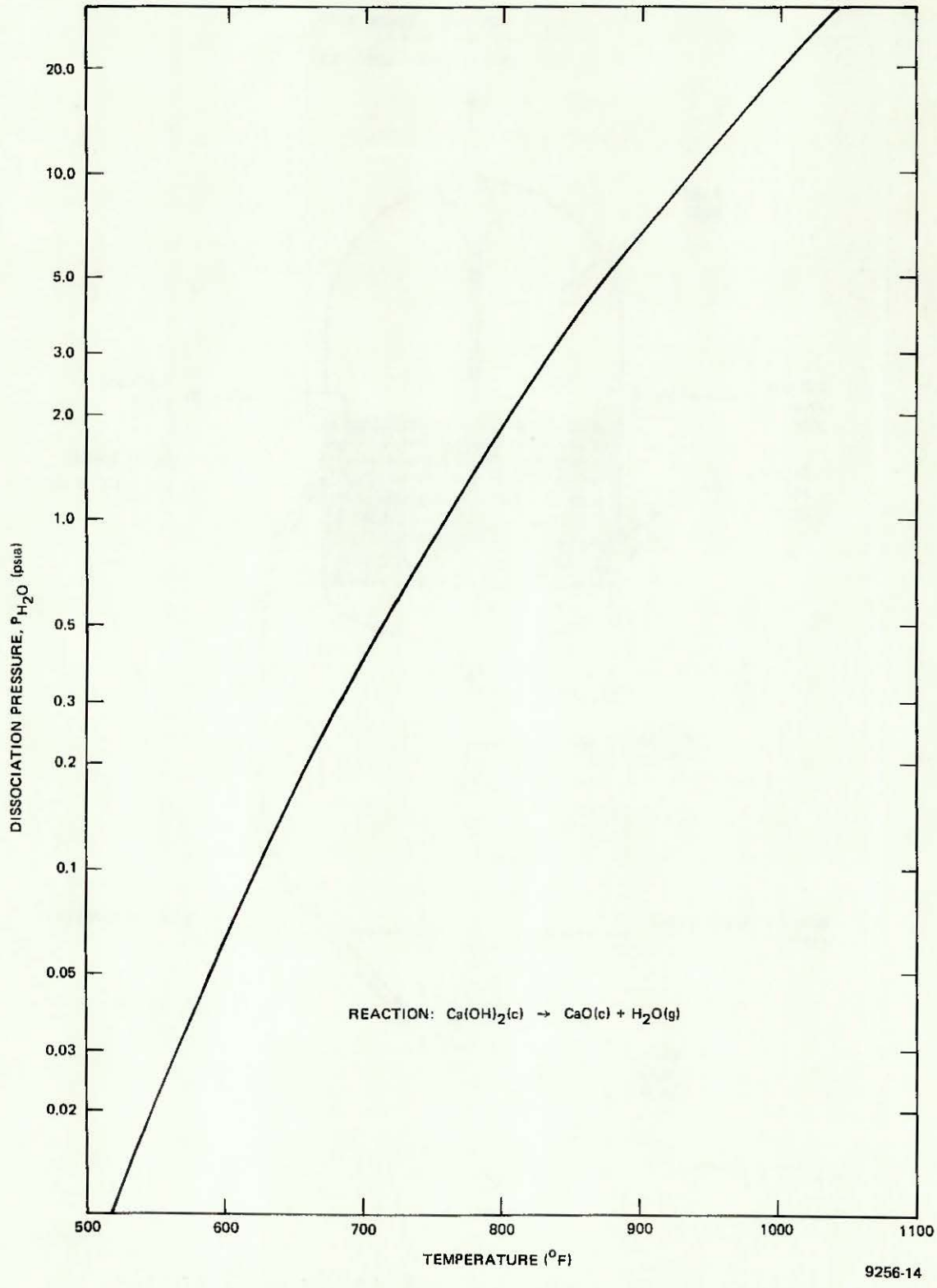

Figure III-5. $Ca(OH)_2$ Equilibrium Dissociation Pressure vs Temperature

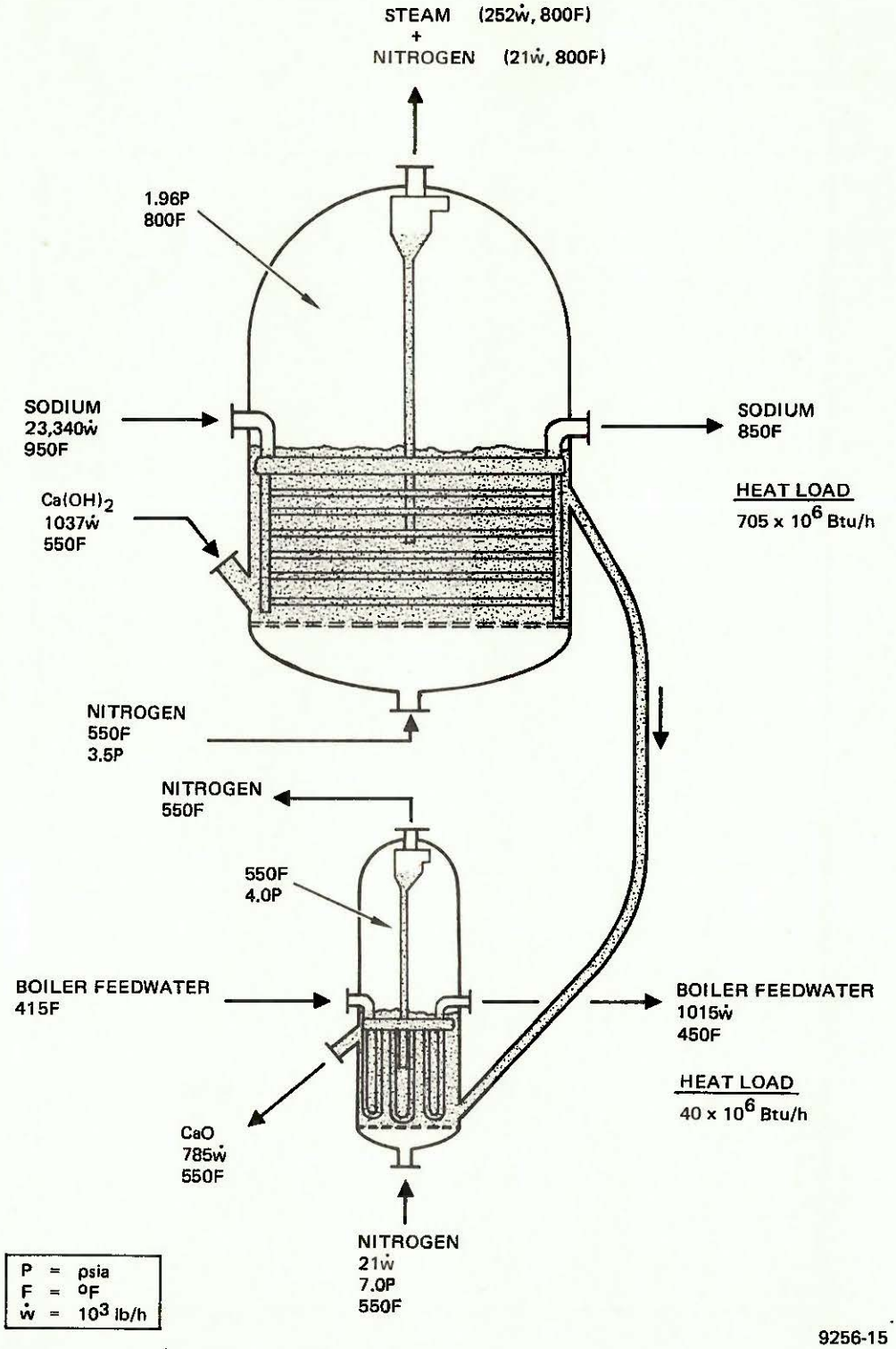

Figure III-6. Dehydration and Heat Recovery Vessels — System Flow Model

where V_B, V_p, and V_{th} are volumes per unit mass for a bulk collection of particles, a single particle, and a theoretical particle without void volume, respectively.

Fluidized-bed correlations use the ρ_p and ϵ_f values, whereas bulk storage volume requirements are determined from ρ_B.

The theoretical densities of CaO and $Ca(OH)_2$ obtained from the literature were 205.9 lb/ft^3 and 146.6 lb/ft^3, respectively. Conoco Coal Company has measured the density (ρ_p) of their CaO particles (approximately spherical, 3000-μ size) to be 94.9 lb/ft^3. This value was used as was an average bulk density (ρ_B) for pebble lime of 57.5 lb/ft^3. These values result in voidage values for CaO of $\epsilon_f = 0.393$, $\epsilon_B = 0.721$, and $\epsilon_p = 0.539$. If the assumption is made that the individual particle sizes of CaO and $Ca(OH)_2$ are the same (i.e., $\epsilon_{f,CaO} = \epsilon_{f,Ca(OH)_2}$), then voidage and density values can be determined for $Ca(OH)_2$ directly from the relative molecular weights of CaO and $Ca(OH)_2$ and the theoretical density of $Ca(OH)_2$. The resulting calculated values for $Ca(OH)_2$ were $\rho_p = 125.3$ lb/ft^3, $\rho_B = 75.9$ lb/ft^3, $\epsilon_B = 0.482$, and $\epsilon_p = 0.145$. The values of $\epsilon_p = 94.9$ lb/ft^3 and $\epsilon_f = 0.393$ used here for CaO compare closely with experimental values of $\epsilon_p = 99.9$ and $\epsilon_f = 0.40$ reported recently in Reference III-3. The assumption of no particle size change on hydration was felt by Conoco to be a fair approximation and is further substantiated by data in Reference III-3 that shows constant lime particle volume upon reaction with SO_2 up to 50% conversion to $CaSO_4$.

2. Fluidized-Bed Reactor Design

The fluidized bed reactors and heat recovery units were designed based on the solids flow requirements given in Figure III-2 for night operation, and a somewhat higher daytime solids flow rate for $Ca(OH)_2$ than was used for the concept shown in Figure III-1 (1,037,000 lb/h versus 934,000 lb/h). The higher flow rate was felt to represent a peak charging rate, and would therefore determine the reactor size. The operating conditions of the fluidized beds analyzed are shown in Figures III-6, III-7, and III-8. In designing the fluidized beds, several design constraints were imposed.

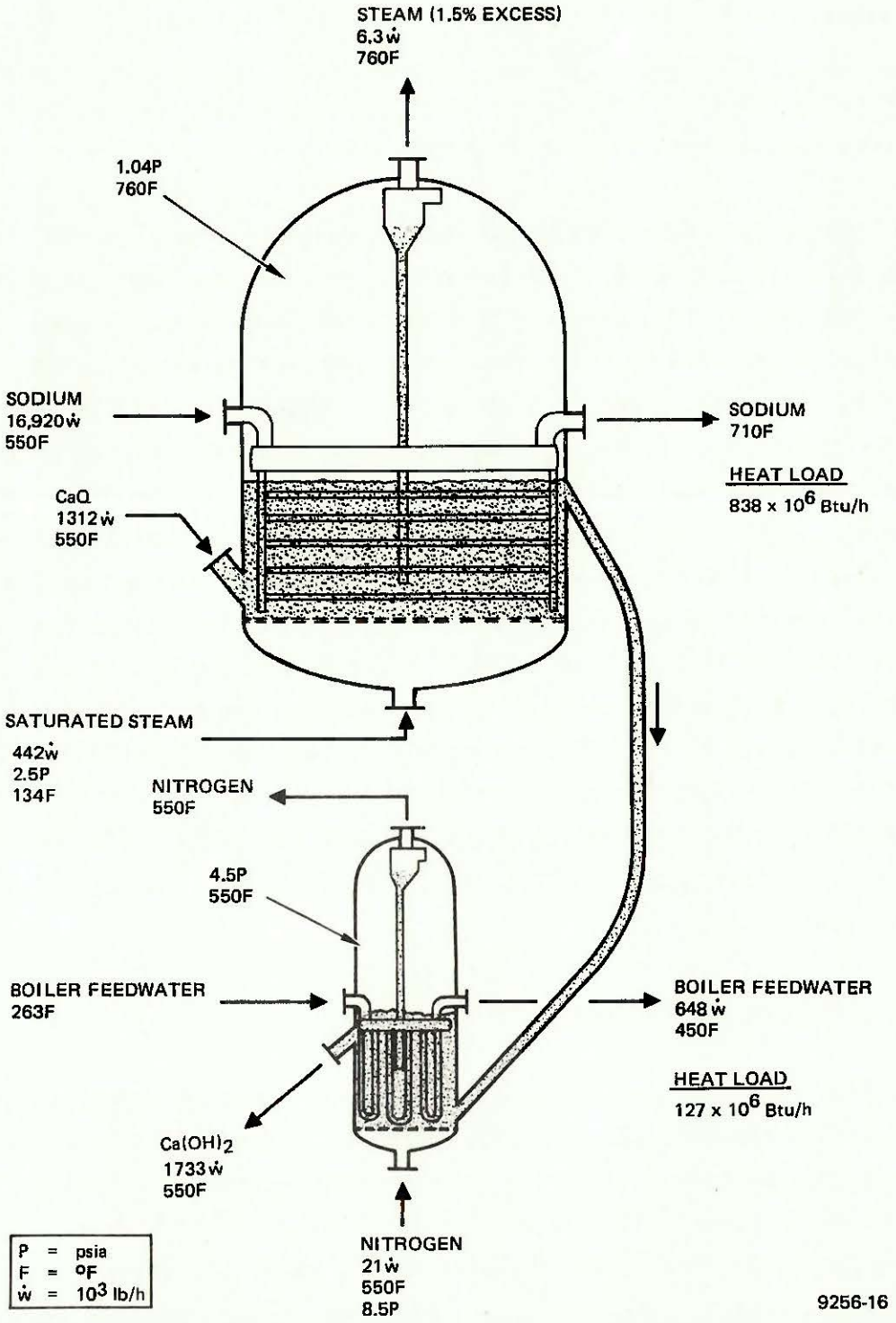

Figure III-7. Low-Temperature Hydration and Heat Recovery Vessels — System Flow Model

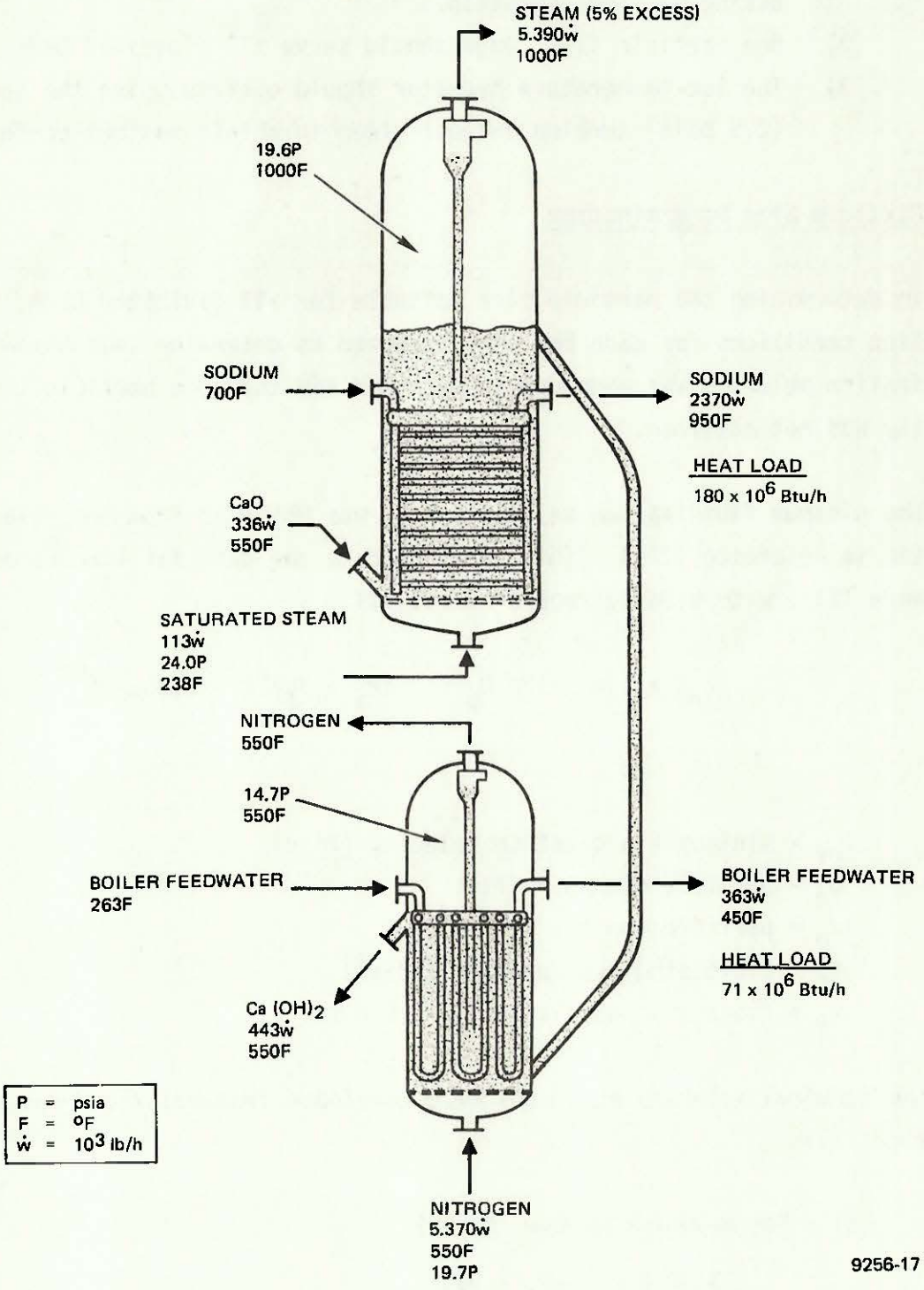

Figure III-8. High-Temperature Hydration and Heat Recovery Vessels — System Flow Model

1) The low-temperature hydration reactor and heat recovery unit should also function as the dehydrator and heat recovery unit during daytime operation.
2) One particle size range should serve all fluidized beds.
3) The low-temperature hydrator should operate using the low-pressure (2.5 psia) turbine exhaust steam to obtain maximum performance.

a. Particle Size Determination

In determining the particle size suitable for all fluidized beds, the operating conditions for each bed were analyzed to determine that a minimum fluidization velocity was exceeded in each bed and that the particle terminal velocity was not attained.

The minimum fluidization velocity, V_{mf}, was obtained from the relationship reported in Reference III-4. This equation fits the data for lime reported in Reference III-3 within an average of about 20%.

$$V_{mf} = 1.4 \times 10^5 \, D_p^{1.82} \, (\rho_p - \rho_f)^{0.94} / 3600 \mu_f^{0.88}$$

where,

V_{mf} = minimum fluidization velocity (ft/s)
D_p = particle diameter (ft)
ρ_p = particle density (lb/ft^3)
ρ_f = fluidizing gas density (lb/ft^3)
μ_f = fluidizing gas viscosity (lb/h-ft)

The terminal velocity equations were developed from relationships given in Reference III-5.

1) For Reynolds Number, Re < 2

$$V_T = \frac{3600 \, g \, D_p^2 \, (\rho_p - \rho_f)}{18 \mu_f}$$

2) For Re = 2 < 500

$$V_T = \left[315.8\ D_p^{1.6}\ (\rho_p - \rho_f)/\mu_f^{0.6}\rho_f^{0.4}\right]^{0.714}$$

3) For Re ≥ 500

$$V_T = \left[97.6\ D_p\ (\rho_p - \rho_f)/\rho_f\right]^{0.5}$$

The velocities are based on the total cross-sectional area of the vessel.

Tables III-1, III-2, and III-3 present V_{mf} and V_T values versus particle size for the six different sets of fluidized-bed conditions. V_{mf} is computed at the reactor inlet pressure for the dehydration reactor and at the exit pressure for the hydration reactors, since this is the point at which minimum gas velocity occurs. V_T is computed for the reactor outlet pressure for the dehydration reactor and for the reactor inlet pressure for the hydration reactors, since these are the locations at which the largest gas velocities occur. This distinction of reactor inlet and outlet conditions was made because of the very large gas volume change through the reactors caused by generation or loss of steam. For the heat recovery units, there is no mass flow change through the bed and relatively little gas velocity change. Consequently, the pressure at the top of the bed or an average pressure was used in determining the gas density.

Selection of a particle size that satisfies the V_{mf} and V_T criteria for all beds was made after a determination of the actual gas velocities. The gas velocities were calculated from the cross-sectional area and the gas flow rate. Results indicated that a very limited particle size range of approximately 300 to 700 μ simultaneously satisfied the V_{mf} and V_T criteria for all the fluidized beds.

b. Reactor Area Determination

To achieve a fluidized state in the solids bed, the pressure drop across the bed must be sufficient to lift the weight of solids in the bed. This

TABLE III-1

FLUIDIZATION MINIMUM AND TERMINAL VELOCITIES VS PARTICLE SIZE
FOR DEHYDRATION AND HEAT RECOVERY VESSELS

D_p (μ)	D_p (ft)	Reactor-Dehydration		Heat Recovery	
		V_{mf}* (ft/s)	V_T† (ft/s)	V_{mf}§ (ft/s)	V_T§ (ft/s)
10	3.28×10^{-5}	1.8×10^{-4}	1.0×10^{-2}	2.0×10^{-4}	9.6×10^{-3}
20	6.56×10^{-5}	6.5×10^{-4}	4.3×10^{-2}	7.3×10^{-4}	3.8×10^{-2}
40	13.12×10^{-5}	2.2×10^{-3}	1.7×10^{-1}	2.5×10^{-3}	1.5×10^{-1}
60	19.68×10^{-5}	4.8×10^{-3}	3.9×10^{-1}	5.4×10^{-3}	3.4×10^{-1}
80	26.24×10^{-5}	8.1×10^{-3}	6.9×10^{-1}	9.1×10^{-3}	6.1×10^{-1}
100	32.8×10^{-5}	1.2×10^{-2}	1.0	1.3×10^{-2}	9.6×10^{-1}
150	4.92×10^{-4}	2.5×10^{-2}	2.4	2.8×10^{-2}	2.1
200	6.56×10^{-4}	4.2×10^{-2}	4.3	4.8×10^{-2}	3.8
250	8.20×10^{-4}	6.4×10^{-2}	6.8	7.2×10^{-2}	5.2
300	9.84×10^{-4}	8.9×10^{-2}	9.8	1.0×10^{-1}	6.5
400	13.12×10^{-4}	1.5×10^{-1}	14.5	1.7×10^{-1}	9.0
500	16.40×10^{-4}	2.2×10^{-1}	18.7	2.5×10^{-1}	11.7
700	22.96×10^{-4}	4.2×10^{-1}	27.5	4.7×10^{-1}	17.1
1000	32.80×10^{-4}	8.0×10^{-1}	41.3	9.0×10^{-1}	25.8
1500	49.21×10^{-4}	1.6	65.7	1.8	41.0
2000	65.61×10^{-4}	2.8	91.4	3.1	57.0
2500	82.02×10^{-4}	4.2	117.9	4.7	73.6
3000	98.42×10^{-4}	5.9	145.2	6.6	88.4

*CaO fluidized with N_2 at 800°F, 3.0 psia (entrance condition)
†CaO fluidized with N_2 and steam at 800°F, 1.96 psia (exit condition)
§CaO fluidized with N_2 at 550°F, 4.5 psia

TABLE III-2

FLUIDIZATION MINIMUM AND TERMINAL VELOCITIES VS PARTICLE SIZE
FOR LOW-TEMPERATURE HYDRATION AND HEAT RECOVERY VESSELS

D_p (μ)	D_p (ft)	Large Reactor-Hydration		Heat Recovery	
		V_{mf}* (ft/s)	V_T† (ft/s)	V_{mf}§ (ft/s)	V_T§ (ft/s)
10	3.28×10^{-5}	3.1×10^{-4}	1.5×10^{-2}	2.7×10^{-4}	1.3×10^{-2}
20	6.56×10^{-5}	1.1×10^{-4}	6.0×10^{-2}	9.5×10^{-4}	5.1×10^{-2}
40	13.12×10^{-5}	3.9×10^{-3}	2.4×10^{-1}	3.3×10^{-3}	2.0×10^{-1}
60	19.68×10^{-5}	8.1×10^{-3}	5.4×10^{-1}	7.0×10^{-3}	4.6×10^{-1}
80	26.24×10^{-5}	1.4×10^{-2}	9.6×10^{-1}	1.2×10^{-2}	8.2×10^{-1}
100	32.8×10^{-5}	2.1×10^{-2}	1.5	1.8×10^{-2}	12.7×10^{-1}
150	4.92×10^{-4}	4.3×10^{-2}	3.4	3.7×10^{-2}	2.9
200	6.56×10^{-4}	7.3×10^{-2}	6.0	6.3×10^{-2}	4.7
250	8.20×10^{-4}	10.1×10^{-2}	9.4	9.4×10^{-2}	6.1
300	9.84×10^{-4}	15.2×10^{-2}	12.9	1.3×10^{-1}	7.5
400	13.12×10^{-4}	2.6×10^{-1}	17.9	2.2×10^{-1}	10.4
500	16.40×10^{-4}	3.9×10^{-1}	23.2	3.3×10^{-1}	13.5
700	22.96×10^{-4}	7.1×10^{-1}	34.0	6.1×10^{-1}	19.8
1000	32.80×10^{-4}	1.4	51.2	1.2	29.8
1500	49.21×10^{-4}	2.8	81.3	2.5	47.3
2000	65.61×10^{-4}	4.8	112.9	4.1	65.7
2500	82.02×10^{-4}	7.2	145.8	6.2	83.9
3000	98.42×10^{-4}	10.1	179.5	8.7	91.9

*$Ca(OH)_2$ fluidized with excess steam at 760°F, P = 1.0 psia (exit condition)
†$Ca(OH)_2$ fluidized with steam at 760°F, P = 2.00 psia (entrance condition)
§$Ca(OH)_2$ fluidized with N_2 at 550°F, P = 5.5 psia

TABLE III-3

FLUIDIZATION MINIMUM AND TERMINAL VELOCITIES VS PARTICLE SIZE FOR HIGH-TEMPERATURE HYDRATION AND HEAT RECOVERY VESSELS

D_p (μ)	D_p (ft)	Small Reactor-Hydration		Heat Recovery	
		V_{mf}* (ft/s)	V_T† (ft/s)	V_{mf}§ (ft/s)	V_T§ (ft/s)
10	3.28×10^{-5}	2.7×10^{-4}	12.8×10^{-3}	2.7×10^{-4}	12.7×10^{-3}
20	6.56×10^{-5}	9.6×10^{-4}	5.1×10^{-2}	9.5×10^{-4}	5.1×10^{-2}
40	13.12×10^{-5}	3.4×10^{-3}	2.0×10^{-1}	3.4×10^{-3}	2.0×10^{-1}
60	19.68×10^{-5}	7.1×10^{-3}	4.6×10^{-1}	7.0×10^{-3}	4.6×10^{-1}
80	26.24×10^{-5}	11.9×10^{-3}	8.2×10^{-1}	11.8×10^{-3}	8.2×10^{-1}
100	32.8×10^{-5}	1.8×10^{-2}	12.8×10^{-1}	1.8×10^{-2}	12.7×10^{-1}
150	4.92×10^{-4}	3.7×10^{-2}	2.9	3.7×10^{-2}	2.6
200	6.56×10^{-4}	6.3×10^{-2}	4.1	6.3×10^{-2}	3.6
250	8.20×10^{-4}	9.5×10^{-2}	5.2	9.4×10^{-2}	4.6
300	9.84×10^{-4}	13.2×10^{-2}	6.5	13.1×10^{-2}	5.7
400	13.12×10^{-4}	2.2×10^{-1}	9.0	2.2×10^{-1}	7.9
500	16.40×10^{-4}	3.4×10^{-1}	11.6	3.3×10^{-1}	10.2
700	22.96×10^{-4}	6.2×10^{-1}	17.0	6.1×10^{-1}	15.0
1000	32.80×10^{-4}	11.8×10^{-1}	25.5	11.8×10^{-1}	22.5
1500	49.21×10^{-4}	2.5	40.6	2.5	35.7
2000	65.61×10^{-4}	4.2	56.4	4.1	45.9
2500	82.02×10^{-4}	6.3	63.8	6.2	51.4
3000	99.42×10^{-4}	8.7	69.9	8.7	56.3

*$Ca(OH)_2$ fluidized with excess steam at 1000°F, 19.6 psia (exit condition)
†$Ca(OH)_2$ fluidized with steam at 1000°F, 21.4 psia (entrance condition)
§$Ca(OH)_2$ fluidized with N_2 at 550°F, 14.7 psia

pressure drop remains essentially constant over the total height of the bed over a wide range of gas velocity from V_{mf} to V_T. Thus, although the bed height (L_f) and voidage (ϵ_f) increase with increasing gas velocity, the total pressure drop (ΔP_f) remains approximately equal to the weight of solids (W_S) divided by the cross-sectional area of the bed A_B, or

$$\Delta P_f = W_S/144A_B \qquad ...(1)$$

where

ΔP_f = total pressure drop across bed (lb/in.^{2})
W_S = total weight of reacted solids in the bed (lb)
A_B = cross-sectional area of the bed (ft^2)

W_S may be expressed in terms of the solids weight flow rate through the bed, $\dot{w}_s$, and the residence time in the bed, t, by

$$W_S = \dot{w}_s t \qquad ...(2)$$

where

$\dot{w}_s$ = flow rate of reacted solids out of the bed (lb/min)
t = residence time of reacted solids in the bed (min)

It should be noted that W_S and $\dot{w}_s$ refer to the product formed by the reaction. This is common procedure, since the product is the predominant species in the bed. Combining Equations 1 and 2 results in an expression for bed area in terms of the significant operational variables.

$$A_B = \dot{w}_s t/144\Delta P_f \qquad ...(3)$$

Each of the variables on the right of Equation 3 has design restrictions. The solids flow rate is exactly specified by the charging rate for daytime operation, or the power level required for nighttime operations. The residence time depends on the reaction rates achievable. Based on the laboratory hydration-dehydration

TABLE III-4

SUMMARY OF FLUIDIZED-BED DESIGN PARAMETERS*

	Dehydration System		Low-Temperature Hydration System		High-Temperature Hydration System	
	Reactor	HRV†	Reactor	HRV	Reactor	HRV
$\dot{w}_s$ (lb/h)	785×10^3	785×10^3	1733×10^3	1733×10^3	433×10^3	433×10^3
t (min)	30	10	12.9	4.5	10	4.3
ΔP_f (lb/in.^{2})	1.15	1.13	1.10	1.13	3.30	3.75
$\dot{w}_g$, in (lb/h)	21×10^3	21×10^3	442×10^3	21×10^3	113×10^3	5.4×10^3
$\dot{w}_g$, out (lb/h)	273×10^3	21×10^3	6.3×10^3	21×10^3	5.4×10^3	5.4×10^3
V_{min} (ft/s)	0.40	0.60	0.52	0.50	0.43	0.50
V_{max} (ft/s)	11.93	0.80	18.3	0.62	7.7	0.67
A_B (ft^2)	2364	808	2364	808	155	59
D_B (ft)	54.9	32.1	54.9	32.1	14.1	8.6
Particle Size Range (μ)	350 to 700	90 to 800	400 to 600	70 to 650	350 to 600	70 to 650

*Based on design conditions shown in Figures II-6, II-7, and III-8
†HRV = Heat Recovery Vessel

cycling work done under this contract and presented in Section II of this report, residence times of approximately 30 min for dehydration and 10 min for hydration were assumed to be adequate to achieve 100% reaction completion. The allowable bed pressure drop is restricted on the hydration cycle to the difference between the turbine exhaust pressure of 2.5 psia (with 25% loss in the gas injector of the reactor) and the equilibrium dissociation pressure at the desired reaction temperature (19.6 psia for 1000^{o}F and 1.04 psia for 760^{o}F). To obtain a high station efficiency, steam should be withdrawn from the turbine at as low a pressure as possible. The low-temperature hydrator uses turbine exhaust steam at 2.5 psia, and the high-temperature hydrator uses turbine steam withdrawn at 24 psia. The vessel area was calculated based on the limitations of the variables in Equation 3.

After a determination of the vessel area was made, the superficial gas velocities, v_g, were determined at the inlet and outlet of the fluidized beds.

$$v_g = \dot{w}_g / 3600\ \rho_g A_B \qquad ...(4)$$

where

v_g = superficial gas velocity (ft/s)
$\dot{w}_g$ = weight flow rate of gas (lb/h)
ρ_g = density of gas (lb/ft^3)

A tabulation of the design parameters for the six different fluidized bed conditions is given in Table III-4. It can be seen that a significant change in gas weight flow rate and superficial velocity occurs through the bed. For the dehydrator, the generation of steam causes high velocities at the exit of the bed. For the hydrators, the velocity is greatest at the entrance of the bed. The maximum and minimum velocities (V_{max} and V_{min}) calculated for each bed were compared with the allowable particle sizes for V_T (= V_{max}) and V_{mf} (= V_{min}) shown in Tables III-1, III-2, and III-3. The resultant acceptable particle size range is shown in Table III-4. It can be seen that the effect of the large velocity change is to narrow the acceptable particle size range. The heat

recovery units that are fluidized with nitrogen have a much wider acceptable range of particle size.

It can also be seen that the bed area and diameter are too large to be considered a single vessel. It was decided that four parallel sets of reactors of one-half the diameter shown in Table III-4 would be an acceptable design. These areas were later adjusted upward to accommodate the blockage introduced by the internal heat exchangers.

c. Heat Exchanger Design

Using the flow conditions and particle size (500 μ) determined for the reactors and heat recovery units, the heat exchanger designs required for the heat loads were determined. Both horizontal and vertical tube correlations were used for each of the six sets of operating conditions shown in Table III-4. The correlations used for the film coefficient were those presented in Reference III-4, which are as follows:

For vertical tubes:

$$h_g = 0.33 C_R \left(\frac{D_p G}{\mu_g}\right)^{0.23} \left(\frac{c_s}{c_g}\right)^{0.8} \left(\frac{\rho_p}{\rho_g}\right)^{0.66} \left(\frac{c_g \rho_g}{k_g}\right)^{0.43} \frac{k_g(1 - \epsilon_f')}{D_p}$$

where

h_g = heat transfer coefficient from the bed to tube wall (Btu/h-ft^2-^{o}F)
C_R = correction factor for nonaxial tube location = 1.6 (dimensionless)
D_p = average diameter of particles (ft)
G = superficial mass velocity of gas through bed (lb/h-ft^2)
μ_g = fluidizing gas viscosity (lb/h-ft)
c_s = heat capacity of solid (Btu/lb-^{o}F)
c_g = heat capacity of fluidizing gas (Btu/lb-^{o}F)
ρ_p = particle density (lb/ft^3)

ρ_g = density of fluidizing gas (lb/ft^3)
k_g = thermal conductivity of the fluidizing gas ($Btu/h\text{-}ft\text{-}^oF$)
ϵ'_f = voidage of bed at the average fluid velocity (dimensionless)

For horizontal tubes:

1) For $R_e < 2500$

$$h_g = 0.066 \left(\frac{c_g \mu_g}{k_g}\right)^{0.3} \left[\left(\frac{D_t G}{\mu_g}\right)\left(\frac{\rho_s}{\rho_g}\right)\left(\frac{1 - \epsilon'_f}{\epsilon'_f}\right)\right]^{0.44} \frac{k_g}{D_t}$$

2) For $R_e \geq 2500$

$$h_g = 420 \left(\frac{C_g \mu_g}{k_g}\right)^{0.3} \left[\left(\frac{D_t G}{\mu_g}\right)\left(\frac{\rho_s}{\rho_g}\right)\left(\frac{\mu_g^2}{D_p^3 \rho_p^2 g}\right)\right]^{0.3} \frac{k_g}{D_t}$$

where

D_t = tube outside diameter (ft)
g = acceleration due to gravity (ft/h^2)

For the heat recovery vessels, a boiler feedwater film coefficient of 300 was assumed in computing the overall heat transfer coefficient.

The bed voidage, ϵ'_f at the average velocity through the bed, was estimated using the relationship given in Reference III-6.

$$\epsilon'_f = \exp\left\{\left[\ln\left(\frac{18N_{Re} + 2.7N_{Re}^{1.6}}{N_{Ga}}\right)\right] \Big/ 4\right\}$$

where

N_{Re} = Reynolds number
N_{Ga} = Galileo number

TABLE III-5

FLUIDIZED-BED HEAT TRANSFER AND DESIGN SUMMARY*

	Dehydration System		Low-Temperature Hydration System		High-Temperature Hydration System	
	Reactor	HRV	Reactor	HRV	Reactor	HRV
h_g, horizontal ($Btu/ft^2\text{-}h\text{-}^oF$)	98†	64	135†	75	124†	56
h_g, vertical ($Btu/ft^2\text{-}h\text{-}^oF$)	35	51†	72	101†	81	101†
A_t (ft)	19,700	2360	19,700	2360	2610	1330
n_t	3770	1100	3770	1100	1920	586
$L_{t,avg}$(ft)	20	8.2	20	8.2	5.2	8.6
A_x (ft^2)	52	6.0	52	6.0	4.2	3.2
L_f' (ft)	7.8	9.3	5.5	8.2	13	8.7
L_T (ft)	46.3	26.1	46.3	26.1	23.5	15.0
D_B' (ft)	28.6	8.5	28.6	8.5	7.4	4.8

*Based on design conditions shown in Figures III-6, III-7, and III-8

†Indicates which tube bundle orientation was selected

The total height of bed in which the tubes are submersed can be calculated from

$$L'_f = \frac{1 - \epsilon'_f}{1 - \epsilon'_f} L_f$$

where

L_f = height of bed in unfluidized state (ft)
L'_f = height of bed in fluidized state (ft)

The total height of the vessel, L_T, was determined by adding the disengaging height (determined from Figure 14 of Reference III-4) to the bed height, L'_f.

Table III-5 gives a summary of the heat exchanger design and the final approximate dimensions of the vessels. The values given are for one of four vessels in parallel, which handle the total system load. In this table, A_t is the tube (1-in. OD) surface area (no tube fins were used), n_t is the number of horizontal or vertical tubes, L_t is the tube length (an average value for horizontal tubes), A_x is the estimated blockage area caused by the tubes (the vessel area was increased by this amount) and D'_B is the vessel inside diameter. Rough sketches of the vessel, tube bundle, and manifolding were submitted, along with the overall dimensions, to Pricing and Estimating, a separate department of the Energy Systems Group, for a cost evaluation.

3. Rotating Drum Reactor Design

Sketches similar to Figures III-6, III-7, and III-8 (except that rotating drums were depicted instead of fluidized beds) were given to Stansteel Corporation personnel for evaluation of reactor sizes and costs. Table III-6 summarizes the design and cost information received from them. The systems study of a power station generating 100 MWe net night power indicated that one large hydration-dehydration reactor would be required, in addition to the components shown in the table.

TABLE III-6

ROTATING DRUM CONFIGURATION AND COST SUMMARY*

Large Hydration-Dehydration Reactor

Number of Drums — 21
Heat Transfer Surface Area (Finned Tubes) — 40,000 ft^2/drum
Motor Drive — 400 hp/motor, 2 motors/drum
Reactor Dimensions — 12 ft OD by 100 ft length
Cost — $1,500,000 each drum assembly

Heat Recovery Vessels for Above Units

Number of Drums — 7
Heat Transfer Surface Area (Bare Tubes) — 7000 ft^2/drum
Motor Drive — 350 hp/motor, 2 motors/drum
HRV Dimensions — 12 ft OD by 100 ft length
Cost — $1,100,000 each drum assembly

Small Hydration Reactor

Number of Drums — 4
Heat Transfer Surface Area (Finned Tubes) — 40,000 ft^2/drum
Motor Drive — 350 hp/motor, 2 motors/drum
Reactor Dimensions — 12 ft OD by 100 ft length
Cost — $1,500,000 each drum assembly

Heat Recovery Vessel for Small Hydration Reactor

Number of Drums — 2
Heat Transfer Surface Area (Some Fins) — 10,000 ft^2/drum
Motor Drive — 350 hp/motor, 2 motors/drum
HRV Dimensions — 12 ft OD by 100 ft length
Cost — $1,200,000 each drum assembly

*Equipment requirements and costs were determined by Stansteel Corporation, based on design conditions shown in Figures III-6, III-7, and III-8 furnished by the Energy Systems Group.

4. Conveying System Design

Pneumatic conveying with recirculation was selected over mechanical conveying for use in this study, primarily because pneumatic conveying was thought to be a better system for transporting hot (550°F) solids over long distances in an airtight system. Conveying distances of 100 ft in both horizontal and vertical directions were used, based on a rough sketch of the storage and reactor vessel area. The method used for analyzing system pressure drop is given in Reference III-7. Equations for system pressure drop, power requirements, and gas temperature rise were programmed, and a wide range of pipe sizes were analyzed. Based on conversations with the Elliot Company, the compressors were designed to not exceed 20,000 ft head rise and an outlet temperature of 750°F. This allowed the use of much lower cost, single-stage compressors. Consideration was also given to minimizing the pressure in the large storage vessels. The final design selection for the pneumatic conveying system is shown in Table III-7.

D. STORAGE SYSTEM DESCRIPTION AND COST

A detailed cost evaluation was made only of those components required to replace the fixed-bed storage system described in Reference III-1. The costs of all other components of the central power station were scaled from Reference III-1 data. A description of the components required and the cost is given in Table III-8. These costs were determined by the Pricing and Estimating Department, based on hardware sketches and design requirements supplied by the Preliminary Engineering Unit. These costs are based on the flow conditions shown in Figures III-2, III-6, III-7, and III-8, which provided a 6-h storage capability for a 115-MWe night operation. They were later adjusted to 100 MWe and 70 MWe night operation. The total cost for the rotating drum reactor and storage concept was obtained by replacing the fluidized-bed costs and the bed recirculation blower costs with the costs listed in Table III-6 (with the addition of one large hydrator-dehydrator unit).

TABLE III-7

PNEUMATIC CONVEYING SYSTEM DESIGN*

Conveying System	Pipe Diameter† (in.)	Pressure Drop (psi)	Total Power Required (kW)	Nitrogen Total Flow (lb/h)
1.037×10^6 lb/h $Ca(OH)_2$ from Storage Vessel to Hydrator	16	5.1	807	62,900
0.785×10^6 lb/h CaO from Dehydrator to Storage Vessel	14	5.1	600	68,700
1.312×10^6 lb/h CaO from Storage Vessel to Low-Temperature Hydrator	14	8.3	1008	75,200
1.733×10^6 lb/h $Ca(OH)_2$ from Low-Temperature Hydrator to Storage Vessel	18	6.7	1320	118,900
0.336×10^6 lb/h CaO from Storage Vessel to High-Temperature Hydrator	12	3.2	871	64,900
0.433×10^6 lb/h $Ca(OH)_2$ from High-Temperature Hydrator to Storage Vessel	10	5.7	341	35,600

*Based on design conditions shown in Figures III-6, III-7, and III-8
†4 lines

TABLE III-8

FLUIDIZED-BED STORAGE SUBSYSTEM INSTALLED COST*

Item No.	Component Description†	Cost ($000)
1.	4 Large Hydrator-Dehydrator Vessels — 29 ft OD by 47 ft height, 2-1/4 Cr - 1 Mo	3,392
2.	4 Large Heat Recovery Vessels — 8.5 ft OD by 26 ft height, A36 steel	478
3.	4 High-Temperature Hydrators — 7.5 ft OD by 24 ft height, 2-1/4 Cr - 1 Mo	564
4.	4 Small Heat Recovery Vessels, 5 ft OD by 15 ft height, A36 steel	236
5.	4 CaO Storage Vessels with 60° Conical Bottom — 43,000 ft^3, 30 ft OD by 79 ft height, A36 steel	3,200
6.	4 $Ca(OH)_2$ Storage Vessels with 60° Conical Bottom — 43,000 ft^3, 30 ft OD by 79 ft height, A36 steel	3,056
7.	4 Feed Bins for Large Hydrator-Dehydrator with 60° Conical Bottom, 1430 ft^3, 10 ft OD by 24 ft height, A36 steel	288
8.	4 Feed Bins for Small Hydrator with 60° Conical Bottom — 365 ft^3, 6 ft OD by 16.5 ft height, A36 steel	84
9.	8 Receiving Bins for Large Heat Recovery Vessel — 357 ft^3 60° Conical Bottom, 6 ft OD by 16 ft height, A36 steel	208
10.	4 Receiving Bins for Small Heat Recovery Vessel — 60° Conical Bottom, 365 ft^3, 6 ft OD by 16.5 ft height, A36 steel	84
11.	Piping with Insulation, Fittings, and Hangers — 800 ft, 6 in.; 4000 ft, 10 in.; 800 ft, 12 in.; 1600 ft, 14 in.; 800 ft, 16 in.; 800 ft, 18 in., carbon steel pipe	1,944
12.	12 Solids Conveying Blowers, 1 Stage Centrifugal — 4 at 740 hp, 4 at 330 hp, 4 at 85 hp, Elliot high-temperature units	782
13.	N_2 Recirculation Blowers, Vacuum Pumps — 4 at 0.5 hp, 4 at 138 hp, 4 at 15 hp, 1 at 260 hp, Elliot high-temperature units	100
14.	Conveying and Gas Shutoff Valves, twelve 14 in., twelve 10 in. twenty-eight 6 in., carbon steel body, Type 316 stainless steel butterfly, 17-4 stem	106
	Total	14,522

*Based on flows shown in Figures III-6, III-7, and III-8; approximately 115 MWe night operation
†Solids feed valves and internal cyclones are included in cost of feed,receiving, and storage vessels

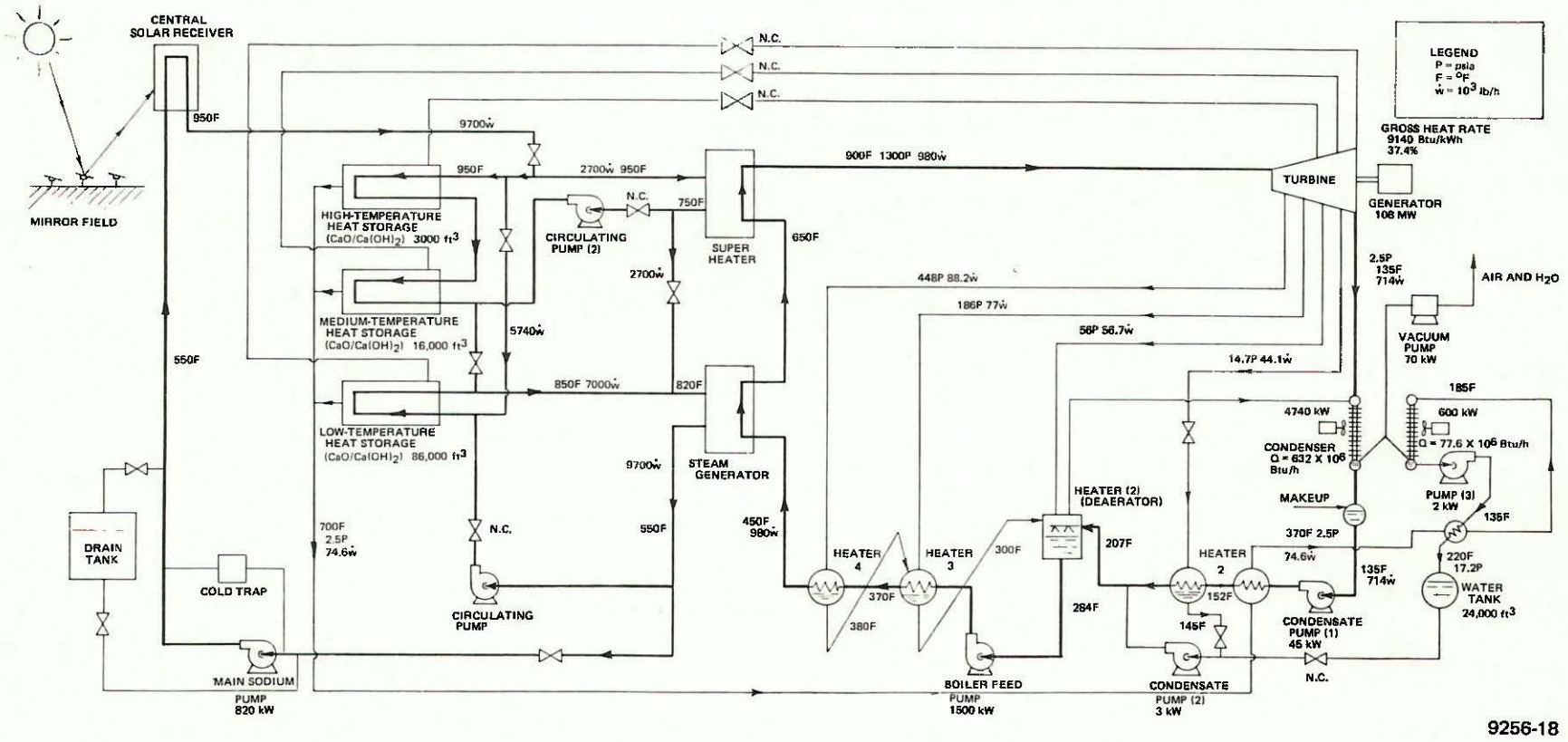

Figure III-9. Flow Diagram of Central Solar Power Plant Coupled With $CaO - Ca(OH)_2$ Fixed-Bed Heat Storage, 100-MW Day Operation

E. ANALYSIS OF POWER STATION OVERALL EFFICIENCY

Daytime, nighttime, and overall station thermal efficiencies were computed for the fluidized-bed and rotating drum concepts at the selected design point of 100-MWe day and 100-MWe night (6-h daily storage capability) operation. A station design point of 100-MWe day and 70-MWe night (6-h daily storage) operation was also computed for the fluidized-bed concept. This latter design was made so that performance and cost results could be compared on an equal basis with the fixed-bed and the HT-43 and hot rock systems described in Reference III-1. Figures III-9, III-10, and III-11 are process flow diagrams for these systems. Figure III-12 shows the design concept for the fixed-bed reactor-storage vessel.

Table III-9 shows a performance comparison for the rotating drum and fluidized bed at 100-MWe night operation and the fluidized-bed, fixed-bed, and HT-43 - hot rocks systems at 70-MWe night operation. Since the net thermal efficiency of the night operation is different from that of daytime operation, the overall station efficiency (η_{oA}) on an annual basis will vary, depending on the ratio of the annual daytime energy production to the annual nighttime production (r_p).

By the definitions, we have

$$\eta_{oA} = \frac{E_a}{Q_a} = \frac{E_d + E_n}{Q_d + Q_n/f_{st}} \qquad \ldots(5)$$

But,

$$Q_d = \frac{E_d}{\eta_d}, \quad Q_n = \frac{E_n}{\eta_n} \qquad \ldots(6)$$

and

$$r_p = \frac{E_d}{E_n} \qquad \ldots(7)$$

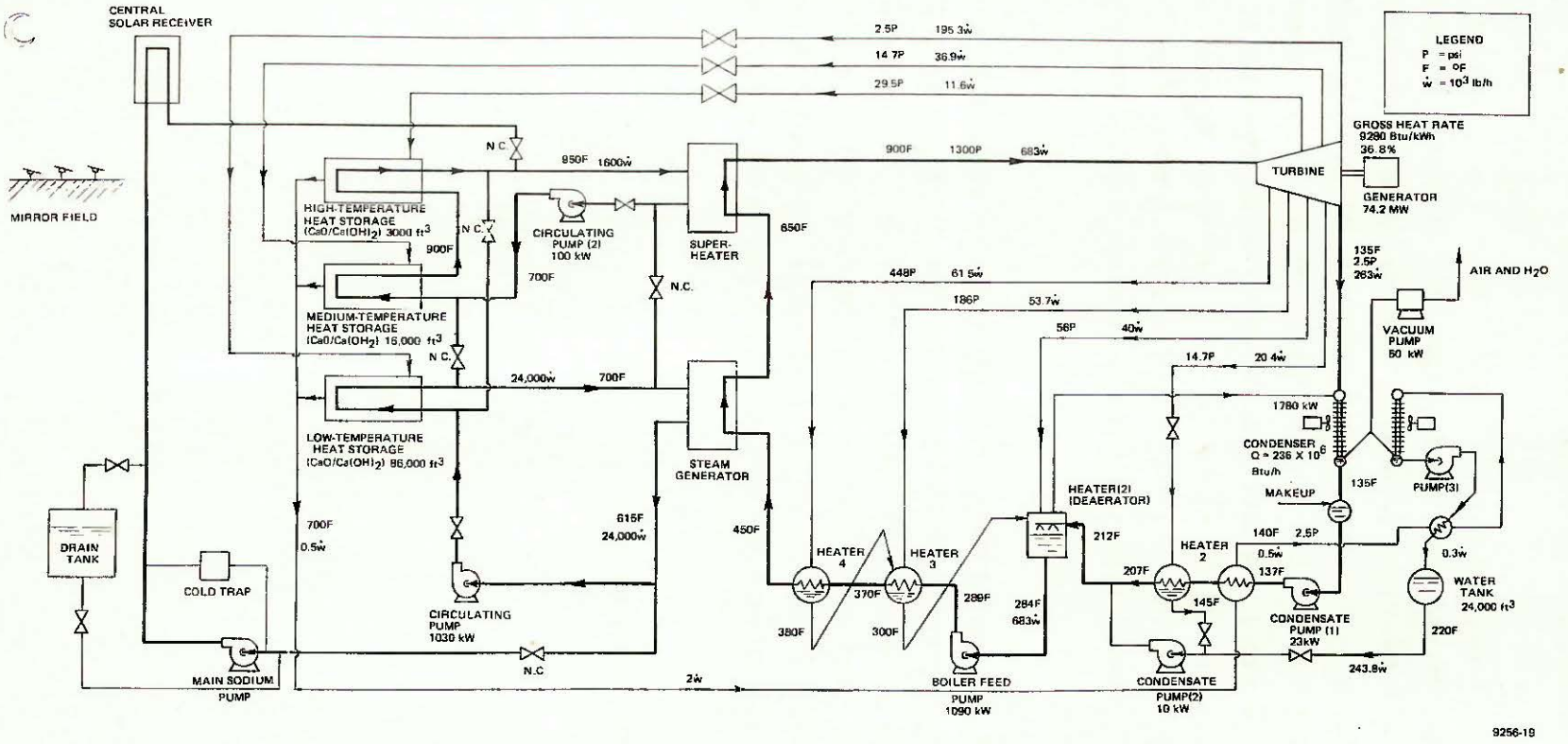

Figure III-10. Flow Diagram of Central Solar Power Plant Coupled With CaO - $Ca(OH)_2$ Fixed-Bed Heat Storage, 70-MW, 6-h Night Operation

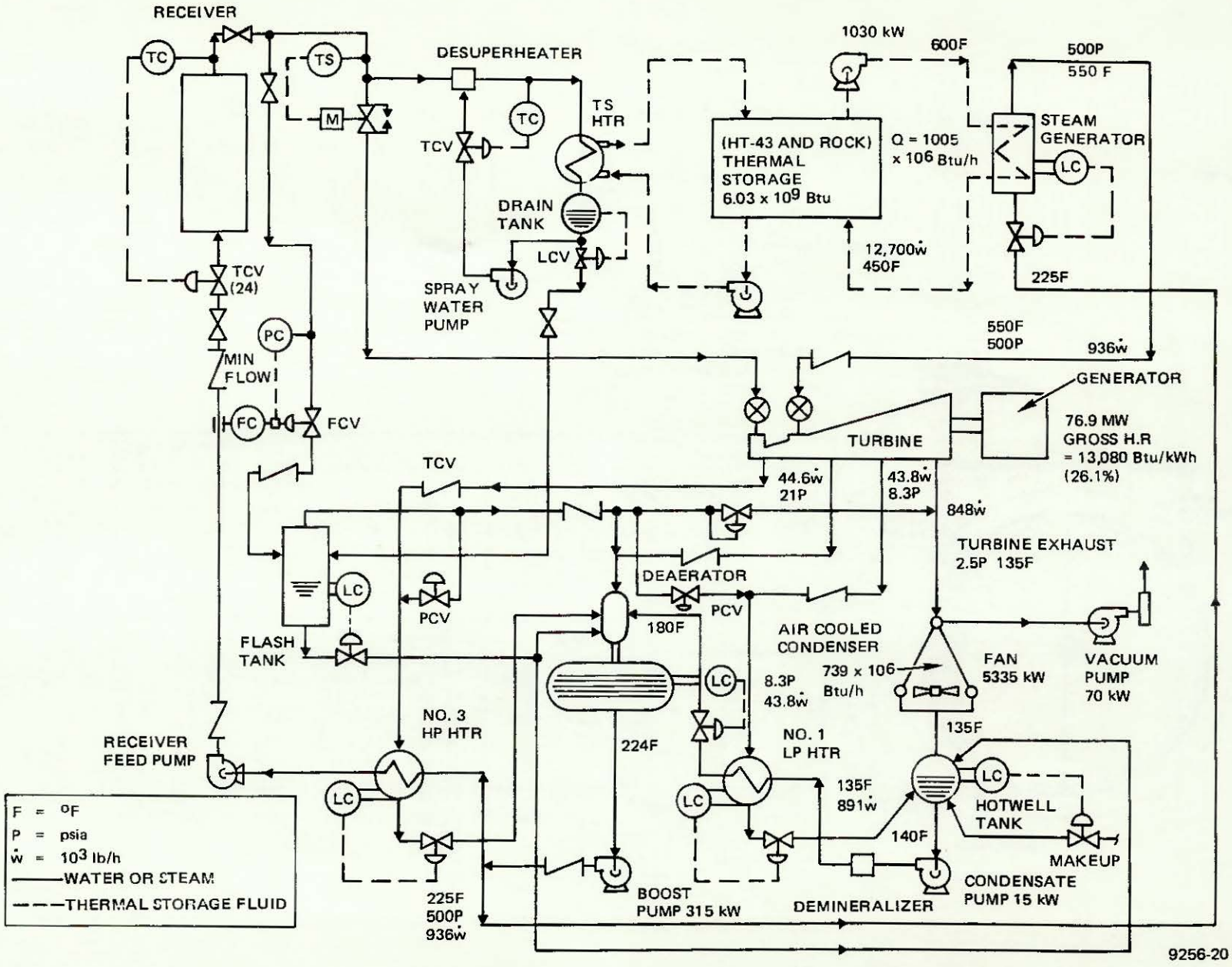

Figure III-11. Flow Diagram of 100-MWe Plant — HT-43 and Hot Rock Heat Storage, 70-MWe Nighttime Operation

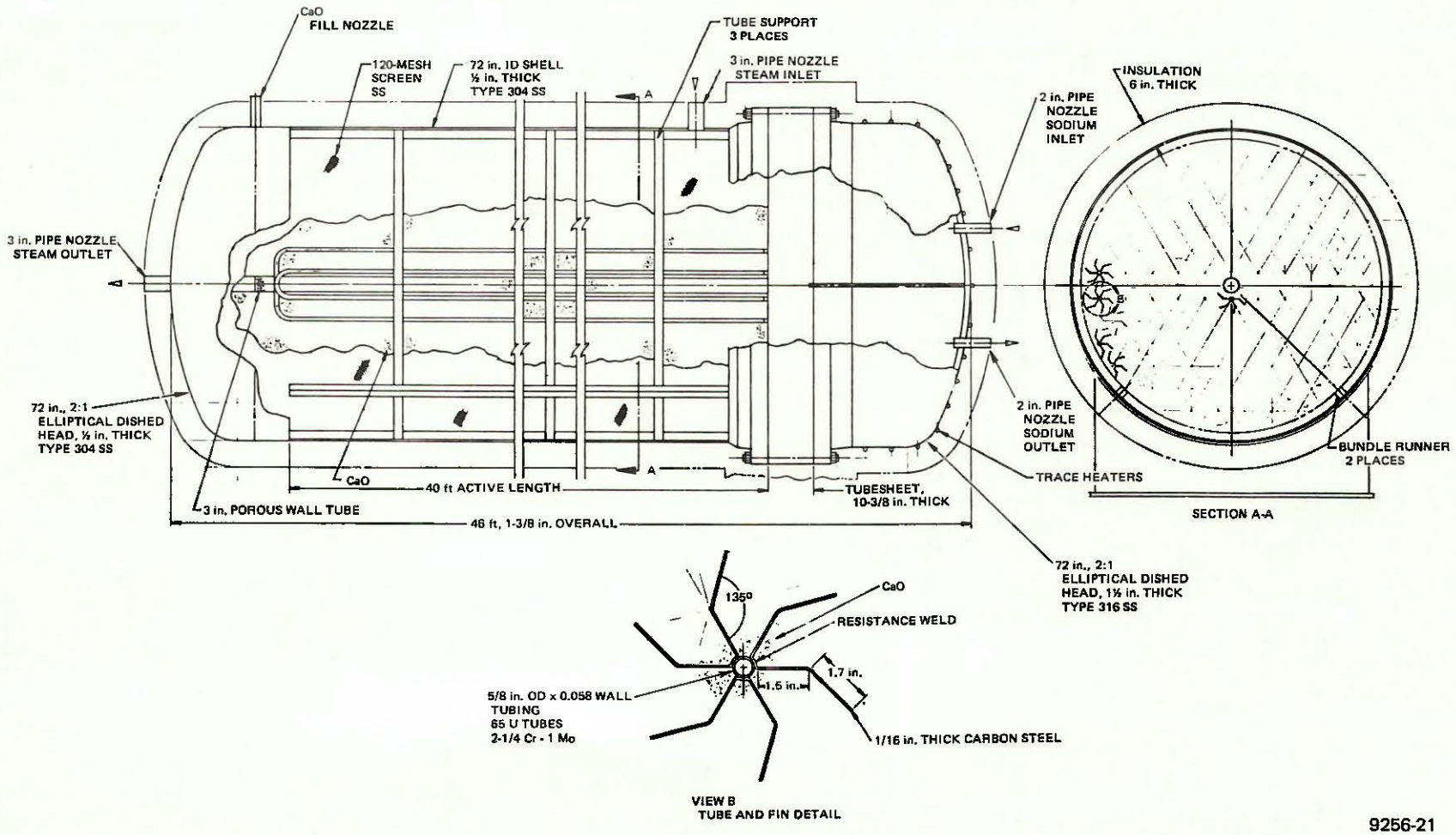

Figure III-12. CaO - $Ca(OH)_2$ Fixed-Bed Storage and Reaction Vessel

TABLE III-9

PERFORMANCE COMPARISION OF STORAGE CONCEPTS
(6-h Daily Storage)

	HT-43* Hot Rocks		CaO - Ca(OH)* Fixed Bed		$CaO - Ca(OH)_2$ Fluidized Bed		$CaO - Ca(OH)_2$ Fluidized Bed		$CaO - Ca(OH)_2$ Rotating Drum	
	Day	Night	Day	Night	Day	Night	Day	Night	Day	Night
Net Power (MWe)	100	70	100	70	100	70	100	100	100	100
Parasitic Power (MWe)	8.0	6.9	8.0	4.2	10.8	5.3	12.5	7.6	24.3	28.8
Steam Temperature (°F)	950	550	900	900	900	900	900	900	900	900
Steam Pressure (psia)	1,800†	500	1,300	1,300	1,300	1,300	1,300	1,300	1,300	1,300
Gross Heat Rate (Btu/kWhe)	8,750	13,000	9,140	9,280	9,164	9,860	9,164	9,860	9,164	9,860
Thermal Efficiency (%)§	36.1	23.8	34.6	34.7	33.7	32.2	33.1	32.2	30.0	26.9
Station Efficiency (%)§	31.1		33.7		31.7		31.0		27.1	

*Values obtained from Reference III-1
†The current design value is 1465 psia
§Refer to page III-41 for definitions of thermal and station efficiencies

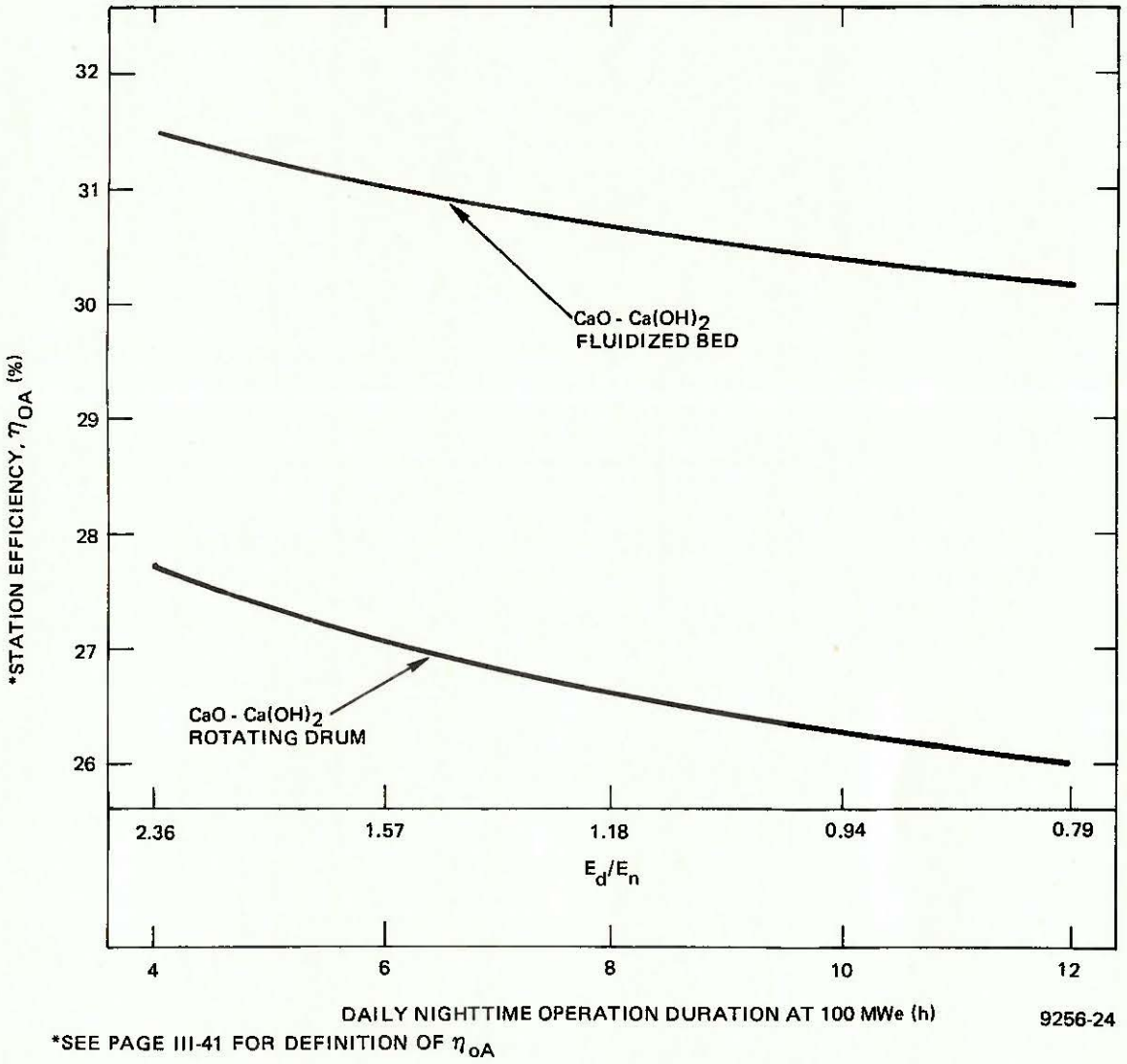

*SEE PAGE III-41 FOR DEFINITION OF η_{oA}

Figure III-13. Overall Station Thermal Efficiency vs Hours of Nighttime Operation at 100 MWe
(E_d is constant at 311.4 x 10^6 kWh/year)

Substituting Equations 6 and 7 into Equation 5 gives

$$\eta_{oA} = \frac{\eta_d \eta_n f_{st}(1 + r_p)}{\eta_d + \eta_n f_{st} r_p} \qquad ...(8)$$

where

E_d = annual net daytime energy production from direct operation (nominal 311.4 x 10^6 kWhe/year)

E_n = annual net night energy production (nominal 138.6 x 10^6 kWhe/year and 198 x 10^6 kWhe/year for 70-MWe and 100-MWe power, respectively, and 6-h daily storage)

η_d, η_n = net station thermal efficiency for the day and night operation, respectively

Q_d, Q_n = thermal energy supplied to the steam generator and superheater (and to the boiler feedwater from fluidized-bed and rotating drum heat recovery vessels) during day and night operation, respectively (kWht/year)

E_a, Q_a = annual net electrical energy production and annual total solar thermal energy collected by the receiver, respectively

f_{st} = fraction of the heat input to the heat storage during daytime that is released during night operation (f_{st} = 1 for the hot rock system, f_{st} = 0.92 for the fixed-bed system, and f_{st} = 0.876 for the fluidized-bed and rotating drum systems)

If $r_{p,t} = r_{p,6}$ for nominal station operation of 6-h nighttime operation (t = 6) at a given power level, then $r_{p,t} = r_{p,6}(6/t)$ for nighttime operation of t hours duration when E_d is kept constant at the nominal value of 311.4 x 10^6 kWhe/year. Numerical values from Equation 8 are plotted for the fluidized-bed and rotating drum systems at 100-MWe night power level in Figure III-13 and for the fixed-bed, fluidized-bed, and hot rock systems at 70-MWe night power level in Figure I-4. Figure III-13 shows that the η_{oA} for the rotating drum is from 3.7 to 4.2% lower than the fluidized-bed system, with the difference increasing with increasing hours of night operation. Figure I-4 shows that η_{oA} for the

TABLE III-10

OPERATING POWER REQUIREMENTS FOR CaO - $Ca(OH)_2$ SYSTEMS*

Component	Fixed Bed 70 MWe Net at Night		Fluidized Bed 70 MWe Net at Night		Fluidized Bed 100 MWe Net at Night		Rotating Drum 100 MWe Net at Night	
	Day	Night	Day	Night	Day	Night	Day	Night
Main Sodium Pump, P7	820	–	1,417	–	2,020	–	2,418	–
Sodium Circulating Pump (High Temperature), P6	–	100	–	90	–	129	–	155
Sodium Circulating Pump (Low Temperature), P5	–	1,030	–	444	–	634	–	759
Boiler Feed Pump, P4	1,500	1,090	1,484	937	1,505	1,338	1,666	1,602
Condensate Pump, P1	45	23	49	20	50	29	55	34
Condensate Pump, P2	3	10	–	13	–	19	–	23
Condensate Pump, P3	2	–	4	–	6	–	7	–
Main Condenser Fan, F1	4,740	1,780	5,155	1,267	5,228	1,813	5,789	2,169
Secondary Condenser Fan, F2	600	–	1,281	58	1,827	83	2,186	99
Main Condenser Vacuum Pump, V1	70	50	49	24	50	35	55	42
Secondary Condenser Vacuum Pump, V2	Incl. above	Incl. above	14	12	20	17	24	21
Secondary Condenser Recycle Pump, V3	–	–	136	–	195	–	233	–
Solids Conveying Blower, B1	–	–	510	1,148	727	1,640	870	1,962
Solids Conveying Blower, B2	–	–	379	806	541	1,152	647	1,378
Solids Conveying Blower, B3	–	–	–	208	–	298	–	356
Nitrogen Recirculating Blower, B4	–	–	225	250	321	358	–	–
Nitrogen Recirculating Blower, B5	–	–	–	28	–	40	–	–
Receiving Bin Vacuum Pump, V4	–	–	1	1	1	1	2	1
Rotating Drum Low-Temperature Dehydrator-Hydrator Motors	–	–	–	–	–	–	8,016	13,073
Rotating Drum High-Temperature Hydrator Motors	–	–	–	–	–	–	–	2,181
Rotating Drum High-Temperature Heat Recovery Motors	–	–	–	–	–	–	–	1,090
Rotating Drum Low-Temperature Heat Recovery Motors	–	–	–	–	–	–	2,340	3,817
Total	7,780	4,083	10,704	5,306	12,491	7,586	24,308	28,762

*Power in kilowatts; all systems are 100 MWe net for day operation

hot rock system is 1.7% lower than the fixed-bed CaO - $Ca(OH)_2$ system at 4 h storage and 4.2% lower at 12 h storage. The increasingly poorer performance of the hot rocks system with increasing night operation is because of the very low efficiency of that system during that time (see Table III-9). The station efficiency for the fluidized-bed system is 1.7% lower than the fixed bed at 4 h storage and 2.5% lower at 12 h daily night operation. The major reason for the performance differences of the CaO - $Ca(OH)_2$ systems is the parasitic power losses. Table III-10 shows a detailed breakdown of these power requirements.

The following assumptions were made for the calculation of the cycle thermal efficiencies in this study and the study of Reference III-1:

1) An internal turbine efficiency of 88% was used for all cases with the exception of night operation of the HT-43 - hot rock system. To take into account the relatively low grade of throttle steam and the high moisture content in the exhaust system, 85% was used for this case.
2) The heat losses from the pipes and equipment are neglected.
3) A combined generator-mechanical efficiency of 98% was used.
4) A pump efficiency of 75% was used for all pumps.
5) A condenser fan efficiency of 75% was used. The temperature increase and pressure drop of the cooling air across the condensers were assumed to be $20^{o}F$ and 1-in. H_2O, respectively.

F. ECONOMIC ANALYSIS AND ASSESSMENT

1. Capital Cost Basis

The power station costs were derived from a study of the HT-43 and hot rock system by McDonnell Douglas Company and described in Reference III-2. Table 2-4 of Reference III-2 gives a cost breakdown for a solar thermal plant (with 100-MWe daytime power capability and 70-MWe nighttime power capability) using a HT-43 and hot rock system with 6-h storage. The values presented in this table were used in this study (increased by 5%/year for 2 years to account for inflation) for the hot rock system with one exception. The thermal storage unit was

TABLE III-11

POWER STATION CAPITAL COST, HT-43 AND HOT ROCK STORAGE SYSTEM*

Component	Cost (1977 Dollars x 10^{-6})			
I. Solar Collection and Transport System				100.7
Collector			80.8	
Integration (Assembly Transport Only)		6.5		
Field Controller Assembly		10.1		
Field Controller	7.1			
Heliostat Cabling	3.0			
Heliostat Assembly		64.2		
Integration	4.4			
Reflector	26.0			
Tracking	4.7			
Drive	17.8			
Heliostat Support	11.3			
Land and Improvement			3.5	
Receiver and Tower			15.8	
Receiver Subsystem		8.0		
Integration	1.0			
Support and Protective Structures	2.0			
Distribution and Collection	0.3			
Absorber	2.8			
Instrumentation	1.6			
Access	0.2			
Miscellaneous	0.1			
Tower Subsystem		4.4		
Riser-Downcomer System		3.4		
Master Control			0.6	
II. Storage Subsystem				14.1
A. Capacity-Related Costs				
Thermal Storage Unit			10.7	
B. Power-Related Costs				
Thermal Charging Assembly			1.3	
Integration Piping and Controls			2.1	
III. Power Generation Subsystem				27.5
Steam Generator			1.9	
Steam Turbine Loop			25.4	
Turbine Generator Plant		16.6		
Electric Plant		2.3		
Structures and Improvements		3.4		
General Plant and Other		3.1		
Circulating Pumps			0.2	
Total Solar Plant				142.3

*100 MWe day, 70 MWe night, 6 h daily storage

increased in cost from 7.2 to 9.7 million dollars because the 90% volumetric storage efficiency used in Reference III-2 should be ~70%. Table III-11 shows the resulting cost breakdown for the HT-43 and hot rock system used in this study.

Table III-12 shows a breakdown of power station costs for the fixed-bed system operating at 100 MWe daytime and 70 MWe nighttime. A detailed breakdown is shown only for those components that differ from the hot rock system. The collector and the land and improvement items were scaled from Table III-11 in proportion to the total solar energy collected. The steam turbine loop was reduced from that of the hot rock system, because a single admission turbine is used rather than the dual admission turbine required for the hot rock system. The costs for the receiver and tower and storage subsystem were obtained from Reference III-1. They were adjusted to incorporate more recent estimates of superheater, steam generator, sodium pump, and heat storage vessel costs.

Table III-13 shows a breakdown of power station costs for the fluidized-bed system operating at 100 MWe daytime and 70 MWe nighttime. A detailed breakdown is shown only for those systems that differ from the fixed-bed system. The storage subsystem cost was scaled directly from the data given in Table III-8.

Tables III-14 and III-15 show power station costs with the fluidized-bed and the rotating drum storage systems. A detailed breakdown is given only for the storage subsystem, since the other components were scaled from similar components in the fixed-bed system.

2. Cost Comparison

A comparison of the total capital investment for a 100-MWe commercial solar power plant is shown in Table III-16 for the fluidized-bed and rotating drum reactor storage systems. The heat storage capacity of both systems is the same — 100-MWe night operation for 6 h, 330 days a year. Both systems produce an equal amount of net electricity annually — 509.4×10^6 kWhe/year.

TABLE III-12

POWER STATION CAPITAL COST, FIXED-BED CaO - $Ca(OH)_2$ STORAGE SYSTEM*

Component	Cost (1977 Dollars x 10^{-6})		
I. Solar Collection and Transport System			93.0
Collector		74.6	
Land and Improvement		3.2	
Receiver and Tower		14.6	
Receiver	4.8		
Riser-Downcomer	3.3		
Piping and Valves	1.0		
Sodium	0.2		
I. and C.	0.2		
Expansion Tank	0.1		
Drain Tank	0.5		
Purification System	0.5		
Inert Gas and Vent	0.5		
Tower	3.5		
Master Control		0.6	
II. Storage Subsystem			17.5
A. Capacity-Related Costs			
Thermal Storage Unit (85 units)		10.7	
Storage Assemblies (85 units)	10.4		
$Ca(OH)_2$, 4067 tons at $60/ton	0.3		
Water Vapor Condenser		1.8	
Water Tank		0.1	
B. Power-Related Costs			
Thermal Charging Assembly, Sodium Pumps		1.6	
Integration Piping and Controls		3.1	
Piping and Valves	1.8		
Sodium	0.1		
Expansion Tank	0.1		
Drain Tank	0.2		
Purification System	0.3		
Instrumentation and Controls	0.2		
Inert Gas and Vent System	0.4		
III. Power Generation Subsystem			29.1
Steam Generator		4.3	
Steam Turbine Loop		24.0	
Circulating Pumps, Sodium Pump		0.8	
Total Solar Plant			139.6

*100 MWe day, 70 MWe night, 6 h daily storage

TABLE III-13

POWER STATION COST, FLUIDIZED-BED CaO - $Ca(OH)_2$ STORAGE SYSTEM*

Component	Cost (1977 Dollars x 10^{-6})	
I. Solar Collection and Transport System		99.8
Collector	79.3	
Land and Improvement	3.4	
Receiver and Tower	15.5	
Master Control	0.6	
II. Storage Subsystem		16.1
A. Capacity-Related Costs		
Thermal Storage Unit	4.1	
CaO Storage Vessels, 4 Units	2.0	
$Ca(OH)_2$ Storage Vessels, 4 Units	1.8	
$Ca(OH)_2$, 4387 tons at $60/ton	0.3	
Water Vapor Condenser	2.0	
Water Tank	0.1	
B. Power-Related Costs		
Thermal Charging Assembly	6.8	
Low-Temperature Hydrator-Dehydrator Vessels, 4 Units	2.0	
Low-Temperature Heat Recovery Vessels, 4 Units	0.3	
High-Temperature Hydrator Vessels, 4 Units	0.4	
High-Temperature Heat Recovery Vessels, 4 Units	0.2	
Feed and Receiving Bins, 20 Units	0.4	
Piping and Valves	1.3	
Sodium Pumps	1.6	
Conveying Blowers	0.5	
Fluidizing Gas Blowers	0.1	
Integration Piping and Controls	3.1	
III. Power Generation Subsystem		29.9
Steam Generator	4.4	
Steam Turbine Loop	24.7	
Circulating Pumps, Sodium Pump	0.8	
Total Solar Plant		145.8

*100 MWe day, 70 MWe night, 6 h daily storage

TABLE III-14

POWER STATION CAPITAL COST, FLUIDIZED-BED CaO - $Ca(OH)_2$ STORAGE SYSTEM*

Component		Cost (1977 Dollars x 10^{-6})
I.	Solar Collection and Transport System	114.6
	Collector	91.9
	Land and Improvement	4.0
	Receiver and Tower	18.0
	Master Control	0.7
II.	Storage Subsystem	23.2
	A. Capacity-Related Costs	
	Thermal Storage Unit	5.8
	CaO Storage Vessels, 4 Units	2.8
	$Ca(OH)_2$ Storage Vessels, 4 Units	2.6
	$Ca(OH)_2$, 6268 tons at $60/ton	0.4
	Water Vapor Condenser	3.1
	Water Tank	0.2
	B. Power-Related Costs	
	Thermal Charging Assembly	9.7
	Low-Temperature Hydrator-Dehydrator Vessels, 4 Units	2.9
	Low-Temperature Heat Recovery Vessels, 4 Units	0.4
	High-Temperature Hydrator Vessels, 4 Units	0.5
	High-Temperature Heat Recovery Vessels, 4 Units	0.2
	Feed and Receiving Bins, 20 Units	0.6
	Piping and Valves	1.9
	Sodium Pumps	2.4
	Conveying Gas Blowers	0.7
	Fluidizing Gas Blowers	0.1
	Integration Piping and Controls	4.4
III.	Power Generation Subsystem	30.4
	Steam Generator	4.5
	Steam Turbine Loop	25.1
	Circulating Pumps	0.8
	Total Solar Plant	168.2

*100 MWe day, 100 MWe night, 6 h daily storage

TABLE III-15

POWER STATION COST, ROTATING DRUM CaO - $Ca(OH)_2$ STORAGE SYSTEM*

Component	Cost (1977 Dollars x 10^{-6})	
I. Solar Collection and Transport System		131.2
Collector	105.2	
Land and Improvement	4.6	
Receiver and Tower	20.6	
Master Control	0.8	
II. Storage Subsystem		69.4
A. Capacity-Related Costs		
Thermal Storage Unit	7.0	
CaO Storage Vessels, 4 Units	3.3	
$Ca(OH)_2$ Storage Vessels, 4 Units	3.2	
$Ca(OH)_2$, 7501 tons at $60/ton	0.5	
Water Vapor Condenser	3.7	
Water Tank	0.2	
B. Power-Related Costs		
Thermal Charging Assembly	52.8	
Low-Temperature Hydrator-Dehydrator, 22 Drum Assemblies	33.0	
Low-Temperature Heat Recovery Drums, 7 Assemblies	7.7	
High-Temperature Hydrator-Dehydrator, 4 Drum Assemblies	6.0	
High-Temperature Heat Recovery Drums, 2 Drum Assemblies	2.4	
Feed and Receiving Bins	0.7	
Piping and Valves	2.2	
Conveying Blowers	0.8	
Integration Piping and Controls	5.7	
III. Power Generation Subsystem		33.6
Steam Generator	5.0	
Steam Turbine Loop	27.7	
Circulating Pumps, Sodium Pump	0.9	
Total Solar Plant		234.2

*100 MWe day, 100 MWe night, 6 h daily storage

TABLE III-16

CAPITAL COST COMPARISON OF FLUIDIZED-BED AND ROTATING DRUM CONCEPTS*

	Fluidized Bed	Rotating Drum
	Cost (1977 dollars x 10^{-6})	
I. Solar Collection and Transport System - $\propto Q_a$	114.6	131.2
Collector	(91.9)	(105.2)
Land and Improvement	(4.0)	(4.6)
Receiver and Tower	(18.0)	(20.6)
Master Control	(0.7)	(0.8)
II. Storage Subsystem	23.2	69.4
A. Capacity-Related Costs - $\propto Q_n$		
Thermal Storage Unit	(5.8)	(7.0)
Water Vapor Condenser	(3.1)	(3.7)
Water Tank	(0.2)	(0.2)
B. Power-Related Costs - $\propto P_n$†		
Thermal Charging Assembly	(9.7)	(52.8)
Integration Piping and Controls	(4.4)	(5.7)
III. Power Generation Subsystem - $\propto P_d$†	30.4	33.6
Steam Generator	(4.5)	(5.0)
Steam Turbine Loop	(25.1)	(27.7)
Circulating Pumps	(0.8)	(0.9)
TOTAL	168.2	234.2

*100 MWe day, 100 MWe night, 6-h daily storage. The annual net energy production is 509.4 x 10^6 kWhe/year, or 1738 x 10^9 Btu/year.

†P_n and P_d are the night and day power generation capability, respectively.

A comparison of the total capital investment for a 100-MWe power plant is shown in Table III-17 for the fluidized-bed, fixed-bed, and HT-43 and hot rock storage systems. The heat storage capacity of these systems is the same — 70-MWe night operation for 6 h, 330 days a year. These three systems all produce an annual net electricity output of 450 kWhe/year.

Table III-16 shows that the cost of the rotating drum system is ~39% higher than the comparable fluidized-bed system. This overwhelming cost difference is caused by the high cost of the large number of rotating drum reactors and the high power required to drive the reactors (resulting in high collector cost).

Table III-17 shows the cost of the fixed-bed system to be only 2% less than that of the hot rock system, and 4% less than that of the fluidized-bed system. It can be seen in Table III-17 that the storage subsystem total cost is somewhat higher for the fixed-bed system compared with the fluidized-bed system. An examination of the cost breakdown of this subsystem shows that the cost of actual storage vessels (thermal storage unit) is significantly lower for the fluidized-bed system ($\$4.1 \times 10^6$ versus $\$10.7 \times 10^6$). The charging components consist only of the sodium recirculation pumps (P5 and P6 in Figure III-3) for the fixed-bed system, but also includes all the items listed in Table III-8 (except for the storage vessels) for the fluidized-bed system. Since the costs in Group II-A (see Tables III-16 and III-17) are proportional to the total energy storage and the costs in Group II-B are proportional to the night power desired, the storage subsystem cost breakdown strongly suggests that for large storage requirements and low night power level, the fluidized-bed system may be more economical than the fixed-bed system.

In order to estimate the plant cost variation with storage capability, the capital cost item of Tables III-16 and III-17 were assumed to vary as follows:

Group I — The capital cost involved in this group is expected to be proportional to the total solar thermal energy collected and used for annual station operation

TABLE III-17

CAPITAL COST COMPARISON OF SOLAR POWER STATION CONCEPTS*

	HT-43 Hot Rocks	$CaO - Ca(OH)_2$ Fixed Bed	$CaO - Ca(OH)_2$ Fluidized Bed
	Cost (1977 dollars x 10^{-6})		
I. Solar Collection and Transport System - $\propto Q_a$	100.7	93.0	99.8
Collector	(80.8)	(74.6)	(79.3)
Land and Improvement	(3.5)	(3.2)	(3.4)
Receiver and Tower	(15.8)	(14.6)	(15.5)
Master Control	(0.6)	(0.6)	(0.6)
II. Storage Subsystem	14.1	17.5	16.1
A. Capacity Related Costs - $\propto Q_n$			
Thermal Storage Unit	(10.7)	(10.7)	(4.1)
Water Vapor Condenser	-	(2.0)	(2.0)
Water Tank	-	(0.1)	(0.1)
B. Power Related Costs - $\propto P_n$†			
Thermal Charging Assembly	(1.3)	(1.6)	(6.8)
Integration Piping and Controls	(2.1)	(3.1)	(3.1)
III. Power Generation Subsystem - $\propto P_d$†	27.5	29.1	29.9
Steam Generator	(1.9)	(4.3)	(4.4)
Steam Turbine Loop	(25.4)	(24.0)	(24.7)
Circulating Pumps	(0.2)	(0.8)	(0.8)
TOTAL	142.3	139.6	145.8

*100 MWe day, 70 MWe night, 6-h daily storage. The annual net energy production is 450.0 x 10^6 kWhe/year, or 1535 x 10^9 Btu/year.

†P_n and P_d are the night and day power generation capabilities, respectively.

where

$r_{p,6} = E_d/E_n$ at 6 h storage = 2.247 at 70-MWe night power level and 1.573 at 100-MWe night power level

CI = total capital investment for a 100-MWe plant with t hours of daily night operation at 70-MWe or 100-MWe power

The total annual energy production, E_a, is given by

$$E_a = E_d + E_{n,6}\,\frac{t}{6} = E_d\left[1 + \frac{1}{r_{p,6}}\left(\frac{t}{6}\right)\right] \qquad ...(11)$$

where

$E_{n,6}$ = total annual net electrical energy produced by 6-h daily night operation = 138.6×10^6 kWhe and 198.0 kWhe for 70-MWe and 100-MWe night power, respectively

The total capital cost and the total annual net electrical power production evaluated using Equations 10 and 11 are shown in Table III-18 for the rotating drum and fluidized-bed systems at 100-MWe power night operation, and in Table III-19 for the fluidized-bed, fixed-bed, and hot rock systems operating at 70-MWe power night operation.

To calculate the annualized cost of electricity for these systems, the annual operation and maintenance costs were assumed to be 1.7% of the total capital cost. Annualized costs were computed for the fluidized-bed, rotating drum and hot rock systems with and without the assumption of an additional yearly 15% replacement of $Ca(OH)_2$ and HT-43. The effect of a 15% material replacement on annualized cost was examined for these systems because of their suspected greater susceptibility to material losses. A cost of \$60/ton (3¢/lb) of $Ca(OH)_2$ and \$1.00/gal. of HT-43 was used. The effect of using a $Ca(OH)_2$ material cost of \$300/ton (15¢/lb) for the fluidized-bed and fixed-bed systems is shown in Table III-20. This high cost represents potential additional material costs for purification of or pelletizing the material.

TABLE III-19

CAPITAL INVESTMENT, OPERATION AND MAINTENANCE COST, AND LEVELIZED BUSBAR COST OF ELECTRICITY FOR 70-MWe NIGHT AND 100-MWe DAY OPERATION*

Hours of Nighttime Operation		4	6	8	10	12	14
Annual Net Energy Production (kWhe x 10^{-6})		403.8	450.0	496.2	542.4	588.6	634.8
E_d/E_n		3.370	2.247	1.685	1.349	1.123	0.963
Capital Costs (1977 \$ x 10^{-6})	HT-43, Hot Rocks	125.2	142.3	159.4	176.5	193.6	210.7
	Fixed Bed	125.2	139.6	154.0	168.3	182.7	197.0
	Fluidized Bed	132.2	145.8	159.4	173.0	186.6	200.3
Maintenance and Operating Cost (1977 \$ x 10^{-6})	HT-43, Hot Rocks	2.13 (2.54)†	2.42 (3.00)	2.7 (3.36)	3.00 (3.72)	3.29 (4.09)	3.58 (4.51)
	Fixed Bed	2.13 —	2.37 —	2.62 —	2.86 —	3.11 —	3.35 —
	Fluidized Bed	2.25 (2.28)	2.48 (2.52)	2.71 (2.76)	2.94 (3.01)	3.17 (3.25)	3.41 (3.50)
Annualized Costs [(\$ x 10^{-6})/year]	HT-43, Hot Rocks	23.4 (24.4)	26.6 (28.0)	29.8 (31.3)	33.0 (34.7)	36.2 (38.1)	39.4 (41.5)
	Fixed Bed	23.4 —	26.1 —	28.8 —	31.5 —	34.2 —	36.9 —
	Fluidized Bed	24.7 (24.8)	27.3 (27.4)	29.8 (29.9)	32.4 (32.5)	34.9 (35.1)	37.5 (37.7)
Levelized Busbar Cost (¢/kWhe)	HT-43, Hot Rocks	5.80 (6.03)	5.92 (6.21)	6.01 (6.31)	6.09 (6.39)	6.15 (6.46)	6.21 (6.54)
	Fixed Bed	5.80 —	5.80 —	5.81 —	5.81 —	5.81 —	5.81 —
	Fluidized Bed	6.13 (6.14)	6.06 (6.08)	6.01 (6.03)	5.97 (6.00)	5.93 (5.96)	5.91 (5.94)

*E_d = constant 311.4 x 10^6 kWhe/year

†Numbers in parenthesis include a 15% yearly replacement of $Ca(OH)_2$ or HT-43, at costs of \$60/ton and \$1/gal., respectively.

TABLE III-20

EFFECT OF HIGH $Ca(OH)_2$ COST ON POWER STATION COSTS FOR 70-MWe NIGHT AND 100-MWe DAY OPERATION*

Hours of Nighttime Operation		4	6	8	10	12	14
Annual Net Energy Production (kWhe x 10^{-6})		403.8	450.0	496.2	542.4	588.6	634.8
E_d/E_n		3.370	2.247	1.685	1.349	1.123	0.963
Capital Costs (1977 \$ x 10^{-6})	Fixed Bed	125.2 (125.9)†	139.6 (140.6)	154.0 (155.3)	168.3 (169.9)	182.7 (184.7)	197.0 (199.3)
	Fluidized Bed	132.2 (132.9)	145.8 (146.9)	159.4 (160.8)	173.0 (174.8)	186.6 (188.7)	200.3 (202.8)
Maintenance and Operating Cost (1977 \$ x 10^{-6})	Fixed Bed	2.13	2.37	2.62	2.86	3.11	3.35
	Fluidized Bed	2.25	2.48	2.71	2.94	3.17	3.41
Annualized Costs [(\$ x 10^{-6})/year]	Fixed Bed	23.4 (23.5)	26.1 (26.3)	28.8 (29.0)	31.5 (31.7)	34.2 (34.5)	36.9 (37.2)
	Fluidized Bed	24.7 (24.8)	27.3 (27.4)	29.8 (30.0)	32.4 (32.6)	34.9 (35.2)	37.5 (37.9)
Levelized Busbar Cost (¢/kWhe)	Fixed Bed	5.80 (5.83)	5.80 (5.84)	5.81 (5.85)	5.81 (5.85)	5.81 (5.86)	5.81 (5.86)
	Fluidized Bed	6.13 (6.15)	6.06 (6.10)	6.01 (6.05)	5.97 (6.02)	5.93 5.98	5.91 5.96)

*E_d = constant 311.4 x 10^6 kWhe/year

†Numbers in parantheses are for a $Ca(OH)_2$ cost of \$300/ton; numbers without parantheses (maintenance and operations costs apply to both cases) are for a $Ca(OH)_2$ cost of \$60/ton

The annualized cost and the levelized cost of electricity in Tables III-18, III-19, and III-20 were calculated using a standardized revenue methodology prepared by the Jet Propulsion Laboratory.[III-8] The nominal values of the parameters used in the calculation are as follows:

Base Year	1977
Year of Start of Commercial Operation	1990
Lifetime (years)	30
Internal Rate of Return (%)	8
Capital Recovery Factor	0.0888
Annualized Fixed Charge Rate	0.1483

No equipment replacement was assumed.

Table III-18 shows that the levelized busbar cost of electricity ($\overline{BBEC}$) for the rotating drum system is 42% higher than for the fluidized-bed system at 4 h storage time, and 34% higher at 12 h storage when no material replacement is assumed. With 15% material replacement, the rotating drum system $\overline{BBEC}$ is 42% and 34% higher than the $\overline{BBEC}$ for the fluidized bed at 4 and 12 h storage, respectively. The $\overline{BBEC}$ cost for the higher power fluidized bed (100-MWe night operation) is 5.99¢/kWhe at 12 h storage. This is about 3% higher than the lowest value shown in Table III-19 (5.80) for the fixed-bed system at 70-MWe night capability.

The effect of 15% yearly material replacement was about the same for both the rotating drum and fluidized-bed systems: The $\overline{BBEC}$ was increased by 2¢/kWhe at 4 h storage and 3¢ to 5¢/kWhe at 12 h storage, with the fluidized-bed system having the smaller increase.

Table III-19 compares the $\overline{BBEC}$ for the fixed-bed, fluidized-bed, and hot rock systems at 70-MWe power for night operations. These values are also plotted in Figure I-5. When no yearly material losses are assumed, the $\overline{BBEC}$ for the hot rock system is equal to that of the fixed-bed system only at the 4-h storage

point. With increasing storage capacity, the $\overline{BBEC}$ for the hot rock system increases rapidly while the fixed-bed $\overline{BBEC}$ remains constant. At 12 h storage, the $\overline{BBEC}$ for the hot rock system is about 6% higher than for the fixed-bed system. When a 15% yearly material loss is assumed for the hot rock system, its $\overline{BBEC}$ is 4 to 11% higher than for the fixed bed system.

The $\overline{BBEC}$ for the fluidized bed, with no yearly material losses, is about 6% higher than for the fixed-bed system at 4 h storage duration, but approaches the fixed-bed value with increasing storage capacity. With a 15% yearly material loss (at \$60/ton), the fluidized-bed $\overline{BBEC}$ is 5.9% higher than the $\overline{BBEC}$ for the fixed bed at 4 h storage and is about 2.6% higher at 12 h storage capability.

Figure I-6 shows a plot $\overline{BBEC}$ versus total annual net electricity for the fixed-bed system at 70-MWe nighttime power, and the fluidized-bed system at both the 70-MWe and 100-MWe nighttime operating power levels. The curve for the fluidized-bed at 70 MWe is very steep and is approaching the fixed-bed curve for high storage capacity. Figure I-6 also indicates that the higher power level mode of operation (100-MWe night) for the fluidized-bed is from 2 to 3% more costly than the 70-MWe (night) fluidized bed.

Table III-20 shows that the effect of increasing the $Ca(OH)_2$ cost from \$60/ton to \$300/ton is to increase the levelized busbar cost by 4¢ to 5¢/kWhe.

G. THE EFFECT OF INCREASED OPERATING TEMPERATURE

The obvious method to improve the power station performance with any of the storage concepts is to increase the temperature level of operation during both daytime and nighttime operation. The HT-43 and hot rocks system, however, was analyzed at steam temperature levels ($950^{o}F$ daytime and $550^{o}F$ nighttime) that are at the upper limits of its capability. The steam operating conditions assumed ($950^{o}F$, 1800 psia daytime and $550^{o}F$, 500 psia nighttime) are higher than proposed ($950^{o}F$, 1465 psia daytime and $525^{o}F$, 385 psia nighttime) in more recent studies by McDonnell Douglas.[III-9] During daytime the steam temperature is limited by practical solar receiver capabilities with a relatively poor heat

TABLE III-21

PERFORMANCE COMPARISON FOR DIFFERENT OPERATING TEMPERATURES*

	Low-Temperature System		High-Temperature System	
	Day	Night	Day	Night
Net Power (MWe)	100	70	100	70
Steam Temperature (^{o}F)	900	900	1000	1000
Steam Pressure (psia)	1300	1300	1800	1800
Thermal Efficiency (%)	33.7	32.2	35.8	34.3
Station Efficiency (%)	31.7		33.8	

*Fluidized-bed systems, 70-MWe night, 6-h storage

transfer fluid (water-steam), and during nighttime the steam temperature is limited by a maximum operating temperature of about 600°F for the HT-43 oil. The dual mode of turbine operation also results in a more complex dual admission turbine.

The sodium - CaO - $Ca(OH)_2$ system, on the other hand, has a much higher operating temperature capability than was used in this detailed study. Liquid sodium can be delivered from the solar receiver at a temperature of ~1200°F, in comparison with the 950°F used in this study. The upper temperature limit for hydration-dehydration of CaO - $Ca(OH)_2$ will probably be limited by its equilibrium dissociation pressure to ~1100°F, where its dissociation pressure is ~50 psia.

Because the sodium - CaO - $Ca(OH)_2$ system has considerable margin for uprating its operation temperature level, a brief study was made of the effect of increasing the system temperature level 100°F. The fluidized-bed system with 100-MWe day and 70-MWe night net power production was studied. The throttle steam inlet conditions were increased to 1800 psia and 1000°F from 1300 psia and 900°F. The steam exit pressure and quality were the same (2.5 psia and 87.5%) in both cases. The temperature of the sodium from the receiver increased from 950°F to 1050°F, and the high-temperature hydrator temperature increased from 1000°F to 1100°F. A detailed thermodynamic analysis was not made of the entire system, but rather an estimate was made of the improvement in the turbine cycle output. The results, however, should be an accurate indication of the effects.

Table III-21 compares the operating conditions and performance for the two 70-MWe fluidized-bed systems. Both day and night thermal efficiencies and the overall station efficiency were increased by 2.1% with operation at the higher temperature level. Table III-22 shows the effect of operating temperature on capital cost. All major subsystems were lower in cost with higher operating temperature, with the largest reduction (7×10^6 dollars) being the solar collection system. The total power station capital cost was reduced from $\$145.8 \times 10^6$ to $\$136.4 \times 10^6$ with higher operating temperature. Table III-23 shows the variation in overall station efficiency and levelized busbar cost over a 4- to 14-h storage range. The overall efficiency difference varied from 2.1 to 2.0%

TABLE III-22

CAPITAL COST COMPARISON FOR DIFFERENT OPERATING TEMPERATURES

	Low-Temperature System (900°F)	High-Temperature System (1000°F)
I. Solar Collection and Transport System — $\propto Q_a$	99.8	92.8
Collector	(79.3)	(74.4)
Land and Improvement	(3.4)	(3.2)
Receiver and Tower	(15.5)	(14.6)
Master Control	(0.6)	(0.6)
II. Storage Subsystem	16.1	15.4
A. Capacity-Related Costs — $\propto Q_n$		
Thermal Storage Unit	(4.1)	(3.8)
Water Vapor Condenser	(2.0)	(2.0)
Water Tank	(0.1)	(0.1)
B. Power-Related Costs — $\propto P_n$		
Thermal Charging Assembly	(6.8)	(6.4)
Integration Piping and Controls	(3.1)	(3.1)
III. Power Generation Subsystem — $\propto P_d$	29.9	28.2
Steam Generator	(4.4)	(4.2)
Steam Turbine Loop	(24.7)	(23.2)
Circulating Pumps	(0.8)	(0.8)
Total†	145.8	136.4

*Fluidized-bed systems, 70-MWe night, 6-h storage
†1977 dollars x 10^{-6}

TABLE III-23

EFFECT OF OPERATING TEMPERATURE ON η_{oA} AND $\overline{BBEC}$*

Nighttime Operation (h)		4	6	8	10	12	14
Annual Net Energy Production (kWne x 10^{-6})		403.8	450.0	496.2	542.4	588.6	634.8
E_d/E_n		3.370	2.247	1.685	1.349	1.123	0.963
Overall Station Efficiency (η_{oA})	Low-Temperature System (900°F steam)	0.322	0.317	0.314	0.311	0.308	0.306
	High-Temperature System (1000°F steam)	0.343	0.338	0.334	0.331	0.328	0.326
Levelized Busbar Cost (¢/kWhe)	Low-Temperature System (900°F steam)	6.13	6.06	6.01	5.97	5.93	5.91
	High-Temperature System (1000°F steam)	5.73	5.67	5.62	5.58	5.55	5.52

*70-MWe night, 100-MWe day, fluidized-bed systems, E_d = constant 311.4 x 10^6 kWhe/year

over the storage range, and the levelized busbar cost difference varied from 0.40¢ to 0.38¢/kWhe over the storage range.

These preliminary results indicate that there is a significant gain in CaO - $Ca(OH)_2$ system performance and a reduction in system cost with operation at 100°F higher steam temperature. This higher operating temperature appears easily achievable technically and should be considered in future detailed system studies.

H. EVALUATION, ASSESSMENT, AND RANKING OF THE SYSTEMS

Based on the results of this systems study and concurrent laboratory studies (under Tasks 1, 2, and 3 of this contract) of the hydration and dehydration characteristics of CaO - $Ca(OH)_2$, an initial assessment and ranking of the three CaO - $Ca(OH)_2$ storage concepts (fixed bed, fluidized bed, and rotating drum) has been made.

Laboratory results on reagent-grade $Ca(OH)_2$ power indicated that nearly 100% dehydration and hydration can be achieved in a reasonable length of time (45 min for dehydration and 15 min for hydration), even after 1000 cycles, on very small-size (~10 g) samples. The cycling tests indicated potential corrosion and material packing problems. The dehydration process also took place with approximately a 10-psi difference between the equilibrium dissociation pressure and the water vapor pressure above the sample. An excessive material packing could cause a restriction to the flow of steam into and out of the bed, with a consequent reduction in the rate of the reaction. For a power station application, as seen in this study, very high steam flow rates are required.

Other laboratory studies did verify that the heat of reaction and the equilibrium dissociation pressure corresponded with JANAF data.

Based on laboratory data obtained to date, the CaO - $Ca(OH)_2$ energy storage concept warrants further study.

The systems studies were carried out using two optimistic assumptions:

1) No external heat losses
2) The hydration and dehydration steam pressures corresponded to the equilibrium dissociation pressure at the solids temperature.

The requirement for a significant pressure difference between the equilibrium and actual will reduce the system efficiency relative to other storage concepts.

Based on this systems study, the CaO - $Ca(OH)_2$ chemical energy storage concept is more economical than the HT-43 and hot rock thermal storage concept. Of the three CaO - $Ca(OH)_2$ systems, the rotating drum concept was 50% more costly to operate and does not warrant further study. Both the fixed-bed and fluidized-bed concepts are worth further study. The fixed-bed concept was more economical for up to 14 h storage, but the fluidized-bed system may be more economical for greater storage capacity. The fluidized-bed system may appear more attractive when using a power station energy model different from the one used here.

Since the fixed-bed system is by far the simpler to operate, it is the preferred system for development if a choice has to be made between them at this time. However, because applications are probable where the fluidized-bed system is less costly, and because operational problems may occur with the fixed bed which can be overcome in a fluidized bed (or vice versa), both concepts should be studied further.

Since the operational characteristics of the fixed and fluidized beds have not been demonstrated on any scale, it is not possible to decide conclusively which is the better system. A test of a 4- to 6-in. scale model with internal heating and cooling with scaled system flows would provide the type of data needed to begin to demonstrate the practicality of the concept. These bench-scale models would provide information on such questions as reaction rate versus driving pressure differential, fixed-bed packing or plugging tendency causing

pressure buildup and loss of contact with heating and cooling surface, the effect the large volume changes on fluidized-bed stability, and the heat transfer rates in each type of bed. The fluidized-bed testing has the prerequisite, however, of locating or fabricating suitable sized stable and reactive particles (300 to 700 μ range).

Once some practical and encouraging experimental data have been obtained, further theoretical reaction modeling studies and systems applications will prove to be useful to the development of the concepts.

REFERENCES

III-1. D. K. Chung, "An Economic Assessment of the Application of a $CaO-Ca(OH)_2$ Thermal Energy Storage System Applied to a Commercial Solar Power Station," N162TI120008 (September 19, 1977)

III-2. Raymon W. Hallet, Jr. and Robert L. Gervais, "Central Receiver Solar Thermal Power System, Phase 1 Final Report," (CDRL Item 1) MacDonnell Douglas Company (January 1976)

III-3. J. Pata and M. Hartman, "Minimum Fluidization Velocities of Lime and Limestone Particles," Ind. Eng. Chem. Process Des. Dev., 17, No. 3 (1978)

III-4. Joseph F. Frantz, "Design for Fluidization," Chem. Eng. (September 17, 1962)

III-5. W. L. Badger and W. L. McCabe, "Elements of Chemical Engineering," 2nd Edition, McGraw-Hill Book Company

III-6. C. Y. Wen and Y. N. Yu, "Mechanics of Fluidization," Chem. Eng. Progr. Symposium Series No. 62, Vol 62 (1966)

III-7. Air Pollution Engineer Manual, 2nd Edition, U.S. Environmental Protection Agency, Publication No. AP-40, pp 365-367

III-8. J. W. Doane, et al., "The Cost of Energy from Utility-Owned Solar Electric Systems," (JPL 5040-29, ERDA/JPL-1012-76/3) Jet Propulsion Laboratory, Pasadena, California (June 1976)

III-9. "Central Receiver Solar Thermal Power System," SAN-1108-76-8, MDC G6776, Volume I Executive Overview, MacDonnell Douglas Corp. (October 1977)

IV. PROBLEM AREAS AND RECOMMENDED SOLUTIONS

Although both fixed-bed and fluidized-bed configurations appear to be viable on the basis of our systems engineering and economic analyses to date, uncertainties remain to be resolved in both systems. Most of the work thus far has been with the fixed-bed configuration. Three areas require additional evaluation: (1) optimization of starting materials, (2) heat and mass transfer over long paths in cyclic operation, and (3) structural materials compatibility.

Optimization of Starting Materials

This requirement exists both in the fixed- and fluidized-bed concepts. The early experiments with fixed beds used a granulated form of active material, while the experimental results discussed in Section II of this report were obtained with a reagent-grade powder. Changes such as caking were observed, but they did not affect chemical reactivity in the configurations tested. Further study before extrapolating to the larger scale of plant reactors, is, however, required. A systematic experimental investigation of particle (or pellet) preparation, shape, and size distribution is needed in order to supply information for engineering designs. The data would be especially useful for the fluidized bed, where, as indicated in Section III of this report, the bed design criteria are satisfied by a relatively narrow range of particle size, 300 to 700 μm.

Heat and Mass Transfer Over Long Paths in Cyclic Operation

The cyclic operations data discussed in this report and in earlier publications were obtained with shallow beds (1/8 to ~3/4 in. thickness), principally to ensure hydration and dehydration in relatively short times. Plant-scale, fixed-bed reactor designs have reaction paths of the order of a meter in length, an extrapolation that requires experimental verification. The needed data could could be obtained from bench-scale experiments with a model reactor whose section provided the desired long path.

Blanketing of the reacting surfaces by noncondensible gases was identified as an operational problem in Section II of this report. The remedy appears to be simply to pump down the system at appropriate intervals.

Structural Materials Compatibility

Although CaO and $Ca(OH)_2$ are not usually considered to be inherently very corrosive materials, interaction with the Type 304 stainless steel structural material was observed in the experiments discussed in Section II of this report. The relatively high operating temperatures (350 to 550°C) are within the known range for sensitization of stainless steel. In the absence of metallographical investigation, however, it is not possible to identify a corrosion mechanism positively and to conduct a systematic evaluation of alternate structural materials (if required). Useful information for future design could be obtained by a metallurgical study of the stainless steel reactors used in our experiments, and by an evaluation of stresses imposed on the reactor components by temperature and volume changes occurring during operation.

A great amount of uncertainty exists in the projected performance of the fluidized bed. Very little experimental work has been done to resolve the open questions. The uncertainties include the dimensional stability of the active material particles; the effects of pneumatic conveying and fluidizing on particle size and physical characteristics; the effects on system performance of bed expansion, particle carryover, fluidization gas velocity, and particle characteristics; and the overall heat and mass transfer rates achievable, in comparison with the high values projected in Section III of this report.

Useful data bearing on all of these questions could be obtained by an experimental investigation on subscale-size reactors. A sound approach would be to start with glass equipment which has a cross section of a few inches in order to permit direct observation of the bed performance. This study would be followed by experiments with larger, metal reactor scale models. Results of the materials optimization investigation (above) could be combined with the experimental reactor study to provide data for future fluidized-bed system design.

V. CONCLUSION

A very substantial amount of information about the CaO - $Ca(OH)_2$ reaction has been developed to date: the reaction is completely reversible, the rates of reaction are acceptable, the heat of reaction is as expected, and the material can be cycled at least 1000 times without inherent degradation.

Thus, although uncertainties remain at this time, inorganic oxide-hydroxide thermal storage appears to be very attractive, especially since the materials are inexpensive. The products of reaction are basically very safe (one of the products is water which is, of course, universally available), the energy density can potentially be very high, the energy can be transported, and the energy can be stored indefinitely.

APPENDIX

RELATED DOCUMENTS

ENERGY SYSTEMS GROUP DOCUMENTS*

1. G. Ervin, "Solar Heat Storage Based on Inorganic Chemical Reactions," NSF-RA-N-75-041, Proceedings of the Workshop on Solar Energy Storage Subsystems for the Heating and Cooling of Buildings, Charlottesville, Virginia, April 16-18, 1975

2. G. Ervin, Jr., D. K. Chung, and T. H. Springer, "A Study of the Use of Inorganic Oxides for Solar Energy Storage for Heating and Cooling of Buildings, Final Report, June 1, 1974 - July 31, 1975," NSF/RANN/SE/GI-44126/FR/75/2, AI-75-63 (October 1975)

3. G. Ervin, "Solar Heat Storage Based on Inorganic Chemical Reactions," Paper presented at the 1965 Solar Energy Congress, July 28 - August 1, 1975, Los Angeles, extended abstract published in the Proceedings of the Congress

4. G. Ervin, "Experimental Test of Gas Heat Transfer System for Hydroxide Heat Storage," AI-ERDA-13176 (October 29, 1976)

5. G. Ervin, "Hydration-Dehydration Cycling of MgO - $Mg(OH)_2$ for Application to Solar Heat Storage Systems," AI-ERDA-13178 (September 30, 1976)

6. G. Bauerle, et al., "Storage of Energy by Inorganic Oxides and Hydroxides," Proceedings of the International Solar Energy Society Meeting, Volume 8, pp 192-218, Winnipeg, Canada, August 16-19, 1976

7. T. Springer, et al., "Inorganic Oxide and Hydroxide Reversible Chemical Storage Systems," ERDA Semiannual Review of Total Energy Systems, Small Electric Applications, Collector Technology, and Research and Development Projects, Lawrence Berkeley Laboratory, July 21-22, 1976

8. T. Springer, et al., "Solar Energy Storage for Heating and Cooling of Buildings, Contract AT(04-3)-701 Task 33, Review of Applications Analysis and Economic Assessments," presented at Sandia Livermore Laboratories on December 10, 1976

9. T. Springer, et al., "ERDA Thermal Energy Storage Program," Information Exchange Meeting, Cleveland, Ohio, September 8-9, 1976

10. D. K. Chung, "Multitubular Reactor Analysis of a MgO - $Mg(OH)_2$ System," AI Internal Document No. TI-001-130-049 (February 13, 1975)

11. J. Guon, "Economic Comparison of Calcium Oxide and 'Hot Rocks' Storage Systems," AI Internal Document No. N162TI160001 (January 27, 1977)

*Energy Systems Group was formerly Atomics International (AI).

12. D. K. Chung, "Effect of Presence of Air on the Rate of Hydration of a MgO - $Mg(OH)_2$ Heat Storage System," AI Internal Document No. N162TI130001 (January 12, 1976)

13. D. K. Chung, "Effect of Presence of Noncondensibles on the Rate of Hydration and Dehydration of Spherical MgO - $Mg(OH)_2$ Pellets," AI Internal Document No. N162TI130002 (March 5, 1976)

14. D. K. Chung, "Application of MgO - $Mg(OH)_2$ and CaO - $Ca(OH)_2$ as a Daily and Seasonal Heat Storage System for Heating and Cooling of Buildings," AI Internal Document No. N162TI130004 (October 27, 1976)

15. D. K. Chung, "Application of Seasonal Solar Heat Storage for Crop Drying, Process Steam Generation, Electrical Power Generation, and Water Pumping," AI Internal Document No. N162TI130006 (October 25, 1978)

16. G. L. Bauerle, "Preliminary Specification for Magnesium Oxide - Hydroxide and Calcium Oxide - Hydroxide Heat Storage Materials," AI Internal Document No. N162TI120001 (October 18, 1976)

17. G. P. Hajela, "Application of MgO - $Mg(OH)_2$ Storage System for Electric Power Generation," AI Internal Document No. N162TI130005 (June 18, 1976)

18. R. D. Rennick, R. L. Gay, and G. Ervin, "Conceptual Fluidized-Bed Design for Calcium Oxide Solar Energy Storage," AI Internal Document No. N162TI130009 (September 27, 1977) (to be released)

19. D. K. Chung, "An Economic Assessment of the Application of a CaO - $Ca(OH)_2$ Thermal Energy Storage System Applied to a Commercial Solar Power Station," AI Internal Document No. N162TI120008 (September 19, 1977) (to be released)

20. G. P. Hajela, "Solar Heating and Cooling of Buildings Using MgO - $Mg(OH)_2$ Thermal Storage," AI Internal Document No. N162TI130007 (September 28, 1977) (to be released))

21. G. Ervin, "Solar Heat Storage Using Chemical Reactions," Journal of Solid-State Chemistry, 22, 1, 51 (1977)

DOCUMENTS BY OTHERS

1. D. R. Glasson, "Reactivity of Lime and Related Oxides. I. Production of Calcium Oxide," J. Appl. Chem., 8, 793 (December 1958)

2. D. R. Glasson,"Reactivity of Lime and Related Oxides. II. Sorption of Water Vapor on Calcium Oxide," J. Appl. Chem., 8, 798 (December 1958)

3. D. R. Glasson, "Reactivity of Lime and Related Oxides. III. Sorption of Liquid Water on Calcium Oxide ('Wet' Hydration)," J. Appl. Chem., 10, 38, (January 1960)

4. D. R. Glasson, "Reactivity of Lime and Related Oxides. IV. Carbonation of Lime," J. Appl. Chem., 10, 41 (January 1960)

5. D. R. Glasson, "Reactivity of Lime and Related Oxides. V. Crystal Changes in Hydrated Lime at Different Temperatures," J. Appl. Chem., 11, 24 (January 1961)

6. D. R. Glasson, "Reactivity of Lime and Related Oxides. VI. Crystal Changes in Carbonated Lime at Different Temperatures," J. Appl. Chem., 11, 28 (January 1961)

7. D. R. Glasson, "Reactivity of Lime and Related Oxides. VII. Crystal Size Variations in Calcium Oxide Produced From Limestone," J. Appl. Chem., 11, 201 (June 1961)

8. D. R. Glasson, "Reactivity of Lime and Related Oxides. VIII. Production of Activated Lime and Magnesia," J. Appl. Chem., 13, 111 (March 1963)

9. D. R. Glasson, "Reactivity of Lime and Related Oxides. IX. Hydration of Magnesium Oxide," J. Appl. Chem., 13, 119 (March 1963)

10. D. R. Glasson, "Reactivity of Lime and Related Oxides. X. Production of Activated Alkaline Earth Carbonates," J. Appl. Chem., 13, 124 (March 1963)

11. D. R. Glasson, "Reactivity of Lime and Related Oxides. XI. Production of Dolomitic Lime," J. Appl. Chem., 14, 121 (March 1964)

12. D. R. Glasson, "Reactivity of Lime and Related Oxides. XII. Hydration of Dolomitic Lime," J. Appl. Chem., 14, 121 (March 1964)

13. D. R. Glasson, "Reactivity of Lime and Related Oxides. XVI. Sintering of Lime," J. Appl. Chem., 17, 91 (April 1967)

14. J.A.C. Samms and B. E. Evans, "Thermal Dissociation of $Ca(OH)_2$ at Elevated Pressures," J. Appl. Chem., 18 (January 1968)

15. R. Barker, "The Reactivity of Calcium Oxide Towards Carbon Dioxide and Its Use for Energy Storage," J. Appl. Chem. Biotechnol., 24, 221 (1974)

16. N. G. Dave and S. K. Chopra, "Preparation and Thermal Decomposition of Calcium Hydroxide Crystals," J. Am. Ceram. Soc., 575 (October 1966)

17. H. P. Cahoon and P. D. Johnson, "Effects of Chemical Additions on the Hydration Rate of Fired Quicklime (CaO)," J. Am. Ceram. Soc., 34(8), 230, (1951)

18. J. F. Gillott, "Carbonation of $Ca(OH)_2$ Investigated by Thermal and X-Ray Diffraction Methods of Analysis," J. Appl. Chem., 17, 185 (July 1967)

19. R. Barker, "The Reversibility of the Reaction $CaCO_3 \rightarrow CaO + CO_2$," J. Appl. Chem. Biotechnol., 23, 733 (1973)

20. P. J. Anderson, R. F. Horlock, and J. F. Oliver, "Interaction of Water With the Magnesium Oxide Surface," Trans. Faraday Soc., 61, 2754-62 (1965)

21. D. S. Coleman and W. F. Ford, "The Effect of Crystallite Size and Porosity on the Hydration of Magnesia," Trans. Brit. Ceram. Soc., 63, 365 (1964)

22. J. E. Lyon, T. U. Fox, and J. W. Lyons, "Phosphate Bonding of Magnesia Refractories," Ceramic Bulletin, 45(12), 1078 (1966)

23. F. Wolf and L. Eckert, "Flocculation and Filtration of Magnesium Hydroxide," Chem. Tech. Berl., 23(3), 169 (1971)

24. R. J. Bratton and G. W. Brindley, "Kinetics of Vapor-Phase Hydration of Magnesium Oxide. Part 3. Effect of Iron Oxides in Solid Solution," Trans. Faraday Soc., 62, 2909 (1966)

25. G. K. Layden and G. W. Brindley, "Kinetics of Vapor-Phase Hydration of Magnesium Oxide," J. Am. Ceram. Soc., 46, No. 11, 518 (November 1963)

26. B. S. Girgis, "Activation Energy Evaluation of $Mg(OH)_2$ Dehydration from Conventional and Isothermal DTA Traces," Trans. J. Brit. Ceram. Soc., 71, 6, 177 (1972)

27. R. J. Bratton and G. W. Brindley, "Kinetics of Vapor-Phase Hydration of Magnesium Oxide. Part 2. Dependence on Temperature and Water Vapor Pressure," Trans. Faraday Soc., 61, 1017 (1965)

28. J. Chown and R. F. Deacon, "The Hydration of Magnesia by Water Vapor," J. Brit. Ceram. Soc., 63(2), 91 (1964)

29. W. F. Giauque, "An Example of the Difficulty in Obtaining Equilibrium Corresponding to a Macrocrystalline Nonvolatile Phase. The Reaction $Mg(OH)_2 \rightarrow MgO + H_2O(g)$," J. Am. Chem. Soc., 71, 3192-4 (1949)

30. W. F. Giauque and R. C. Archibald, "The Entropy of Water From the Third Law of Thermodymanics. The Dissociation Pressure and Calorimetric Heat of the Reaction $Mg(OH)_2 \rightarrow MgO + H_2O$. The Heat Capacities of $Mg(OH)_2$ and MgO from 20 to 300 K," J. Am. Chem. Soc., 59, 561-0 (1937)

31. D. T. Livey, et al., "The Properties of MgO Powders Prepared by the Decomposition of $Mg(OH)_2$," Trans. Brit. Ceram. Soc., 56, 217-36 (1957)

32. J. P. McWilliams and A. N. Hixson, "Thermal Decomposition of Manganese Sulfate," Ind. Eng. Chem., Process Des. Dev., 15, No. 3 (1976)

33. M. Selvaratnam and P. D. Garn, "Kinetics of Thermal Decompositions: An Improvement in Data Treatment," J. Am. Ceram. Soc., 59 (7-8), 376 (1976)

34. C. N. Satterfield and P. J. Cadle, "Diffusion in Commercially Manufactured Pelleted Catalysts," I&EC Process Design and Development, 7(2), 256 (1968)

35. B. M. Fabuss, et al., "Kinetics of Thermal Cracking of Paraffinic and Napthenic Fuels at Elevated Pressures," I&EC Process Design and Development, 3(1), 33 (1964)

36. J. Shen and J. M. Smith, "Diffusional Effects in Gas-Solid Reactions," I&EC Fundamentals, 4(3), 293 (1965)

37. P. Schneider and J. M. Smith, "Chromatographic Study of Surface Diffusion," J. AIChE, 14(6), 886 (1968)

38. J. B. Rivarola and J. M. Smith, "Effectiveness Factors with Surface Diffusion," I&EC Fundamentals, 3(4), 308 (1964)

39. C. N. Satterfield and P. J. Cadle, "Gaseous Diffusion and Flow in Commercial Catalysts at Pressure Levels Above Atmospheric," I&EC Fundamentals, 7(2), 202 (1968)

40. J. H. Krasuk and J. M. Smith, "Effectiveness Factors with Surface Diffusion," I&EC Fundamentals, 4(1), 102 (1965)

41. N. Wakao and J. M. Smith, "Diffusion and Reaction in Porous Catalysts," I&EC Fundamentals, 3(2), 123 (1964)

42. S. Masamune and J. M. Smith, "Adsorption of Ethyl Alcohol on Silica Gel," J. AIChE, 11(1), 41 (1965)

43. A. W. Searcy and D. Beruto, "Kinetics of Endothermic Decomposition Reactions. I. Steady-State Chemical Steps," J. Phys. Chem., 80(4), 425 (1976)

44. B. Valdman and R. Hughes, "A Simple Method of Calculating Effectiveness Factors for Heterogeneous Catalytic Gas-Solid Reactions," J. AIChE, 22(1), 192 (1976)

45. J. H. Sharp, G. W. Brindley, and B. N. Narahari Achar, "Numerical Data for Some Commonly Used Solid-State Reaction Equations," J. Amer. Ceram. Soc., 49(7), 379 (1966)

46. R. E. Cunningham and A. Calvelo, "Kinetic Expressions for Reaction Rate in Noncatalytic Solid-Gas Systems," Ind. Eng. Chem. Fundam., 9(3), 505 (1970)

47. R. L. Stone, "Apparatus for Differential Thermal Analysis Under Controlled Partial Pressures of H_2O, CO_2, or Other Gases," J. Am. Ceram. Soc., 35(3), 76 (1952)

48. R. L. Stone, "Differential Thermal Analysis of Kaolin Group Minerals Under Controlled Partial Pressures of H_2O," J. Am. Ceram. Soc., 35(4), 90 (1952)

49. T. Z. Harmathy, "Simultaneous Moisture and Heat Transfer in Porous Systems with Particular Reference to Drying," I&EC Fundamentals, 8(1), 92 (1969)

50. W. E. Wentworth and E. Chem, "Simple Thermal Decomposition Reactions for Storage of Solar Thermal Energy," Solar Energy, 18, 205 (1976)

51. R. W. Hallet, Jr. and R. L. Gervais, "Central Receiver Solar Thermal Power System, Phase 1 Final Report," MacDonnell Douglas Company (January 1976)

52. J. W. Doane, et al., "The Cost of Energy from Utility-Owned Solar Electric Systems," (JPL 5040-29, ERDA/JPL-1012-76/3) Jet Propulsion Laboratory, Pasadena, California (June 1976)

53. J. F. Frantz, "Design for Fluidization," Chem. Eng. (September 17, 1962)

54. W. L. Badger and W. L. McCabe, Elements of Chemical Engineering, 2nd Edition, McGraw-Hill Book Company

55. C. Y. Wen and Y. N. Yu, "Mechanics of Fluidization," Chem. Eng. Progr. Symposium Series No. 62, 62 (1966)

56. Air Pollution Engineer Manual, 2nd Edition, U.S. Environmental Protection Agency, Publication No. AP-40, pp 365-367

57. J. Pata and M. Hartman, "Minimum Fluidization Velocities of Lime and Limestone Particles," Ind. Engr. Chem. Process Des. Dev., 17, No. 3 (1978)

58. H. Littman et al., "Fluidization Fundamentals and Application," Chemical Engineering Progress Symposium Series 105, 66 (1970)

59. M. A. Bergougnou et al., "Fundamental Processes in Fluidized Beds," Chemical Engineering Progress Symposium Series 101, 66 (1970)

60. "Fluidization and Fluid-Particle Systems," D. L. Keairns, Editor, A.I.Ch.E. Symposium Series 141, 70 (1974)

61. "Fluidization Theories and Applications," J. S. Halow, Editor, A.I.Ch.E. Symposium Series 161, 73 (1977)

62. J. M. Smith, Chemical Engineering Kinetics, 2nd Edition, McGraw-Hill, New York (1970)

63. L. S. Caretto and K. Nobe, "Effects of Pore Diffusion in the Catalytic Oxidation of Ethylene," A.I.Ch.E.J., 15, 18-24 (1969)

64. G. L. Bauerle, S. C. Wu, and K. Nobe, "Parametric and Durability Studies of NO_x Reduction with NH_3 on V_2O_5 Catalysts," I&EC Prod. Res. Develop., 17, 117-22 (1978)

65. G. L. Bauerle, S. C. Wu, and K. Nobe, "Parametric and Durability Studies of NO_x Reduction with NH_3 on Fe-Cr Oxide Catalysts," I&EC Prod. Res. Develop., 17, 123-8 (1978)

66. I. Fujii and K. Tsuchiya, "Experimental Study of Thermal Energy Storage by Use of Reversible Chemical Reactions," Paper presented at International Conference on Alternative Energy Sources, Miami, FL, December 5-7, 1977

67. D. R. Stull and H. Prophet, JANAF Thermochemical Tables, Nat. Stand. Ref. Data Serv., Nat. Bur. Stand., 37 (June 1971) and supplements for 1974 and 1975

68. R. S. Mikhail, S. Brunauer, and L. E. Copeland, "Kinetics of the Thermal Decomposition of Calcium Hydroxide," J. Colloidal Interface Sci., 21, 394-404 (1966)

69. J. H. Flynn and L. A. Wall, "General Treatment of the Thermogravimetry of Polymers," Journal of Research, U.S. Nat. Bur. Stand., 70A, 487-523 (1966)

70. C. D. Doyle, J. Appl. Polymer. Sci., 6, 639 (1962)

71. "Central Receiver Solar Thermal Power System," SAN-1108-76-8, MDC G6776, Volume I Executive Ovewview, MacDonnell Douglas Corp. (October 1977)

UNLIMITED RELEASE

INITIAL DISTRIBUTION

U. S. Department of Energy
Division of Energy Storage Systems
Washington, D. C. 20545
Attn: J. Gahimer (5)
G. Pezdirtz
J. H. Swisher

Australian National University
Department of Engineering Physics
Canberra, A.C.T. 2600
AUSTRALIA
Attn: P. O. Carden

Electric Power Research Institute
P. O. Box 10412
Palo Alto, California 94304
Attn: B. Mehta

Corporate Research and Development
General Electric
Schenectady, New York 12301
Attn: J. W. Flock

Gilbert Associates, Inc.
P. O. Box 1498
Reading, Pennsylvania 19603
Attn: H. Chen

NASA-Lewis Research Center
Cleveland, Ohio 44101
Attn: J. Calogeras
W. J. Masica

Oak Ridge National Laboratory
Oak Ridge, Tennessee 37830
Attn: R. Graves

Rocket Research Company
York Center
Redmond, Washington 98052
Attn: R. D. Smith

Atomics International Division
Rockwell International
8900 DeSota Avenue
Canoga Park, California 91304
Attn: T. Springer (15)

Solar Energy Research Institute
1536 Cole Boulevard
Golden, Colorado 80401
Attn: C. Wyman

C. J. Swet
Route 4, Box 258
Mt. Airy, Maryland 21771

R. W. Mar, 8313
M. Nickols, 8313
J. J. Iannucci, 8326
T. T. Bramlette, 8452
J. D. Fish, 8452
W. G. Wilson, 8453
Publications Division, 8265, for TIC (27)
Publications Division, 8265/Technical Library Processes and Systems Division, 3141
Technical Library Processes and Systems Division, 3141 (2)
Library and Security Classification Division, 8266 (3)

Org.	Bldg.	Name	Rec'd by*	Org.	Bldg.	Name	Rec'd by*

*Recipient must initial on classified documents.

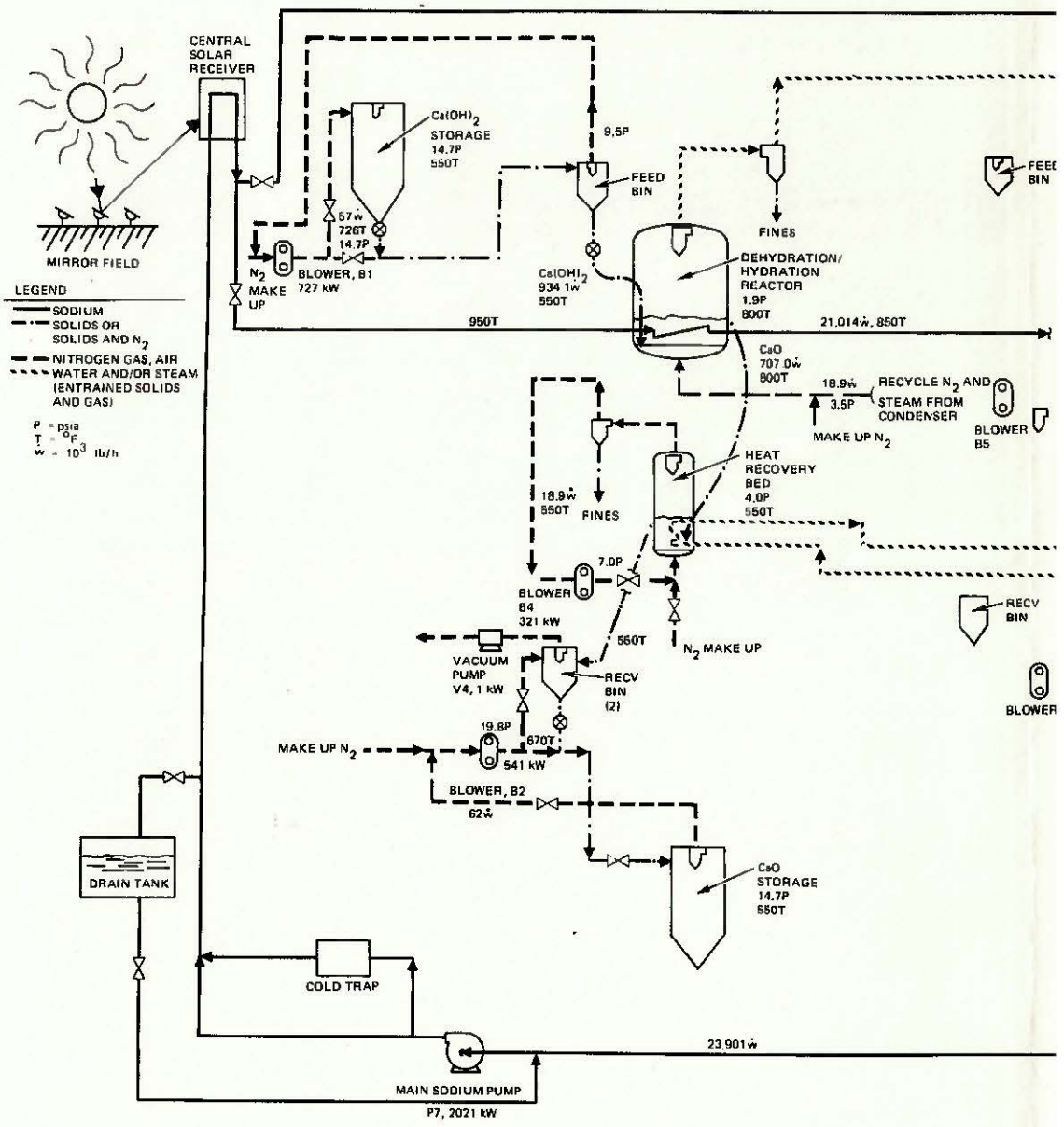
CENTRAL SOLAR RECEIVER
MIRROR FIELD
LEGEND
SODIUM
SOLIDS OR SOLIDS AND N_2
NITROGEN GAS, AIR WATER AND/OR STEAM (ENTRAINED SOLIDS AND GAS)
P = psia
T = °F
ẇ = 10^3 lb/h
$Ca(OH)_2$ STORAGE 14.7P 550T
57ẇ 726T 14.7P
N_2 MAKE UP
BLOWER, B1 727 kW
9.5P
FEED BIN
FINES
$Ca(OH)_2$ 934.1ẇ 550T
DEHYDRATION/ HYDRATION REACTOR 1.9P 800T
950T
21,014ẇ, 850T
CaO 707.0ẇ 800T
18.9ẇ
3.5P
RECYCLE N_2 AND STEAM FROM CONDENSER
MAKE UP N_2
BLOWER B5
HEAT RECOVERY BED 4.0P 550T
18.9ẇ 550T
FINES
7.0P
BLOWER B4 321 kW
560T
N_2 MAKE UP
VACUUM PUMP V4, 1 kW
RECV BIN (2)
RECV BIN
BLOWER
19.8P
670T
541 kW
MAKE UP N_2
BLOWER, B2 62ẇ
CaO STORAGE 14.7P 550T
DRAIN TANK
COLD TRAP
23.901ẇ
MAIN SODIUM PUMP P7, 2021 kW

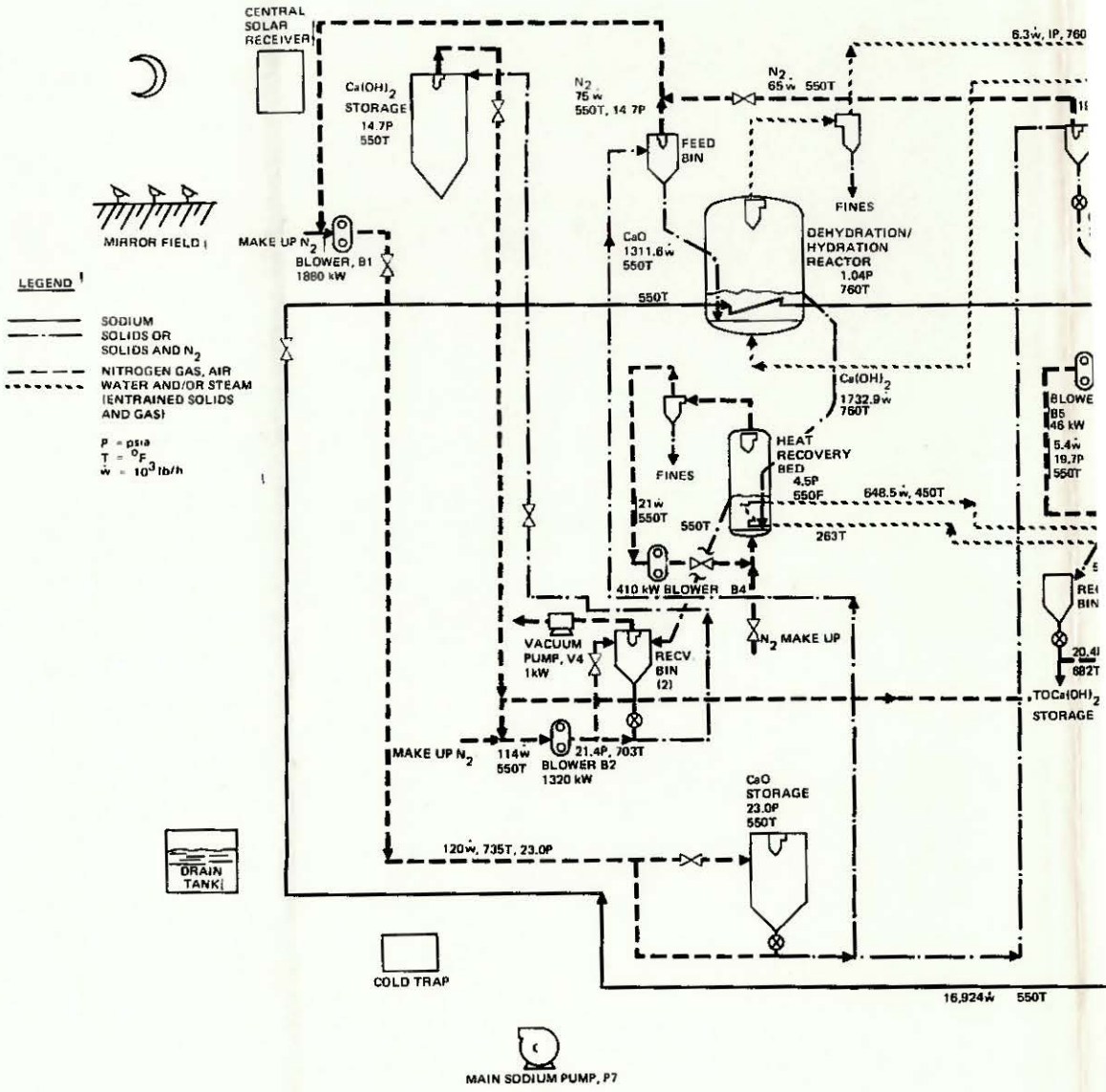
CENTRAL SOLAR RECEIVER
MIRROR FIELD
LEGEND
SODIUM
SOLIDS OR SOLIDS AND N_2
NITROGEN GAS, AIR WATER AND/OR STEAM (ENTRAINED SOLIDS AND GAS)
P = psia
T = °F
ẇ = 10^3 lb/h
$Ca(OH)_2$ STORAGE 14.7P 550T
N_2 75ẇ 550T, 14.7P
N_2 65ẇ 550T
6.3ẇ, IP, 760
FEED BIN
FINES
MAKE UP N_2
BLOWER, B1 1880 kW
CaO 1311.6ẇ 550T
DEHYDRATION/ HYDRATION REACTOR 1.04P 760T
550T
$Ca(OH)_2$ 1732.9ẇ 760T
FINES
HEAT RECOVERY BED 4.5P 550F
648.5ẇ, 450T
21ẇ 550T
550T
263T
410 kW BLOWER, B4
VACUUM PUMP, V4 1kW
RECV BIN (2)
N_2 MAKE UP
TO $Ca(OH)_2$ STORAGE
MAKE UP N_2
114ẇ 550T
21.4P, 703T
BLOWER B2 1320 kW
CaO STORAGE 23.0P 550T
120ẇ, 735T, 23.0P
DRAIN TANK
COLD TRAP
16,924ẇ 550T
MAIN SODIUM PUMP, P7

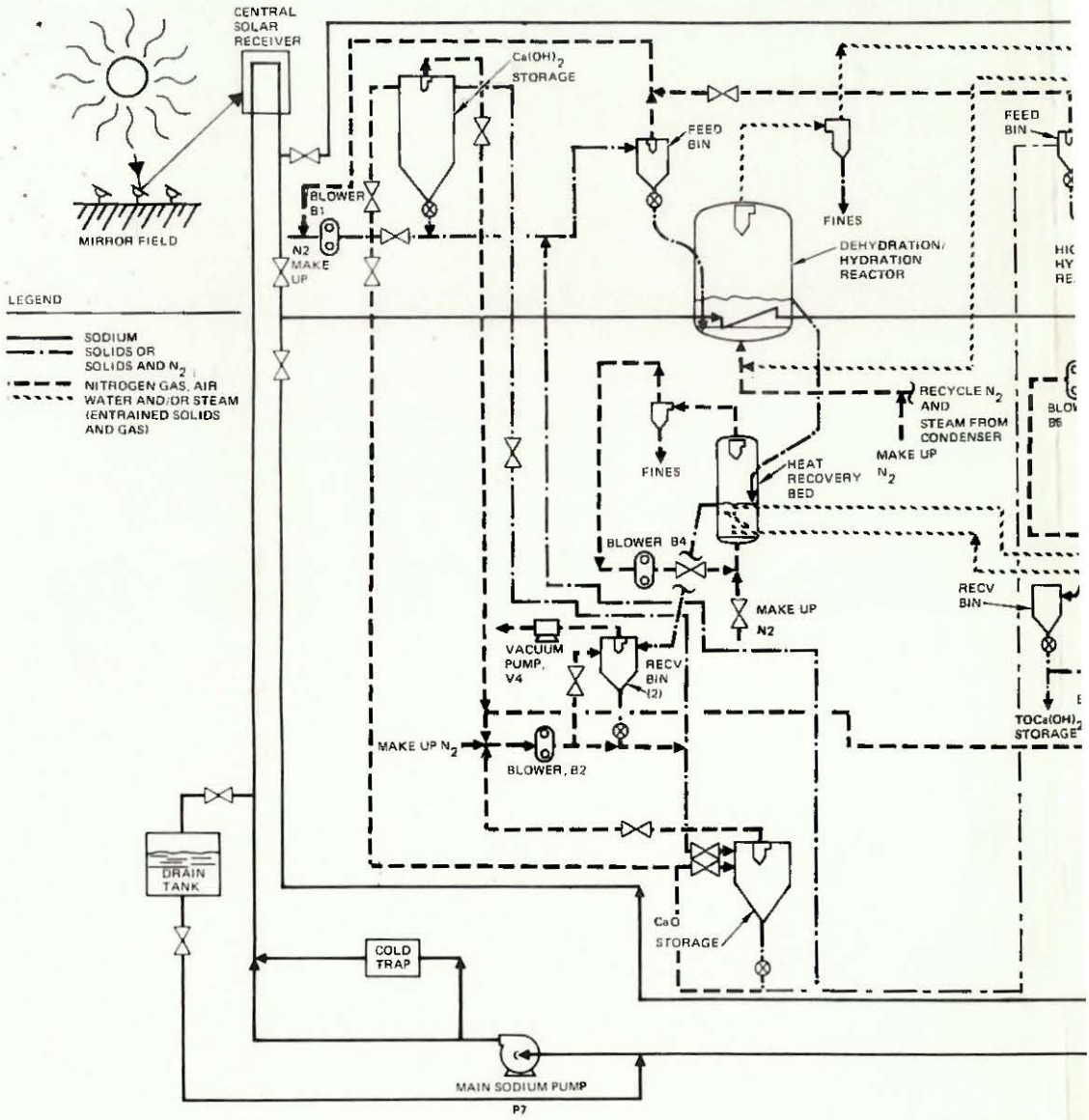
CENTRAL SOLAR RECEIVER
MIRROR FIELD
LEGEND
SODIUM
SOLIDS OR SOLIDS AND N_2
NITROGEN GAS, AIR WATER AND/OR STEAM (ENTRAINED SOLIDS AND GAS)
$Ca(OH)_2$ STORAGE
BLOWER B1
N_2 MAKE UP
FEED BIN
FINES
DEHYDRATION/ HYDRATION REACTOR
RECYCLE N_2 AND STEAM FROM CONDENSER
MAKE UP N_2
HEAT RECOVERY BED
BLOWER B4
MAKE UP N_2
RECV BIN
VACUUM PUMP, V4
RECV BIN (2)
MAKE UP N_2
BLOWER, B2
DRAIN TANK
CaO STORAGE
COLD TRAP
MAIN SODIUM PUMP
P7